PUNCHING SHEAR OF SELF-CONSOLIDATED TWO-WAY SLABS

by

Hossameldeen Bakr, B.Sc. (Hons.)

A thesis submitted to the

School of Graduate Studies

in partial fulfillment of the requirement for the degree of

Master of Engineering

Faculty of Engineering & Applied Science

Memorial University of Newfoundland

May 2015

St. John’s Newfoundland Canada

Abstract

An experimental program was conducted to investigate the structural behaviour of two-way slabs made with Self-consolidating concrete (SCC). Four different SCC mixtures were developed with targeted compressive strength of 30 MPa. Mixtures A and B contained maximum coarse aggregate size of 10 mm, and coarse to fine aggregate ratio (C/F) of 0.70 and 1.20, respectively. Mixtures C and D contained a larger coarse aggregate size of 20 mm, and (C/F) of 0.70 and 1.20, respectively. The properties of the fresh and hardened concrete for each mixture were measured.

Each concrete mixture was used to construct three slabs with different thicknesses of 150 mm, 200 mm, and 250 mm. Thus, a total of twelve slabs were tested in the experimental program. All test slabs had a reinforcement ratio of approximately 1.0%. Hence, the main parameters in the experimental program were the coarse aggregate size, coarse to fine aggregate ratio, and slab depth. The structural behaviour of the slabs was examined under static monotonic load with regard to the deformations, strains in the reinforcement and concrete, ultimate capacity, modes of failure, and crack development.

The C/F ratio and maximum aggregate size do not show significant influence on the slab deformation characteristics such as deflection, stiffness, ductility and energy absorption, steel and concrete strains and cracking characteristics. The slab thickness has the most significant effect among the test parameters on the behaviour of the test slabs. The depth and aggregate size are the most influential parameters on the capacity of the slab; increasing the slab thickness lead to a decrease in the normalized shear

strength of the slab while increasing the aggregate size lead to an increase in the normalized shear strength of the slab.

The Critical Shear Crack Theory (CSCT) by Muttoni (2008) is able to reasonably predict the structural behaviour of the test slabs. However, the predictions of the capacity by the CSCT had a high scatter. In addition, the test results did not show any clear trend in the relationship between the aggregate size and the slab rotation.

The Canadian Code (CSA A23.3-04), the American Code (ACI 318-11) and the British Code (BS8110-97) give safe predictions of the capacity of the SCC test slabs. The predictions of those codes are more conservative and have less scatter when applied to SCC slabs with 20 mm coarse aggregate size compared to those with 10 mm coarse aggregate size. Therefore, these codes can be safely used to check the punching shear capacity of SCC slabs without the need of any modification to the equations used for such shear check. The predictions of the Eurocode (EC2) are unsafe for most of the slabs with thicknesses of 200 mm and 250 mm. Hence, further research is needed to examine the use of EC2 in the design of SCC slabs for punching shear.

Acknowledgement

I am deeply indebted to my thesis supervisors and research advisors; Dr. Amgad Hussein, Head of Department of Civil Engineering at Memorial University of Newfoundland, and Dr. Assem Hassan, Assistant Professor of Civil Engineering. Grateful acknowledgment is due for their sincere support, valuable guidance, fruitful discussions, and comments throughout the courses of this study. I would like to thank them for giving me this great opportunity; it was a rewarding experience, both professionally and personally.

I would also like to thank the staff at Civil Department Laboratory who have helped me a lot, made my work easier, and added pleasant moments to my work; Matthew Curtis and Shawn Organ. I would like to extend my appreciation to Mrs. Moya Crocker, Ms. Colleen Mahoney, and Ms. Nicole Parisi in the graduate studies office who have showed great assistant and guidance through my time at Memorial University.

I also wish to acknowledge the support and cooperation of my colleagues, and classmates during my study at Memorial University. I would like to particularly thank Hossam Al-Alalaily for his amazing friendship; support and encouragement throughout the course of my studies, and Md. Shahriar Nizam for his encouraging energetic spirit, cheerful personality and optimism.

I would like to express my gratitude to the Prof. Hatem Mustafa; professor in the Civil Department in Cairo University who supported and helped me to start my master

program at Memorial University. In addition, I can't forget the support and belief from my best friends: Omar Hegazy, Hazem H. El Anwar, Ali F. Helwa, Shehab W. Agaiby, and Shorouk M. Soliman who supported me as they always have despite the thousands of miles that were between us.

I would like also to deliver my gratitude and appreciation to my best manager ever Ms.Dina Sami, for all the support, and professional experience she gave to me during my time at PDi. I am thankful for her valuable advices and continued encouragement during my journey at Memorial University.

Finally, special appreciation and sincere deep gratitude are due to my precious parents Magdy K. Ahmed, and Abeer Shawki, my brother Hazem M. Karam, my sister Reem M. Karam, and my great grandmother Tahia Abdul-Ati for their patience, encouragement, and their continuous love and support throughout my stay in St. John’s. Dad and Mum, I owe you everything, I would be nothing without you. Thanks for everything you did and you still doing for me. Thank you for being there.

Table of Contents

List of Figures

List of Tables

Abbreviations

ACI	American Concrete Institute
ASTM	American Society for Testing and Materials
BR	Blocking Ratio (L-Box Test)
BS	British Standard
C/F	Coarse to Fine aggregate ratio
CA	Maximum coarse aggregate
CDT	Crack displacement transducers
CSA	Canadian Society Association
CSCT	Critical Shear Crack Theory
EFNARC	European Federation of National Associations Representing for
EC	European Code
FA	Fine aggregate
HRWR	High Range Water Reducer
MCFT	Modified Compression Field Theory
NC	Normal Concrete
SCC	Self-consolidating concrete

ϕ_c	Resistance factor of concrete
a	Reinforcement length (Yield Line Pattern)
a_g	maximum aggregate size
c	side length of square column (distance from extreme compression fibre to neutral axis)
b_0	perimeter of critical section for shear in slabs and footings
d	depth to the lower reinforcement for flexural calculations and the average depth of the reinforcement layer for the punching shear calculation
d_{ave}	average of effective depth in directions of slab
d_g	maximum coarse aggregate size
d_{g_0}	Reference aggregate size (16 mm (0.63 in))
E_s	Modulus of Elasticity of reinforcement

EI_0	flexural stiffness before cracking
EI_1	Tangential flexural stiffness after cracking
f_c'	Uniaxial compressive strength of concrete (cylinder strength)
f_r	Tensile Strength
f_{ck}	Characteristics compressive cylinder strength of concrete (European practice)
f_{ct}	Tensile strength of concrete
f_y	Yield strength for the reinforcement bars
h	Slab thickness
I_{ch}	Characteristic length
P_{flex}	Theoretical flexural capacity
P_{test}	Experimental punching shear strength
P_{th}	Theoretical punching shear strength (Based on Muttoni's Formula)
u	Perimeter of the critical section at 1.5d (British Standard)
u_1	Perimeter of the critical section at 2.0d (European Standard)
V_R	Shear strength
v_{ci}	aggregate interlock capacity at crack
v_n	nominal shear strength resistance
v_u	Shear stress due to factored load
w	Crack width (total relative displacement between lips of crack)
β	Ratio of the long side to the short side
λ	modification factor reflecting reduced mechanical properties of lightweight concrete
ρ	Reinforcement ratio factor
ψ	Rotation of slab outside the column region
m_{cr}	Cracking moment per unit width
m_r	Radial moment per unit width
m_t	Tangential moment per unit width
m_R	Nominal moment capacity per unit width
m_{Rd}	Design moment capacity per unit width
r	Radius
r_0	Radius of the critical shear crack
r_1	Radius of the zone in which cracking is stabilized

r_c	Radius of a circular column
r_{cr}	Radius of cracked zone
r_q	Radius of the load introduction at the perimeter
r_s	Radius of circular isolated slab element
r_y	Radius of yielded zone
$\Delta\phi$	Angle of a slab sector
γc	Partial safety factor for concrete
χ_1	Curvature in stabilized cracking
χ_{cr}	Curvature at cracking
χ_r	Curvature in radial direction
χ_t	Curvature in tangential direction
χ_y	Yielding curvature
χ_{TS}	Decrease in curvature due to tension stiffening

Chapter 1

Introduction

1.1 General

Self-consolidating concrete (SCC) was first used in Japan in the 1980s. It is also known as Self-compacting concrete. It was mainly produced to be used in congested reinforced structures (Goodier 2003). SCC has a high ability to flow under its own weight within highly congested reinforced concrete structures without segregation or destruction of mixture homogeneity, and provide good consolidation without need for internal or external compaction (Hassan et al. 2010). The high flowability is the main characteristic of SCC when compared with normal concrete (NC). SCC can be developed by adding superplasticizer to the NC mixtures. An SCC mixture has a higher fine aggregate content to improve the flowability and avoid any segregation.

These advantages are the reason for the wide use of the SCC as a construction material in applications such as residential and industrial buildings, garages, walls, and bridges. However, the use of SCC is still limited due to the increased fine aggregate content which is believed to result in a reduction in the shear strength of a structural member. The increased fine content may cause a reduction in aggregate interlock which is considered to be the main resisting factor for shear stresses (Lin and Chen 2012). Thus, in the past few years, extensive studies have been conducted on the shear failure mechanism of SCC reinforced beams Lin et al. (2012) and Hassan

et al. (2008). However, no investigations have been reported on the structural behaviour of SCC reinforced slabs failing due to punching shear stresses. Hence, there is a need to study the punching shear in SCC two-way slabs since it has a brittle mode of failure. Brittle failure occurs without warning.

The provisions of the design codes (CSA 23.3-04, ACI 318-11, BS 8110-97, and EC2) for punching failure are based on empirical formulas. These formulas were developed based on research conducted on NC structural members. Thus, it is necessary to examine the application of the code equations in the design of SCC slabs for punching shear.

A rational mechanical model was proposed by Muttoni (2008) and subsequently formed the basis for punching shear provisions in the latest edition of the Model Code (2010). The model includes the effect of the coarse aggregate size to predict the behaviour and capacity of the two-way slabs based on the load-rotation relationship. No other rational model or code equation accounts for the coarse aggregate size effect on the behaviour and capacity of the two-way slab. From the literature, the model gives good predictions for the NC slabs.

1.2 Research Scope and Objectives

The current research program was designed to investigate the structural behaviour of SCC reinforced two-way slabs. For this purpose, twelve full scale interior slab-column connections were constructed using four SCC mixtures of different coarse aggregate sizes and C/F aggregate ratios; each of those mixtures was used to cast three slabs of different thicknesses. Thus, the main parameters for the slab-column connections were the aggregate size the C/F aggregate ratio and the slab thickness.

Firstly, the fresh and mechanical properties of the four developed SCC mixtures were determined. The fresh properties were tested during the casting process by performing slump flow, V-Funnel, and L-Box test. Then, after 28 days, and in the day of testing the slab, the mechanical properties were determined by performing the compressive strength, and the flexure strength tests. Secondly, the slabs were tested in the structural lab by applying concentric load and recording the test data using data acquisition system. Then, the recorded data was processed and analysed in terms of deflection, strain in the reinforcement and concrete, crack development, and ultimate capacity. Finally, the experimental data was compared with current design codes and the Critical Shear Crack Theory (CSCT) which was proposed by Muttoni (2008) and subsequently formed the basis for punching shear provisions in the latest edition of the Model Code (2010).

The main objectives of this research work are summarized as follow;

1- Investigate the structural behaviour and characteristics (deflections, ductility, stiffness, ductility, energy absorption, strains, and crack development) of the SCC two-way slabs.

2- Provide experimental data for SCC reinforced two-way slabs that show the influence of the slab thickness, maximum coarse aggregate size and the C/F aggregate ratio on the structural behaviour and the punching shear capacity of SCC two-way slabs.

3- Investigate the validity of the currently used equations and formulas proposed by the different codes and standards (CSA A23.3-04, ACI318-11, BS8110-97, and EC2), and the CSCT proposed by Muttoni (2008) in predicting the failure behaviour and punching shear capacities of reinforced two-ways slabs constructed using SCC.

1.3 Thesis Outline

Chapter 1, Introduction, presents a brief background on SCC and the punching shear as a possible mode of failure in two-way slabs, and an overview on the current research scope, objectives, and outlines.

Chapter 2, Literature Review, is divided into three parts: the first part presents relevant research work on SCC fresh properties, and reviews the experimental investigation work done on SCC beams showing the influence of parameters similar to those used in the current study. The second part reviews the previous relevant research conducted on two-way slabs made with normal concrete (NC), and presents the recently proposed approaches and formulation accounting for the failure behaviour of two-way slabs. Finally, the third part presents the current codes provisions for the punching shear behaviour in the two-way slabs.

Chapter 3, Experimental Program, is divided into two parts: the first part presents the material proportions, standard testing procedure, the fresh and mechanical properties; and discussion of the results. The second part presents the details of the experimental program such as the test slabs, instrumentation arrangements, and the testing procedure.

Chapter 4, Results & Discussion reports the test results and observations obtained during the testing process. This chapter also includes discussion and comparison of these results with those obtained from different codes predications and other stated formulations.

Chapter 5, Conclusion, summarizes all conclusions made based on the experimental analysis and test observations.

Chapter 2

Literature Review

2.1 Introduction

This Chapter is divided into three parts: the first part presents relevant research on SCC materials, and reviews the previous experimental investigations conducted on SCC beams highlighting the influence of different parameters on their shear characteristics. The second part reviews the previous relevant research carried out to investigate NC two-way slabs, and the recent proposed approaches and formulation accounting for the failure behaviour of the two-way slabs. Finally, the third part presents the current codes provisions for the punching shear behaviour in the two-way slabs.

2.2 Self-Consolidating Concrete

The fresh properties of the SCC are believed to be the most significant difference when compared with the NC. This is reflected by the different characteristics such as flowability, filling ability, passing ability and segregation. The fresh properties of SCC are measured by standard equipment and there are certain limits specified in the standards and specification (EFNARC - 2005) to ensure the quality and consistency of the produced mixes. These properties are also influenced by the admixtures and proportions used. Studies were conducted by many researchers using a wide range of mixes to determine the influence of such parameters. This section reviews few

research work done in which the effect of using different coarse aggregate size, and aggregate volume on the fresh properties of SCC mixes was studied.

The coarse aggregate characteristics (shape, maximum size, and grading) are believed to highly influence the SCC mixtures. Khaleel et al. (2011) conducted an experimental work to study the influence of the maximum coarse aggregate size and type on the fresh properties of SCC (flowability, filling ability, passing ability and segregation). In their research, three different types of coarse aggregate were used: uncrushed gravel, crushed gravel, and crushed limestone, and two different sizes of 10 and 20 mm for each type of the used aggregate. The fresh properties tests in their study were performed as specified by the European Federation of National Associations Representing for Concrete (EFNARC - 2005).

The results showed that the T_{50cm}, time taken for concrete to reach the 500 mm spread circle,for mixtures of 10 mm coarse aggregate size which represents the flowability showed lower values compared with mixtures of 20 mm coarse aggregate size. The flowability was measured again using the V-Funnel test. Increasing the coarse aggregate size from 10 to 20 mm resulted in a significant increase in the initial V-Funnel time (T_f). The L-Box was then used to determine the influence on the passing ability. The recorded values of the Blocking Ratio (BR) factor were lower for mixtures with 20 mm coarse aggregate size. The lower values of the BR when a larger coarse aggregate size was used represented a higher possibility of blocking. The mechanical properties were studied as well for all mixtures, and a decrease in the compressive strength and flexure strength was recorded for all mixture with 10 mm coarse aggregate size. This was attributed to the higher bond when smaller coarse aggregate is used since the small particles have larger surface area compared to the 20

mm coarse aggregate size. Khaleel et al. (2011) concluded that mixtures of smaller coarse aggregate size showed better flowability, higher passing ability, and improved mechanical properties.

Another study was conducted by Krishna et al. (2010) to account for the influence of using different coarse aggregate size. In their experiment a total of eight mixes were examined. These mixes included only four SCC mixtures with the same proportions. However, four different coarse aggregate sizes of 10, 12.5, 16, and 20 mm were used. The standard fresh properties tests were conducted in the following order: slump flow diameter, J-Ring, L-Box and V-Funnel. The mechanical properties were then tested according to EFNARC – 2005. The resulting fresh properties for this research work are listed in Table 2.1. They were found in good agreement with the results of the research conducted by Khaleel et al. (2011) presented earlier in this section. The results confirmed that using a smaller coarse aggregate size provided better fresh properties for the concrete mixture as the T_{50cm} and T_f are found to be longer in case of larger coarse aggregate size is used. In the meantime, the possibility of blocking becomes higher when a larger coarse aggregate size is used, and this can be seen form the L-Box ratios listed; the lower ratios were measured for mixtures with larger coarse aggregate size. Krishna et al. (2010) also concluded that, increasing the coarse aggregate size results in a higher possibility for segregation.

Table 0.1: Fresh Properties of Self-Consolidating Concrete, Krishna et al. (2010)

Mix ID	C.A Size (mm)	Slump Dia. (650-850 mm)	T_{50cm} (2-5 sec)	V-Funnel (6-12 sec)	L-Box (0.8-1.0)
SCC20	20	650	5	12	0.80
SCC16	16	670	4.2	11.5	0.85
SCC12.5	12.5	710	3.6	10	0.90
SCC10	10	725	3	9.3	0.92

On the other hand, the results of the hardened properties of SCC mixtures contradicted with those presented by Khaleel et al. (2011). The results showed a slight improvement in the compressive strength, the tensile strength, and the flexure strength with increasing the coarse aggregate size form 10 mm to 20 mm.

Researchers have carried out experimental investigations to have a better understanding of the SCC structural behaviour and the effect of using different coarse aggregate sizes on the beams' shear mechanisms. Most of these studies were based on a comparison between SCC and NC beams. The most recent studies are presented among the reviews in this section.

Hassan et al. (2008) conducted an experimental investigation in which the shear strength and cracking behaviour of ten SCC beams were compared with similar ten NC reinforced beams. The same parameters were used except the following: beam depth varied between 150 and 750 mm, and longitudinal reinforcement ratio varied between 1% and 2%. The results showed slightly lower shear strengths for the SCC beams. However, no significant change was observed in the pre-cracking stage between NC and SCC beams. The authors concluded that using a lower reinforcement ratio resulted in wider crack widths in beams with reinforcement ratio of 1% compared with those of 2% reinforcement ratio. When the shear strengths were calculated using the equations provided by the Canadian code (CSA A23.3-04) and the American Code (ACI 318-11); the CSA conservatively predicted the shear capacities for both types of beams (SCC and NC). However, the ACI was found to

overestimate the shear strength for less number of the tested beams. It was noted that the ACI predication was less conservative for the rest of tested beams.

The shear behaviour of SCC beams was also studied by Lin et al. (2012). Twenty four beams were tested to compare the behaviour of SCC with that of NC. The beams were divided into three groups each with eight beams; two groups of SCC beams, and one group of NC. Different parameters were tested as follows: concrete strength, shear span-depth ratio (a/d), spacing of the shear reinforcement, and the amount of coarse aggregate in the SCC mixture. The authors compared the capacity of the beams to those predicted using current ACI code. When the two groups of SCC beams were compared, the group which had the larger coarse aggregate size had higher shear strength compared to those with smaller aggregates that had the same compressive strength and shear span-depth ratio. This finding confirmed the influence of the coarse aggregate size on the shear strength. The ACI predictions was found to underestimate the ultimate shear capacity for beams with larger aggregate size by an average of 72% and for the group of smaller aggregate size by an average of 55%. The investigation showed the need to account for the coarse aggregate size in the current code prediction.

2.3 Punching Shear of Two-Way Slabs

This section presents a review of studies conducted on the structural behaviour of two-way slabs failing under punching shear stresses. These reviews included both experimental and theoretical based studies. It should be noted that all the current available investigations were conducted using NC two-way slabs. There is no available experimental investigation that was reported in the literature for SCC reinforced slabs. The theoretical studies presented were based on databank of experimental work done on two-way slabs. The experimental studies presented

focused on those that examined the effect of aggregate size and depth. The influence of these parameters is similar to those used in the current study.

2.3.1 Previous Experimental Investigations

A) Slab Thickness

The size effect was detected and defined in 1980s. In the research conducted by Bazant and Kim (1984), the size effect was investigated by testing nine micro circular concrete slabs with rectangular columns. The slabs had a constant maximum coarse aggregate size of 1.59 mm. The slab thickness used varied as follows: 25 mm, 50 mm, and 100 mm. The slabs were divided into three groups based on the curing process, and each of these groups included three slabs of the three different sizes mentioned. All slabs were designed to fail under punching shear failure.

The authors concluded from the load-deflection curves that a brittle failure occurred in the slabs instead of what was agreed by that time; that plastic failure occurs in a slab. The author also criticized that the size effect for the structure members is ignored by the design codes. Nonetheless, some research work investigations confirmed the influence of the size effect. More brittle failure behaviour was detected for thick slabs; this finding was considered a confirmation for the size effect due to the slab depth rather than aggregate size. The authors proposed the following equation to predict the punching shear capacity;

$$v_u = k_1 f_c' \left(1 + k_2 . \frac{d}{b}\right) \quad (0.1)$$

This formula was proposed based on theoretical derivation using the plastic limit analysis. It yielded reasonable predicted values for the punching shear strength. However, the size effect was insignificantly determined by this equation.

An experimental program was carried out by Rizk et al. (2011) to investigate the influence of the slab size on the punching shear resistance. Five thick square slabs were tested. The slabs were 300 mm and 400 mm thick with side dimension of 2650 mm. The slabs were loaded through a small column stub 400 × 400 mm. Four slabs were cast using high strength concrete and one using normal concrete. Shear reinforcement was used in one of the high strength concrete slab. The results of the punching shear strength showed good agreement with the values predicted using the CEB-FIP Model Code (1990). The ACI 318-11 code was found to underestimate the punching shear strength for all slabs by an average of 17% except for one high strength concrete slab. This high strength slab had the lowest reinforcement ratio and the predicted value was overestimated by 19%. It was highlighted by the authors that the experimental shear strength was different in two slabs. The slabs had different concrete strength, similar slab thickness and reinforcement ratio. Both slabs were designed to fail under punching shear stresses. This finding showed that having a constant number for the size effect factor depending on the slab depth only, as used in major design codes, may not account for the size effect and it should also include the concrete compressive strength.

Two modifications were proposed by the authors to the ACI318-11 code for punching shear as follows:

$$V_{c-eq} = 0.33.\sqrt{f_c'}\left(\frac{I_{ch}}{h}\right)^{0.33}(100\rho)^{0.33}b_o d \quad (0.2)$$

The proposed formula included the control perimeter, concrete strength, reinforcement ratio, and brittleness ratio (h/I_{ch}) to the power of 0.33; the second modification is adding a term for the reinforcement ratio to the power of 0.33.

Birkle and Dilger (2008) conducted similar work to investigate the influence of the slab thickness on the punching strength of the two-way slabs. A total of nine slabs were tested. The slabs were divided into three series and each series has three slabs with three different thicknesses (160 mm, 230 mm, and 300 mm). Series 1 was used to examine the size effect for slabs without shear reinforcement. The slabs were formed in octagonal shape with eight supports as shown in Figure 2.1. The slabs were loaded using a rectangular column that varied in dimensions with the slab thickness.

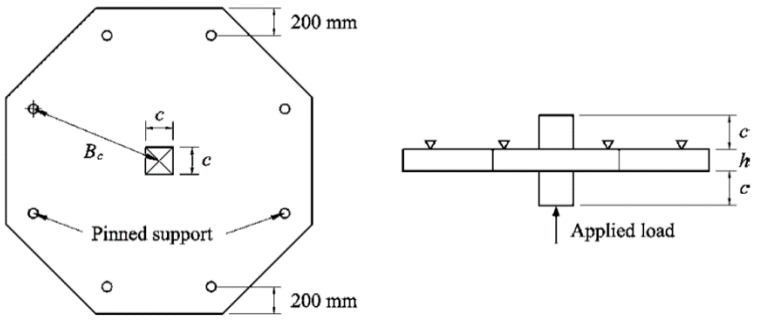

Figure 0.1: Layout of Test Slabs, Birkle and Dilger (2008)

A concrete cover of 20 mm was used. The reinforcement bars had a nominal yield strength of 400 MPa. The reinforcement ratio was decreased with increasing the slab thickness as follows, 1.54%, 1.30%, and 1.10%. The nominal compressive strength at 28 days was 32 MPa. The load-deflection curves for the three slabs showed an expected behaviour of brittle failure. The authors discussed the CSA A23.3-04 code provisions in accounting for the size effect for slabs with effective depths higher than

300 mm. They suggested adding a size effect factor for the slabs with depths approximately equals to 220 mm. Furthermore, the author presented a new proposal to account for the punching shear resistance by adding a coefficient for the reinforcement ratio; since the reinforcement ration has an influence in addition to the influence of the concrete strength and the slab thickness. The authors proposed the following equation for punching shear resistance:

$$v_n = 16 \left(\frac{f_c' . \rho}{d}\right)^{1/3} \geq \sqrt{f_c' \text{ (MPa)}} \tag{0.3}$$

B) Coarse Aggregate Size

The coarse aggregate size effect on the punching shear behaviour of the two-way slabs was first examined by Guandalini et al. (2009) in addition to slabs size. Eleven square slabs with variable thicknesses, maximum coarse aggregate sizes and reinforcement ratios were tested. The slabs were divided into three groups based on the slab dimensions. The first group of slabs with a size of 3.0 m × 3.0 m × 250 mm included six slabs of variable maximum aggregate size and reinforcement ratios. The second group included only one slab of size 6.0 m × 6.0 m × 300 mm which is double size of the first group. The third group included four slabs half size of the first group with variable slab thickness and reinforcement's ratios, and a constant maximum aggregate size of 16 mm. The compressive strength ranged between 27.6 MPa and 34.7 MPa. Only one slab reached a higher strength of 40 MPa. The authors considered the small variation as insignificant and neglected its influence on the punching shear strength. All slabs failed under punching shear. The influence of using different coarse aggregate size was pronounced when two slabs having the same slab thickness and reinforcement ratio were compared. The slab with coarse aggregate size equal to 16 mm was found to exhibit a greater deformation than the slab with a smaller

aggregate size of 4 mm. The size effect was also confirmed by the author when the slabs of higher slab thickness resulted in higher punching shear capacity.

The test results were compared to the predictions of ACI 318-11. The American Code was found to be conservative in predicting the punching shear capacity except for the doubled size slab, the capacity of that slab was over estimated by 30%. This finding was attributed to ignoring reinforcement ratio and the size effect in the code equation.

2.3.2 Theoretical Investigations

The only available model in the literature that accounts for the effect of coarse aggregate size on the slab behaviour and punching shear capacity of two-way slab is the Critical Shear Crack Theory (CSCT) that was first introduced by Muttoni and Schwartz (2008).

The basic assumption of this theory is that the roughness and the opening of the critical shear crack govern the shear strength of any cracked structural member. This theory introduced a good description of the punching shear behaviour of two-way slabs. For any two-way slab subjected to load, this load is resisted by the full concrete section until this load reaches a certain limit where the concrete section is cracked. At the cracked section, tensile stresses start to develop. The shear strength is believed to be influenced by the coarse aggregate size and roughness. This contribution of the existing coarse aggregate is demonstrated in Figure 2.2.

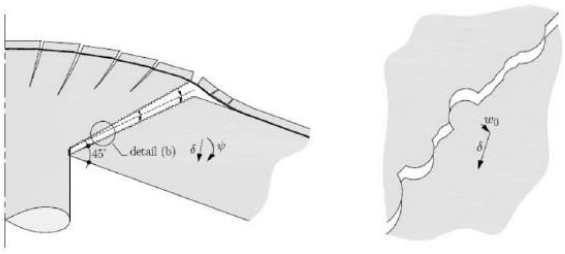

Figure 0.2: Aggregate Interlocking, Fib technical report bulletin 57, (2010)

The friction and strength that are present in the two-way slabs are due to the aggregate interlock. This strength is believed to decrease with increasing the crack angle and the shear crack opening. Based on this provision, a simplified failure criterion was presented by Muttoni and Ruiz (2009) as:

$$\frac{V_R}{bd} = \sqrt{f_c}\, f\,(w, d_g) \tag{0.4}$$

Where V_R represents the shear strength of the concrete member with effective shear depth d, f_c is the compressive strength of the concrete, w is the critical shear crack width, and d_g is the maximum coarse aggregate size. The punching shear strength is a function of the critical shear crack opening and roughness. A revised assumption was then proposed by Muttoni (2008) which attributed the critical shear crack width w to the slab rotation ψ and the effective shear depth; that is w is proportional to ψd as demonstrated in Figure 2.3.

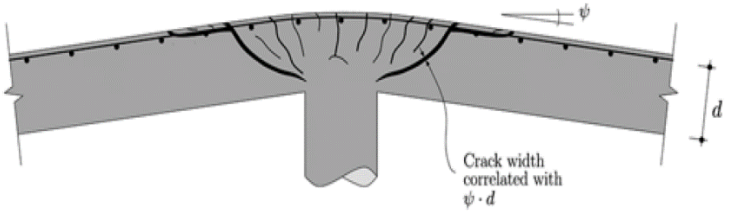

Figure 0.3: Correlation between Crack Width, Slab Depth, and the Slab Rotation, Muttoni (2008)

Based on this assumption the following simplified equation was presented to account for the amount of shear stress transferred at any critical shear crack. As given in Eq 2.5, the revised formula used the square root of the compressive strength of the concrete and included both slab depth and slab rotation.

$$\frac{V_R}{b_o d^3 \sqrt{f_c'}} = \frac{1}{1+(\frac{\psi d}{4\ mm})^2} \tag{0.5}$$

Muttoni (2003) added the effect of the coarse aggregate size in a new formulation given by Eq. 2.6. This modification was based on provision by Walraven (1981) and Vecchio and Collins (1986) where they proposed that the strength added by the roughness of the critical shear crack can be accounted for by dividing the nominal crack width by the coarse aggregate size (d_{go} + d_g). Where, d_{go} is the reference aggregate size taken as 16 mm (0.63 in), and d_g is the maximum coarse aggregate size used.

$$\frac{V_R}{b_o d\ \sqrt{f_c'}} = \frac{3/4}{1 + 15\frac{\psi d}{d_{g0} + d_g}} \tag{0.6}$$

In addition to the failure criterion presented, Muttoni et al. (2009) presented a quadrilinear numerical equation as given by Eq. 2.7. This formulation is to predict the behaviour of the two-way slabs at different load increments until the failure. It was based on assuming the portion of slab outside the critical shear crack is deflecting as a rigid body at a conical shape. This follows the assumption made by Kinnunen and Nylander (1960). It can be seen from the equation that the cracked and uncracked stiffness were accounted for, and explicitly the reinforcement ratio used in the slab reinforcing.

$$V_R = \frac{2\pi}{r_q - r_c}\begin{pmatrix} -m_r\ r_0 + m_R\ \langle r_y - r_0 \rangle + EI_1\ \psi\ \langle \ln(r_1) - \ln(r_y) \rangle + \\ EI_1\ \chi_{TS}\ \langle r_1 - r_y \rangle + m_{cr}\ \langle r_{cr} - r_1 \rangle + EI_0\ \psi\ \langle \ln(r_s) - \ln(r_{cr}) \rangle \end{pmatrix} \tag{0.7}$$

where

$$EI_1 = \rho.\beta.E_s.d^3.\left(1-\frac{c}{d}\right).\left(1-\frac{c}{3d}\right)$$

$$c = \rho.\beta.\frac{E_s}{E_c}.d.\left(\sqrt{1+\frac{2.E_c}{\rho.\beta.E_s}}-1\right)$$

The punching shear failure capacity is determined at the intersection point of both the failure criterion and load-rotation curve determined by Eq. 2.6 and 2.7 respectively. This is clarified in Figure 2.4 in which the load-rotation relation for different slabs with different reinforcement ratios is identified by solid lines, and the failure criterion for slabs with different thickness is defined by the dotted line.

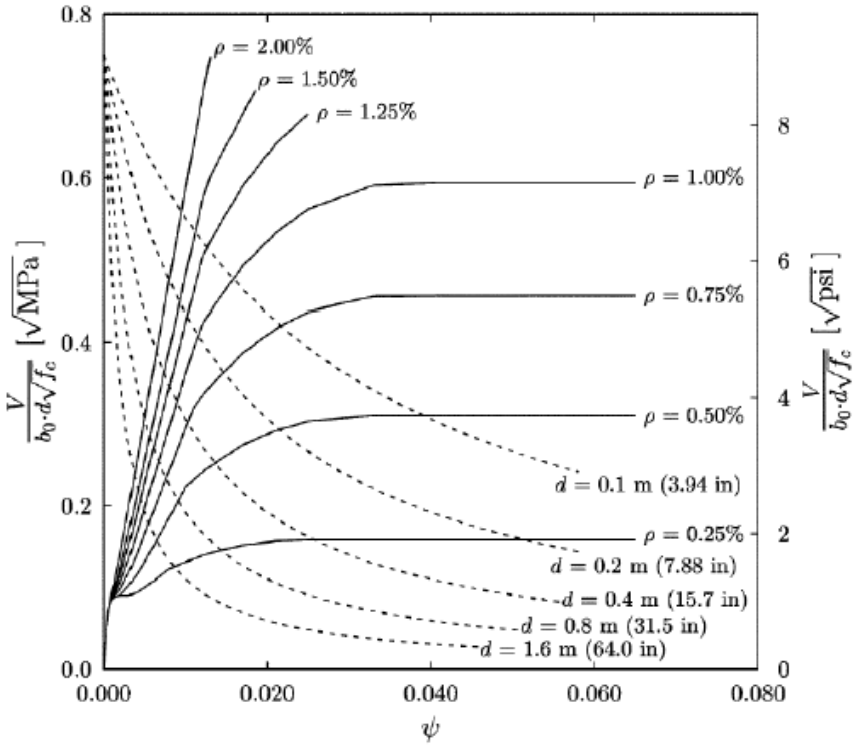

Figure 0.4: Load-Rotation vs. the Failure Criterion, Muttoni (2008)

The accuracy of the proposed formula was examined by comparing the load-rotation relation resulted by using this formulation with the actual relation resulted for

different for slabs with different reinforcement ratios tested by Kinnunen and Nylander (1960). This comparison showed an acceptable accuracy for both the numerical quadrilinear and failure criterion to predict the failure behaviour and punching shear strength as shown in Figure 2.5.

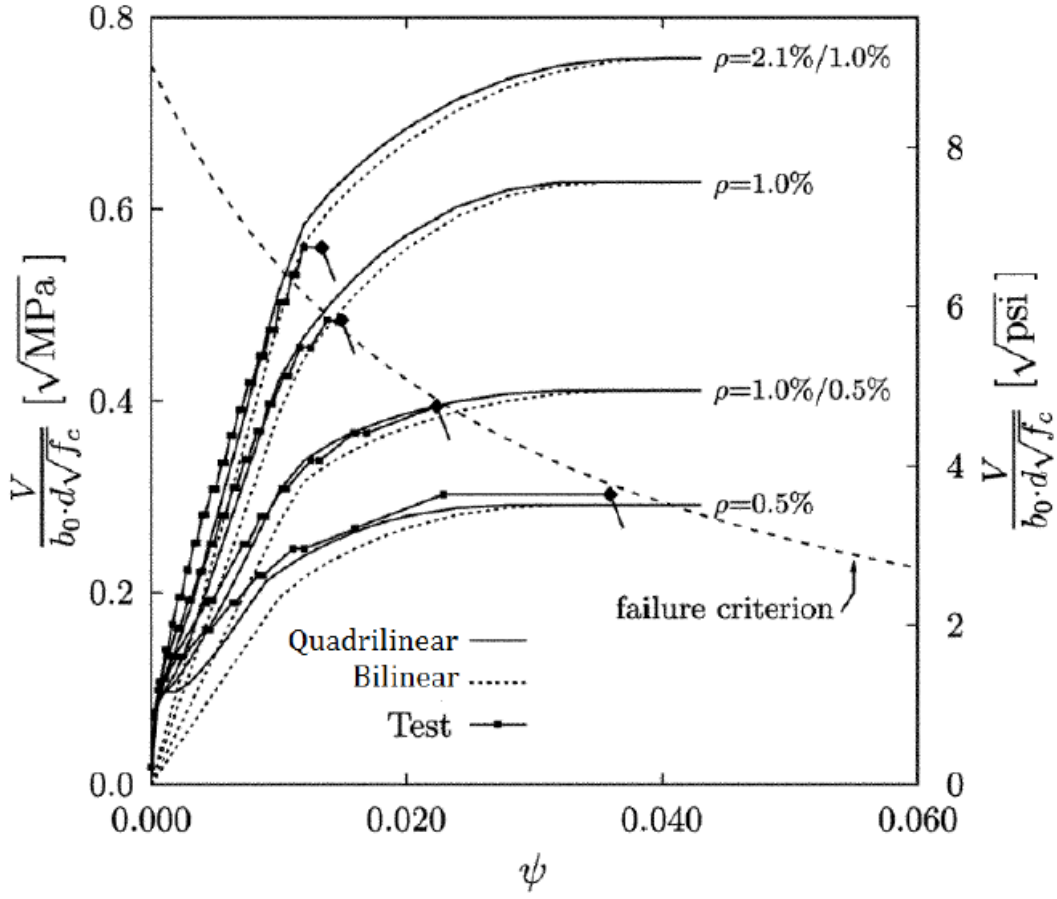

Figure 0. Comparison of Load-Rotation Curves for Tests and for the Proposed Numerical Formulation, Muttoni (2008)

Figure 2.6 shows the results for slabs tested by Guandalini et al. (2009). As shown from the figure, the two slabs PG-2b and PG-4 are confirming the accuracy of the failure criterion expressed in Eq. 2.6 which was proposed to account for the effect of the maximum coarse aggregate size used where both slabs have the same slab thickness and reinforcement ratio. Slab PG-2b with aggregate size equal to 16 mm

was found to exhibit a greater deformation than slab PG-4 with smaller aggregate size of 4 mm.

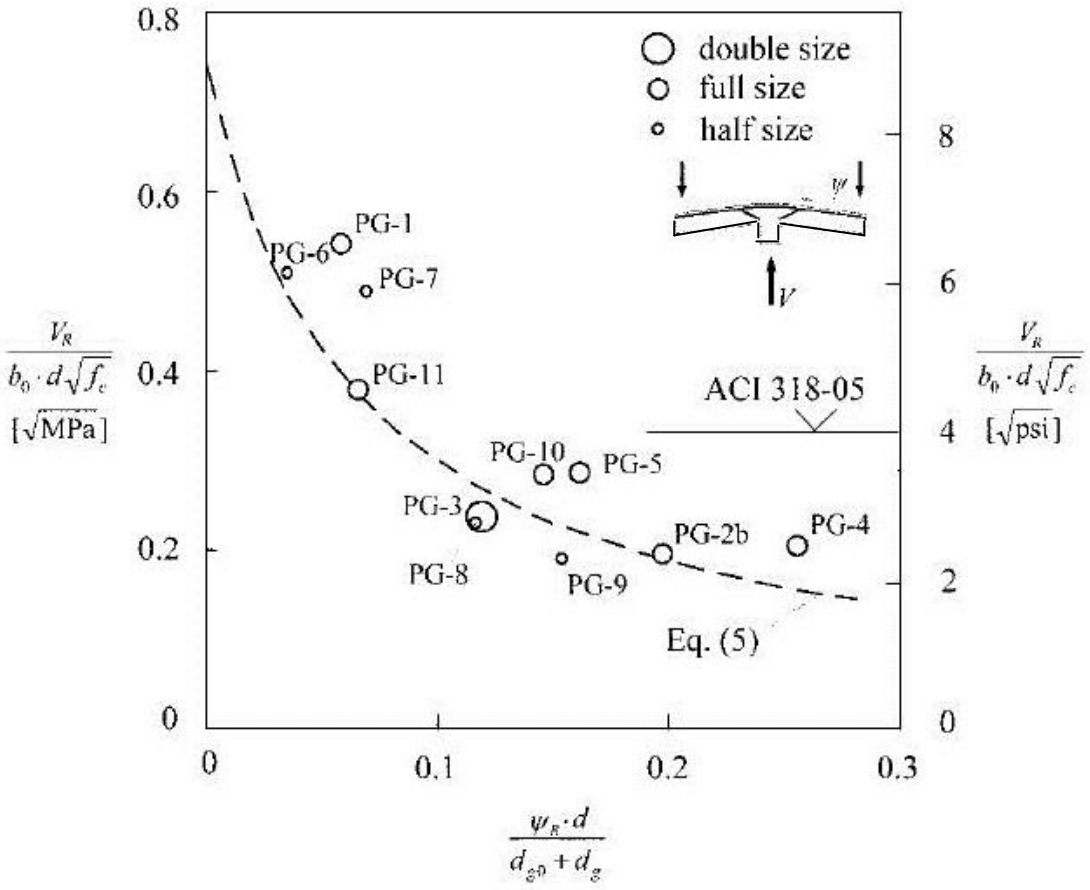

Figure 0.5: Test Results Compared with Failure Criterion, Guandalini et al. (2009)

2.4 Codes Provision for Punching Shear Strength of Two-Way Slabs

This section presents the code design equations for the punching-shear strength as specified by four widely used different codes. The codes are the Canadian Code CSA A23.3-04, the American Code ACI318-11, the British Code BS8110-97, and the European Code EC2 (2010).

2.4.1 Canadian Code [CSA 23.3-04] Provision

The Canadian code provision CSA A23.3-04 for checking the punching shear strength of two-way slabs is based on Eq. 2.8, where v_f is the shear stresses due to factored loads and v_r is the factored shear resistance;

$$v_f = \frac{V_f}{b_o.d} \leq v_r \tag{0.8}$$

The shear stresses are calculated at the critical shear perimeter located at distance *d*/2 from the column face and *d* is the average effective depth of the slab. The shear resistance depends on the concrete compressive strength, the effective depth, and the load location. The shear stress resistance v_c is determined as the smallest value of those obtained from Eq. 2.9 to 2.11.

$$v_c = \left(1 + \frac{2}{\beta_c}\right).0.19.\emptyset_c.\lambda.\sqrt{f_c'} \tag{0.9}$$

$$v_c = \left(\frac{\alpha_s d}{b_o} + 0.19\right).\emptyset_c.\lambda.\sqrt{f_c'} \tag{0.10}$$

$$v_c = 0.38.\emptyset_c.\lambda.\sqrt{f_c'} \tag{0.11}$$

where β_c is the ratio of long side to short side of the column, λ is the concrete density factor; λ = 1 for normal density concrete; and λ = 0.85 for semi-low-density concrete; and λ = 0.75 for low-density concrete, ϕ_c is the resistance factor for concrete, f_c' is the specified compressive strength of concrete, α_s is adjusting factor (α_s = 4 for interior columns, 3 for edge columns, and 2 for corner columns), and b_o is perimeter of the critical section.

2.4.2 The American Code [ACI 318-11] Provision

The American code provision for punching shear of the two-way slabs is based on Eq. 2.12, where v_u *is* the shear stress due to factored loads and v_c is the ultimate punching shear strength of concrete;

$$v_u = \frac{V_u}{b_o d} \leq \phi . v_c \tag{0.12}$$

Similar to the Canadian Code CSA A23.3-04 the American Code assumes the critical punching shear perimeter is located at *d*/2 from the column face, and the shear stress resistance; v_c shall be the smallest of the Eq. 2.13 to 2.15.

$$v_c = 0.083 \left(\frac{\alpha_s d}{b_o} + 0.2 \right) . \lambda . \sqrt{f_c'} \tag{0.13}$$

$$v_c = \left(1 + \frac{2}{\beta} \right) . \lambda . \sqrt{f_c'} \tag{0.14}$$

$$v_c = 0.33 . \lambda . \sqrt{f_c'} \tag{0.15}$$

where β is the ratio of long side to short side of the column, λ = 1 for normal weight concrete and λ = 0.85 for semi lightweight concrete, ϕ_c is the resistance factor for concrete, f_c' is the concrete cylinder compressive strength, α_s = 40 for interior columns; 30 for edge columns; and 20 for corner columns, and b_o is the perimeter of the critical section.

2.4.3 The British Code [BS 8110-97] Provision

The British code provision is based on Eq. 2.16, where the shear stresses are calculated at the critical shear perimeter located at distance 1.50*d* from the column face. The shear resistance according to the British Standard is calculated taking into account the concrete strength, the flexural reinforcement ratio, the effective slab depth and the size effect:

$$V_{BS} = 0.79.\left(100\rho\frac{f_c'/0.78}{25}\right)^{1/3}(400/d)^{1/4}u.d \quad (0.16)$$

where $V_{B.S}$ is the shear load capacity of the two-way slabs, ρ is the reinforcement ratio factor, f_c' is the concrete cylinder compressive strength, d is the effective depth of the slab, and u is the perimeter of the critical section at 1.5d from the column face. The BS 8110-97 code was superseded by Eurocode (EC2) in 2010.

2.4.4 The European Code [EC2] Provision

In the European code (EC2, 2010) the punching shear capacity of two-way slabs without shear reinforcement $V_{Rd,c}$ is taken as the least value of Eq. 2.17 and 2.18 expressed below. The critical shear perimeter in this code is located at distance 2.0d from the column face.

$$V_{Rd,c} = 0.18.k\left(100\rho_1 f_{ck}\right)^{1/3}u_1 d \quad (0.17)$$

But not less than;

$$V_{Rd,c} = 0.035.k^{3/2}f_{ck}^{1/2}.u_1 d \quad (0.18)$$

$$k = 1 + \sqrt{200/d} \leq 2.0$$

Where d is the effective depth, k is the size effect coefficient, ρ_1 is the reinforcement ratio, f_{ck} is the characteristics compressive strength of the concrete mixture, and u_1 is the punching perimeter located at distance 2.0d from the column face.

2.5 Research Summary

The literature review presented in this chapter showed the structural performance of self-consolidating concrete was only tested in concrete beams. It should be noted that no research has been conducted on two-way SCC slabs in terms of both experimental results and rational investigations. In this thesis, an experimental program is designed and conducted to investigate the effect of three different parameters (slab thickness, maximum coarse aggregate size and the C/F aggregate ratio) on the behaviour of two-way SCC reinforced slabs. The investigation would be an initiative to understand the punching behaviour SCC slabs and the experimental results will provide

needed data for SCC slabs. Based on the experimental study, a comparison between the currently used different codes provisions will be conducted. Finally, the experimental data will be compared as well with the CSCT proposed by Muttoni (2008). The CSCT includes the effect of slab thickness and aggregate size to predict for the behaviour and capacity of two-way slabs but has never been applied to SCC slabs.

Chapter 3

Experimental Program

3.1 Introduction

A detailed description of the experiment is presented in this chapter. This description includes; the materials used in preparing the slabs, details of the test slabs, and the instrumentations used to obtain the different measurements. In the first part, the concrete mixtures proportions, mixing procedure, and the results of the fresh and hardened concrete properties are discussed followed by the properties of reinforcement used. In the second part, typical details of the test slabs and the preparation of the specimen are presented. Then, in the last section, the testing frame is described and all the transducers used for measuring deflections, strains, and cracking are listed; describing their installation procedure, functions, and arrangement. The test procedure and the collection of the data are mentioned at the end of the chapter.

3.2 Self-Consolidating Concrete (SCC) Mixtures

3.2.1 Concrete Mixtures

Four different concrete mixtures were used in the current experimental work. The mixtures were designed to achieve a compressive strength of 30 MPa after 28 days. The mixtures proportions are listed in Table 3.1. Variable C/F aggregate ratio and coarse aggregate size were used. The concrete mixtures used in casting the slabs were supplied from a local batch plant. The chemical admixtures were added to the

concrete mixture after it arrived at the structures lab. The amount of HRWR was varied for each concrete mixture to maintain a slump flow diameter of 650 ± 50 mm.

Table 0.1: Mixtures Proportions

Materials	Group A	Group B	Group C	Group D
Binder Amount (kg/m^3)	500	500	500	500
Cement (kg/m^3)	200	200	200	200
FA (kg/m^3)	300	300	300	300
C/F Ratio	0.70	1.20	0.70	1.20
CA Size (mm)	10	10	20	20
CA (kg/m^3)	653	865	653	865
FA (kg/m^3)	933	721	933	721
Water (L/m^3)	200	200	200	200
HRWR (L/m^3)	0.93	0.78	1.30	1.10

A high strength concrete mixture was used for the slabs' columns. It was designed to achieve a compressive strength of 60 MPa at the day of testing the slab, to avoid any premature failure of the column during testing. The column mixture was produced in the concrete laboratory at MUN using a 120 liter capacity mixer and the mixing proportions are listed in Table 3.2.

Table 0.2: Columns Concrete Mixtures Proportions

Materials	Proportions
Binder Amount (kg/m^3)	500
Cement (kg/m^3)	450
Silica Fume (kg/m^3)	50
C/F Ratio	1.00
CA Size (mm)	10
CA (kg/m^3)	658
FA (kg/m^3)	658
Water (L/m^3)	175
HRWR Glenium 7700 (L/m^3)	6.5

Type GU Portland cement with a specific gravity of 3.15 was used for all slabs and columns. Class F fly ash similar to ASTM Type I with a specific gravity of 2.26 was used as a supplementary cementing material. The chemical properties of the cement and fly ash are shown in Table 3.3 as provided by the manufacturer.

Table 0.3: Chemical Properties of Cement and Other SCM's

Chemical Properties %	Cement	Fly Ash
SiO2	19.6	52
Al2O3	5.5	23
Fe2O3	2.4	11
FeO	-	-
TiO2	-	-
C	-	-
P2O5	-	-
SO4	-	-
CaO	62.4	5
MgO	2.5	-
Cr2O3	-	-
MnO	-	-
SrO	-	-
BaO	-	-
Na2O	-	-
C3S	52.3	-
C2S	16.8	-
C3A	10.5	-
C4AF	7.2	-
K2O	-	-
L.O.I.	2.1	-

A high-range water-reducing admixture (commercial name is Glenium 7700) was used to achieve the required slump flow diameter of SCC mixtures. Natural sand with a specific gravity of 2.70 and water absorption of 1% was used for all mixtures. The used coarse aggregate was crushed granite with maximum size of 10 and 20 mm and with a specific gravity of 2.70 and water absorption of 1%.

3.2.2 Fresh Properties

For each of the four designed mixture the standard fresh properties tests were carried out to ensure that all mixture satisfies the SCC requirements. The mixtures proportions are listed in Table 3.1, where a coarse aggregate size of 10 mm was used in Mixtures A and B, while 20 mm aggregate size was used in Mixtures C and D. Mixtures A and C contained a C/F of 0.70 while Mixtures B and D contained 1.2 C/F. The standard fresh properties tests were performed following the same order of the data listed in Table 3.4.

Table 0.4: Fresh properties tests of SCC Mixtures

Test Method	Measured Property	Unit	Criteria
Slump Flow		mm	≥ 520 mm, ≤ 900
T_{50cm} Slump Flow	Flowability	sec	2s – 5s
V-Funnel		sec	≤ 27s
L-Box	Passing Ability	(H_2/H_1)	≥ 0.75

3.2.2.1 Slump Flow Diameter & T_{50cm} Tests

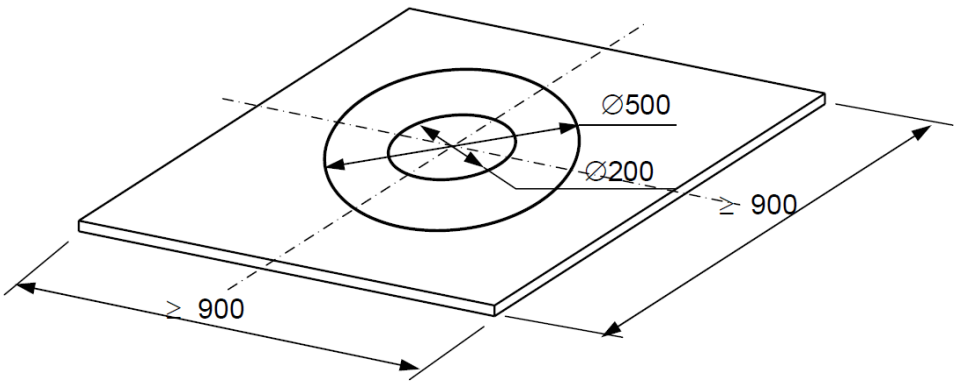

Figure 0.1: Slump Flow Testing Plate (EFNARC - 2005)

Testing the fresh properties of the concrete mixtures started with measuring the slump flow diameter by filling the slump cone with concrete and holding it for 2 second, and then the cone was lifted upward smoothly in time interval of 3 – 5 seconds. Once the

cone is lifted up, the concrete started to flow under its own weight over the 900 mm square metal plate shown in Figure 3.1. This test was performed according to ASTM C1611 specification. To measure the T_{50cm}, a stopwatch was used to record the time from the start of moving the cone upward until the concrete reaches a 500 mm diameter. The slump diameter was measured in two perpendicular diameters after the concrete stopped flowing. The recorded readings of both tests for all mixtures are listed in Table 3.5.

The T_{50cm} and the slump flow diameter both give a good indication for the mixture flowability. The flowability is defined as the ability of the concrete to flow in the form work under its own weight. The higher the slump diameter indicates a higher flowability, For the T_{50cm} a shorter time to reach the 50 cm diameter indicates more flowability. The acceptable ranges for both tests are indicated in Table 3.4.

3.2.2.2 V-Funnel Test

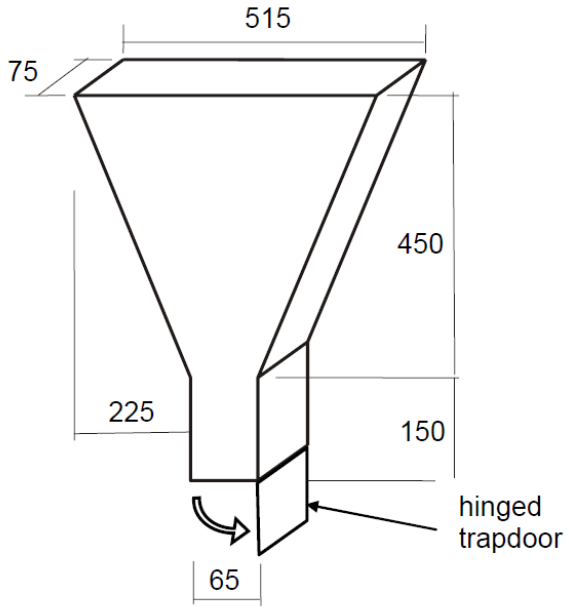

Figure 0.2: V-Funnel Test (EFNARC - 2005)

After finishing the slump flow test, the V-Funnel test was then performed. This test was performed according the European Guidelines (EDNARC - 2005). The V-shaped funnel, see Figure 3.2, was filled with 12 liter of the concrete mixture. Then a stopwatch was used to record the time the concrete takes to flow through the apparatus. The purpose of this test is to determine the flowability; also it gives an indication for the mixture segregation and viscosity. Shorter flow time indicates a higher flowability, but it should be within the acceptable range indicated in Table 3.4 as specified by (EDNARC - 2005)

3.2.2.3 L-Box Test

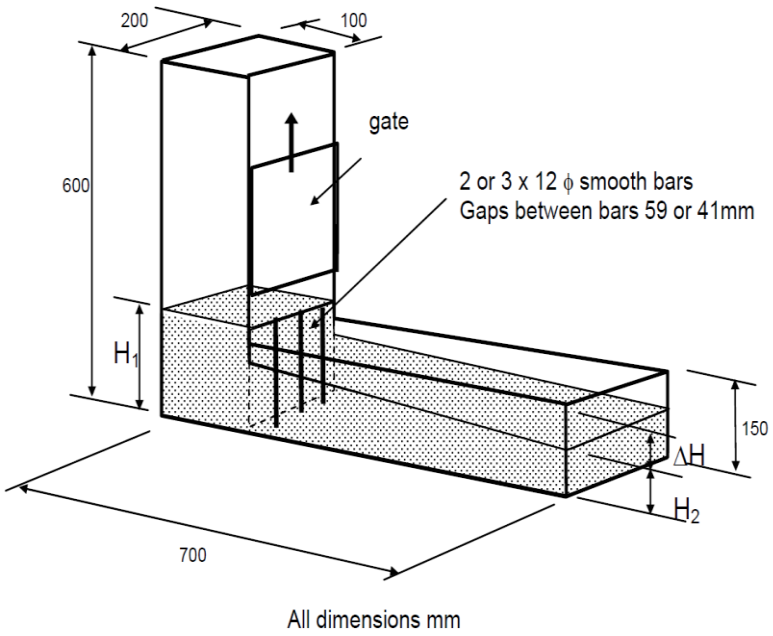

Figure 0.3: L-Box Test (EFNARC - 2005)

The L-Box test is the third test to assess the passing ability of SCC through reinforcement bars, see Figure 3.3. The vertical part was filled with concrete after levelling of the L-Box horizontally. The gate was kept closed for 60 ± 10 seconds after filling the concrete. After opening the gate, the concrete was left to flow under its own weight, and the heights H_1 and H_2 were measured to determine the passing

ability factor by dividing H_2/H_1. The readings are listed in Table 3.5 for all tested mixtures and compared with the accepted ranges specified by (EFNARC - 2005).

3.2.2.4 Fresh Properties Testing Results

In this section, all the fresh properties results for the four mixtures are presented and discussed. The required amount of concrete was delivered from local batch plant in a concrete truck. The designed amount of HRWR to maintain the 650 ± 50 mm slump flow diameter was added upon the arrival of the concrete truck at Memorial University structural lab. The slump flow diameter was then checked before pouring the concrete into the forms to confirm achieving the targeted slump flow diameter.

Testing the fresh properties of the SCC mixtures was carried out during the casting process and after confirming the targeted slump flow diameter. All the recorded readings are listed in Table 3.5. The T_{50cm} is found to increase with increasing the C/F aggregate ratio from 0.70 to 1.20. A similar increasing trend of the T_{50cm} with increasing the coarse aggregate size from 10 to 20 mm was observed by comparing mixtures B and D. This finding is in good agreement with Khaleel et al. (2011). An opposite finding was observed when the T_{50cm} for mixture A is compared with that of mixture C. However, this can be attributed to the large increase in the slump flow diameter from 600 mm to 780 due to uncontrolled conditions.

During the casting process, the initial V-Funnel time T_f was measured. The resulted T_f for all mixtures is within the acceptable ranges indicated in Table 3.4. It can be seen from the data listed in Table 3.5 that the T_f for mixture B is shorter than the T_f for mixture D; where they were cast using the same C/F ratio and coarse aggregate size of 10 mm and 20 mm, respectively. Thus it can be concluded that increasing the coarse

aggregate size results in increasing the T_f. It should be noted that the resulted values agree with a similar study carried out by Krishna et al. (2010) where four mixtures of different coarse aggregate sizes were used. On the other hand, No significant effect was observed for changing the C/F aggregate ratio in the current study. A scatter in the results of the $T_{f,}$ was observed. It is not possible to provide a conclusive explanation to this scatter due to the limited number of mixtures in the current study.

Both the T_{50cm} of the slump flow test and the T_f of the V-Funnel test are good indicators for the concrete flowability and viscosity, as mentioned previously. Mixtures with a longer times measured indicate a higher viscosity and low flowability. Figure 3.4 clearly shows that increasing the coarse aggregate size has more influence in increasing the T_{50cm} compared to the effect of the C/F ratio.

Table 0.5: Slump Flow, V-Funnel, and L-Box

Mixtures	Slump Flow		V-Funnel	L-Box	HRWR
	Dia. (mm)	T_{50cm} (sec)	T_f (sec)	H2/H1	L/m^3
Mix. A	600	1:20	5:30	0.76	0.93
Mix. B	650	1:25	2:40	0.55	0.78
Mix. C	780	1:15	2:54	0.75	1.30
Mix. D	630	3:00	9:00	0.73	1.10

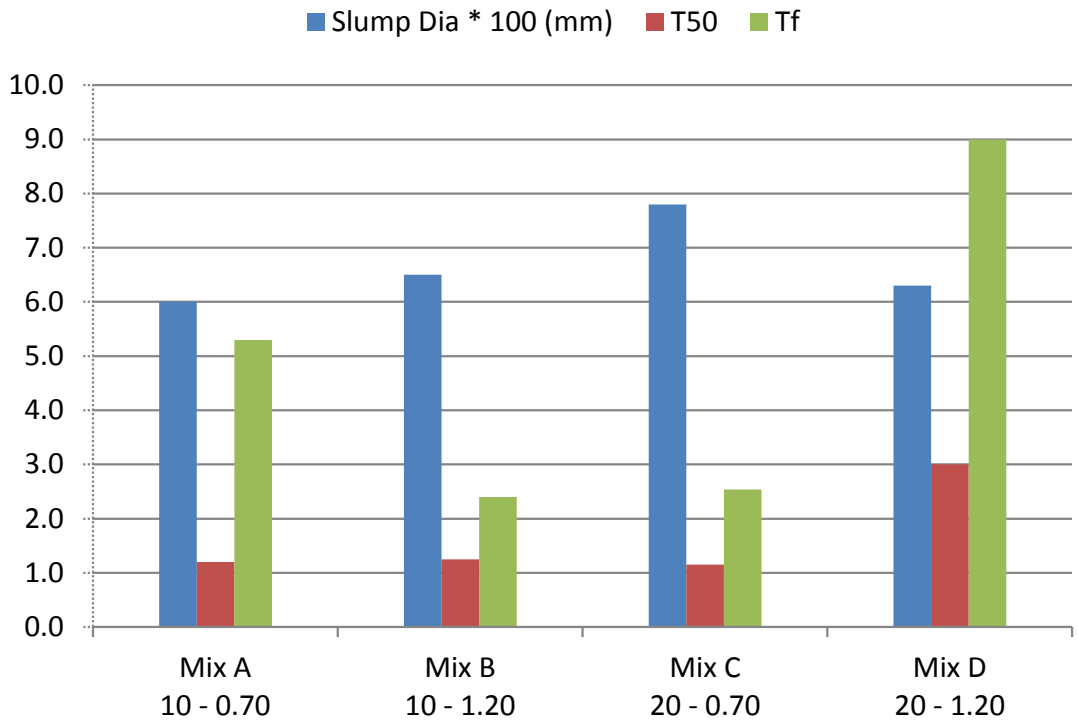

Figure 0.4: Slump Diameter, T_{50cm}, and T_f for Concrete Mixtures

(Note: The slump diameter values mentioned in Figure 3.4 has to be divided by 100 to give the actual test readings)

Although all mixtures had an acceptable value for the T_{50cm}, the passing ability of mixtures B and D did not meet the acceptable range of values as indicated by EFNARC - 2005 and listed in Table 3.4. From the L-Box test results given in Table 3.5 and shown in Figure 3.5 a slight decrease was found in the blocking ratio with increasing the coarse aggregate size from 10 mm in mixtures A and B to 20 mm in mixtures C and D. Khaleel et al. (2011) found a similar trend when the coarse aggregate was increased from 10 mm to 20 mm in their study. The slight change in the L-Box blocking ratio when comparing mixture A with C can be attributed to the larger slump flow diameter of mixture C. If both mixtures have a similar slump flow diameter; a larger difference could be seen. In a similar study carried out by Krishna

et al. (2010) a gradual decrease in the L-Box ratio was observed with increasing the aggregate size from 10 mm to 20 mm.

Figure 3.6 shows a significant decrease in the passing ability with increasing the C/F ratio from 0.70 to 1.20. Such decreasing values are expected since increasing the C/F ratio causes a higher possibility for the coarse aggregate to accumulate at the reinforced bars behind the L-Box gate causing blockage for the concrete to flow. It should be noted that segregation is more likely to occur when either a larger coarse aggregate or C/F ration are used.

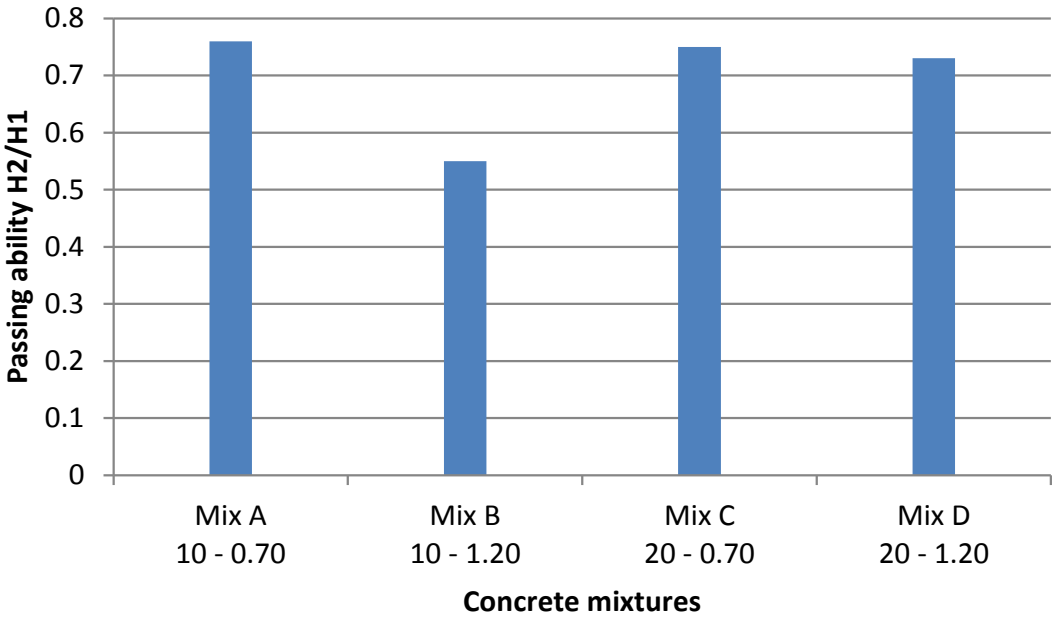

Figure 0.5: Effect of C/F and Coarse Aggregate Size on the Passing Ability

Finally, the influence of changing the coarse aggregate size and the C/F aggregate ratio on the demand for HRWR to achieve the desired slump flow diameter of 650 ± 50 mm was examined. Figure 3.6 shows that, for mixtures having the same coarse aggregate size, when the C/F ratio was increased from 0.70 to 1.20, the required

amount of the HRWR decreased by 16.1% and 15.4% for mixtures of 10 mm and 20 mm coarse aggregate size, respectively.

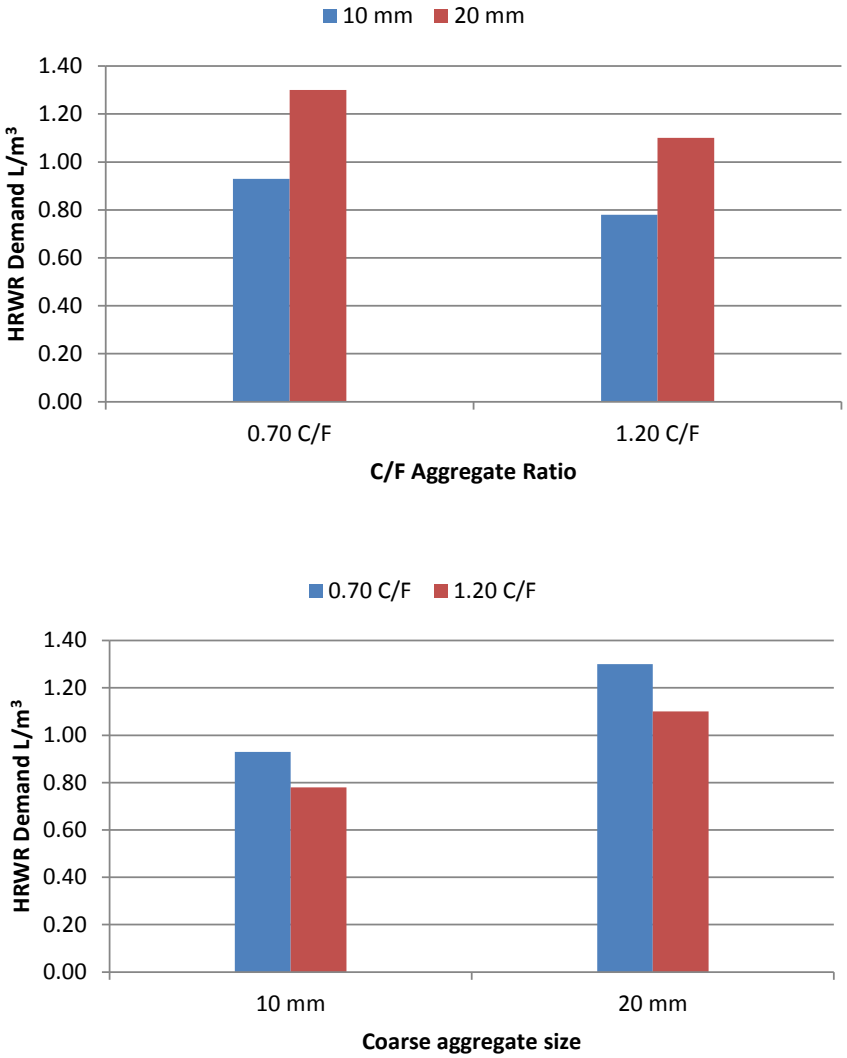

Figure 0.6 : Effect of C/F and Coarse Aggregate Size on the HRWR Demand

The influence of changing the coarse aggregate size on the required amount of the HRWR for mixtures having the same C/F ratio is illustrated by the data shown in Figure 3.6 and the results listed in Table 3.5. The results show that the demand for the HRWR increased with increasing the coarse aggregate size. The amount required increased for the mixtures with the 20 mm coarse aggregate size by 29% compared to that required for the mixtures using the 10 mm coarse aggregate size for the C/F ratios used.

3.2.3 Mechanical Properties

In this section, the mechanical properties of the hardened concrete are presented. All tests were performed according the procedure specified by ASTM standards. The compressive strength, and the modulus of rupture were tested and the results are listed in Table 3.6.

3.2.3.1 Compressive Strength and Modulus of Elasticity

The concrete compressive strength for each slab was obtained in accordance with ASTM C39-04. For each slabs three (100 mm x 200 mm) cylinders were cast for the compressive strength test. The cylinders were kept at the same location the slabs were stored after casting. The cylinders were tested at the same day of testing the slab. The compression testing machine is shown in Figure 3.7. The load was applied at a rate of 0.25 MPa/second. All cylinders were capped with a high strength sulphur compounds. The compressive strengths of the cylinders are listed in Table 3.6. Each result represents the average of the compressive strengths of three cylinders.

Figure 0.7: The Concrete Compression Testing Machine

3.2.3.2 Flexure Tensile Strength

The modulus of rupture for each mixture is measured according to ASTM C78. Four prisms of dimensions 100 x 100 x 400 mm were cast for each mixture at the same day of casting the slabs. The prisms were kept at the same location of the slabs and were cured under the same conditions. The prisms were tested on the day of testing the slab for each concrete mixture. The tests were carried out using four point bending test. An MTS actuator was used to apply load at stress rate of 0.015 MPa/second. Figure 3.8 shows a picture taken during testing one sample in the MTS test frame.

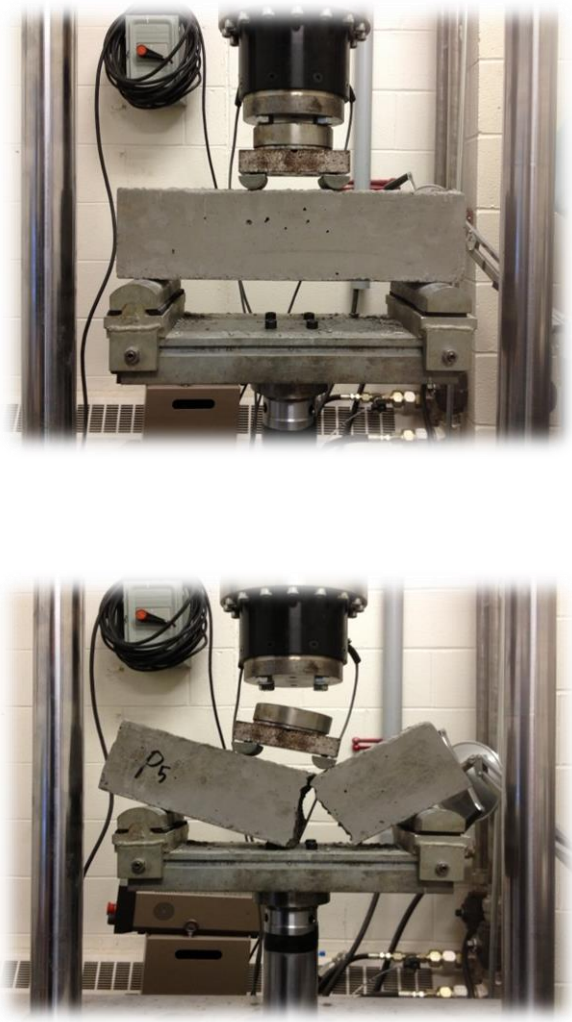

Figure 0.8: Flexure Strength Test [Before and After Test]

The average of all prisms is listed in Table 3.6 for each mixture. The values of the modulus of rupture of the specimen were found to be in reasonable agreement with those calculated using the CSA A23.3 - 04 Code equation

$$f_r = 0.6 \,.\, \lambda \,.\, \sqrt{f_c'} \quad \text{(MPa)}$$

Table 0.6: Mechanical Properties of the Tested Slabs:

Mixture	Size (mm)	C/F	Compressive Strength (MPa)			Measured f_r (MPa)	Calc. f_r (MPa)	$\frac{f_r}{\sqrt{f_c'}}$
			150 mm	200 mm	250 mm			
Mix. A	10	0.70	24.5	26.0	27.0	--	--	--
Mix. B	10	1.20	29.0	30.0	32.0	3.64	3.30	0.66
Mix. C	20	0.70	25.5	26.0	27.0	3.44	3.06	0.68
Mix. D	20	1.20	24.0	24.5	25.0	3.47	2.96	0.70

3.3 Mechanical Properties of the Reinforcement

Grade 400 reinforcement bars with two different diameters were used in the tests. A uniaxial tension tests were carried out on the 15M and 20M bars to determine the yield strength and the modulus of elasticity of the bars. Three samples were tested for each bar diameter and the average of the results was used. Each sample was 800 mm long. Two strain gauges were mounted at the middle of each bar, and on both sides of a bar to measure the strain development. The test samples were placed in a universal testing machine as shown in Figures 3.9 and 3.10. Special grips were used at the top and bottom ends. The free length of the bar between the grips of the machine was 400 mm. The test machine has a capacity of 1335-KN. The data recorded from the load cell and the strain gauges were collected by the data acquisition system used.

All the samples were tested until ruptures as shown in Figure 3.10. The average yield strength was found to be 443 and 432 MPa for 15M and 20M bars, respectively as listed in Table 3.7. The yield strain of the 15M bar was found to be 2200 με while for the 20M bar was 2100 με.

Figure 0.9: The Universal Testing Machine

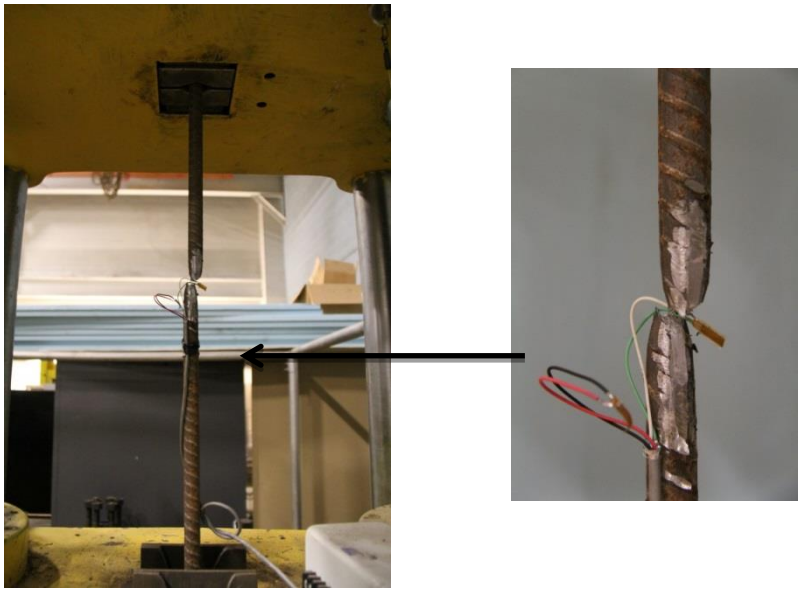

Figure 0.10: A Typical Bar in the Machine after Rupture

Table 0.7: Mechanical Properties of the 400 Grade Bars Tested

Bar Designation	Yielding Strength f_y (MPa)	Yield Strain με
15M	443	2200
20M	428	2100

3.4 Test Slabs

Details of a typical test specimen are shown in Figure 3.11. Dimensioning and reinforcement details for the different groups are listed in Table 3.8. All slabs had side dimensions of 1900 mm. The slabs were concentrically loaded through a 250 x 250 mm square column stub.

The main variables were the slab thickness, coarse aggregate size, and C/F aggregate ration. The twelve slabs were divided into four groups (Group A, B, C and D). Each group was cast using different concrete mixture. The slabs within each group had different thicknesses, 150, 200 and 250. The target reinforcement ratio was 1% and slightly varied for the slabs with different thicknesses to maintain the same spacing between reinforcement. The flexural reinforcement ratios were 1.01%, 1.08% and 0.91% for the slabs with thicknesses 150, 200 and 250 mm respectively.

The target compressive strength for all slabs was 30 MPa. The only sizes of coarse aggregate used were of 10 and 20 mm. The 10 mm coarse aggregate size was used for groups A and B, and C/F aggregate ratios of 0.70 and 1.20 were used for groups A and B, respectively. Similarly, group C and D were mixed using 20 mm coarse aggregate size, and C/F ratios of 0.70 and 1.20 respectively. All these data are detailed in Tables 3.8.

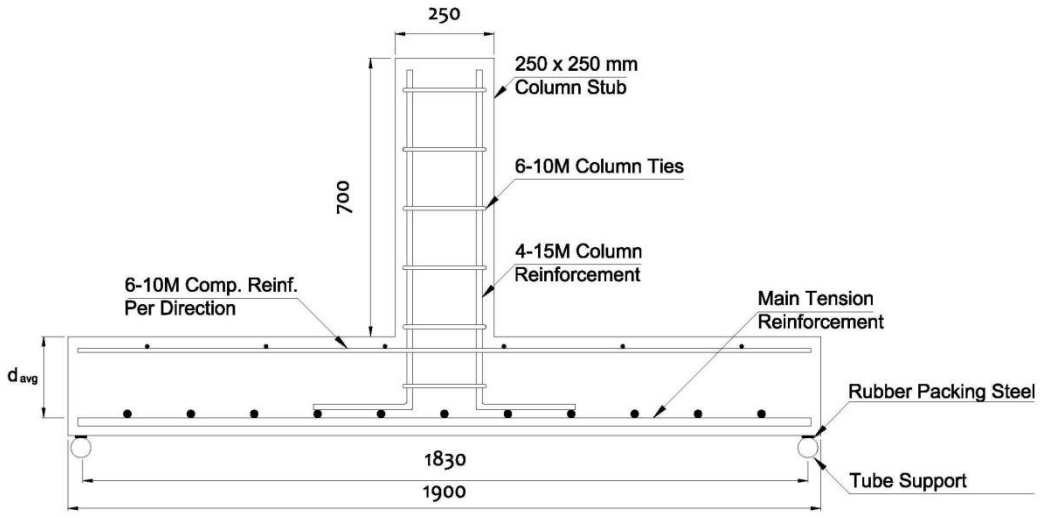

Figure 0.11: Typical Test Slab Specimen

Table 0.8: Details of Test Slabs

Group No.	Agg. Size (mm)	C/F Ratio (%)	Slab No.	Rein. Ratio ρ (%)	Slab Thick. (mm)	Bar Size (mm)	Bar Spacing (mm)	Cover (mm)	Average Depth (mm)
A	10	0.70	SCA150	1.01	150	15M	180	25	110
			SCA200	1.08	200	20M	180		155
			SCA250	0.91	250	20M	160		205
B	10	1.20	SCB150	1.01	150	15M	180	25	110
			SCB200	1.08	200	20M	180		155
			SCB250	0.91	250	20M	160		205
C	20	0.70	SCC150	1.01	150	15M	180	25	110
			SCC200	1.08	200	20M	180		155
			SCC250	0.91	250	20M	160		205
D	20	1.20	SCD150	1.01	150	15M	180	25	110
			SCD200	1.08	200	20M	180		155
			SCD250	0.91	250	20M	160		205

3.5 Form work

Each concrete mixture was used to cast three slabs. The slabs had the same dimensions (1900 mm × 1900 mm) but with three different depths; 150 mm, 200 mm and 250 mm. For casting the 150 mm slab thickness; a permanent steel form work at MUN's concrete lab was always used, see Figure 3.12. The steel platform is supported on W-Shape columns which are connected with I-beams. A square steel plate with 7 mm thickness and 2.0 m width in each direction is placed on the I-beams. Four removable steel sides with a height of 150 mm are installed as a formwork boundary.

Figure 3.13 shows the wooden formworks used for casting both slabs with 200 mm and 250 mm thickness. They are directly supported on the floor at the structural lab at MUN. They are constructed using a 18 mm thick square wooden sheet, stiffened from the bottom using 25 mm lumbers. Finally the four removable wooden sides are attached to the base and tied together in a way to confirm having a net inside area of 1900 mm × 1900 mm. Figure 3.14 shows the lab condition during the casting process

Figure 0.12: Steel Formwork for casting the 150 mm Thick Slabs

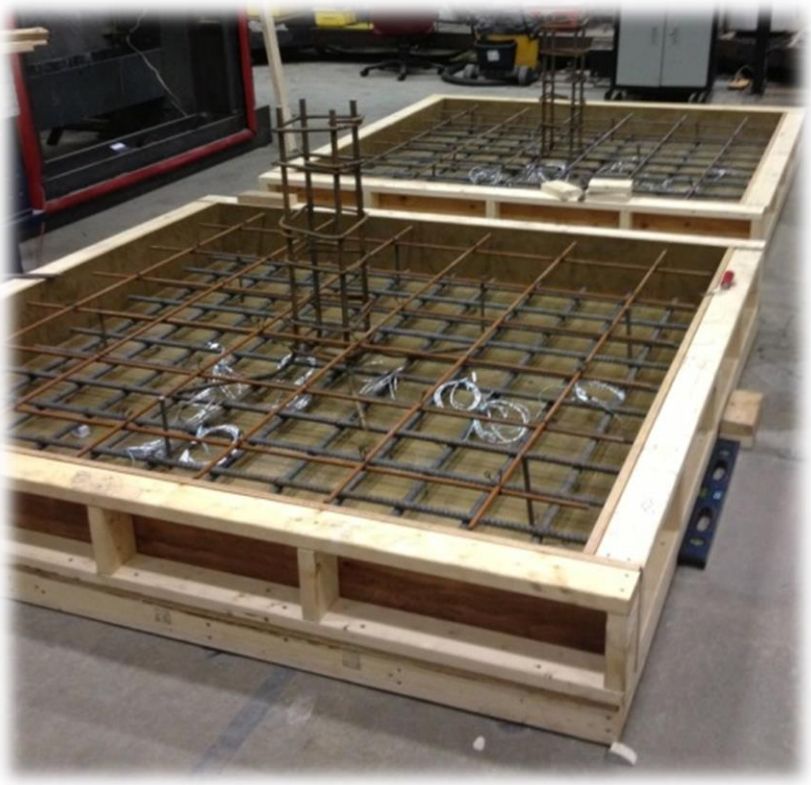

Figure 0.13: Wooden Formwork for Casting the 200 mm & 250 mm Thick Slabs

Figure 0.14: A Photograph during the Casting Process

3.6 Curing

The slabs were cured during the first seven days by spraying water over the exposed surface. The early curing is an effective method to reduce shrinkage cracks. Improper curing can result in shrinkage cracks that appear on the surface of the slabs.

3.7 Test Setup

A steel frame, located in the structural lab at Memorial University of Newfoundland was used for testing all slabs. This frame was built using W and channel steel sections as shown in Figures 3.15. The Frame was anchored to the 76.0 mm (30 in.) lab floor and was designed to be Self-reacting. The four edges of the test slab were supported on 32 mm diameter rods welded on the vertical steel W sections. A 3.0 mm layer of rubber was placed along the contact line between the rods and the slabs to minimize the resulted friction. All slabs were casted in a horizontal position and were placed for testing in a vertical position.

Figure 0.15: The Testing Frame

3.8 Instrumentation and Measurements

3.8.1 Loading System

A hydraulic actuator was fixed to the frame and used to apply the concentric load on the column stub. The hydraulic jack has a maximum capacity of 1783 kN. Thehe applied load and the displacement were measured internally by a pressure transducer and a linear voltage displacement transducer (LVDT), respectively.

3.8.2 Deflections

The deflections at different locations on the tension side were measured using four LVDTs arranged as shown in Figure 0.16. Two Additional LVDT's were placed on the compression side to measure the differential deflection within the punching perimeter. The data from the LVDTs were logged into the data acquisition system.

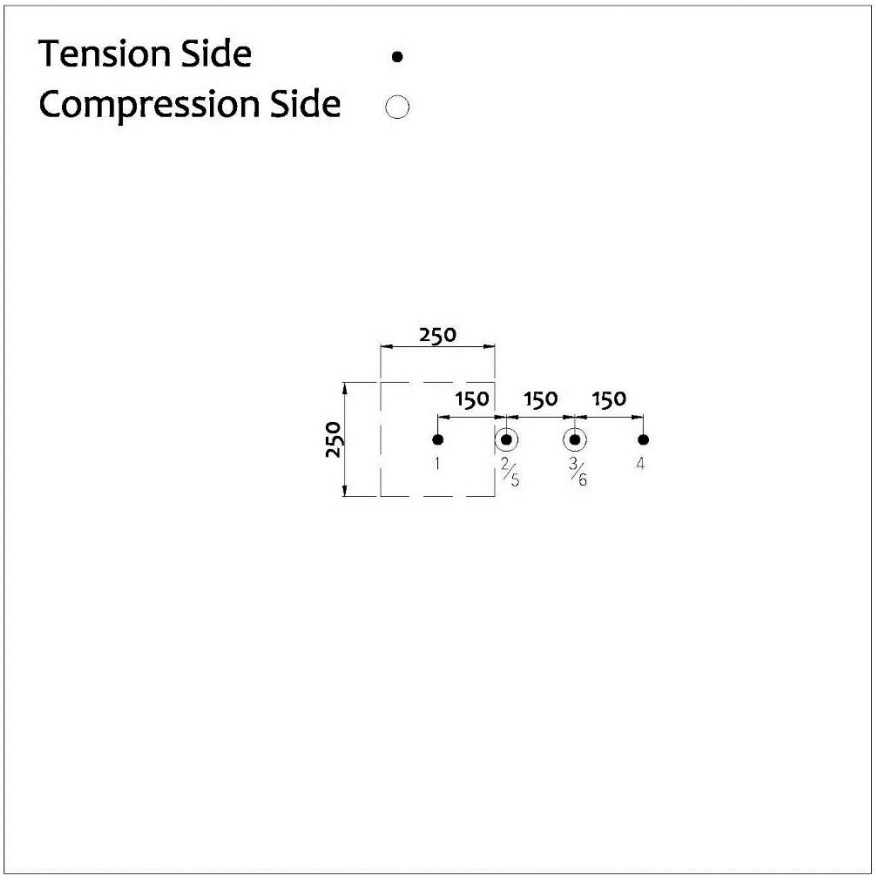

Figure 0.16: LVDTs Arrangements in a Typical Test – Plan View

3.8.3 Steel Strains

The stains in the reinforcement were measured at various locations. These locations were selected to detect the maximum strains in the reinforcement and the strain variation in both radial and tangential directions. Figure 3.17 shows the strain gauge arrangements used in all test slabs. Placing more than three gauges on the same bar was avoided by placing the gauges required over two separate bars, since the presence of strain gauge causes a loss of bond between the concrete and the reinforcement bar at that location. An electrical strain Gauge with gauge factor 2.075 ± 0.5% and resistance of 120 ± 0.30% Ω at 24℃ was placed on the steel surface after grinding the surface, see Figure 3.18 which shows a sample of a strain gauge installation. The normal use temperature range for the strain measurement is -75℃ to 175℃. The gauges were coated with a protective sealant and then covered with a rubber splicing tape to protect them against any possible water damage during concrete casting. Bondable terminals were used on both sets of leads to prevent forces transmitted along the main lead wire from damaging the strain gauges or degrading their performance.

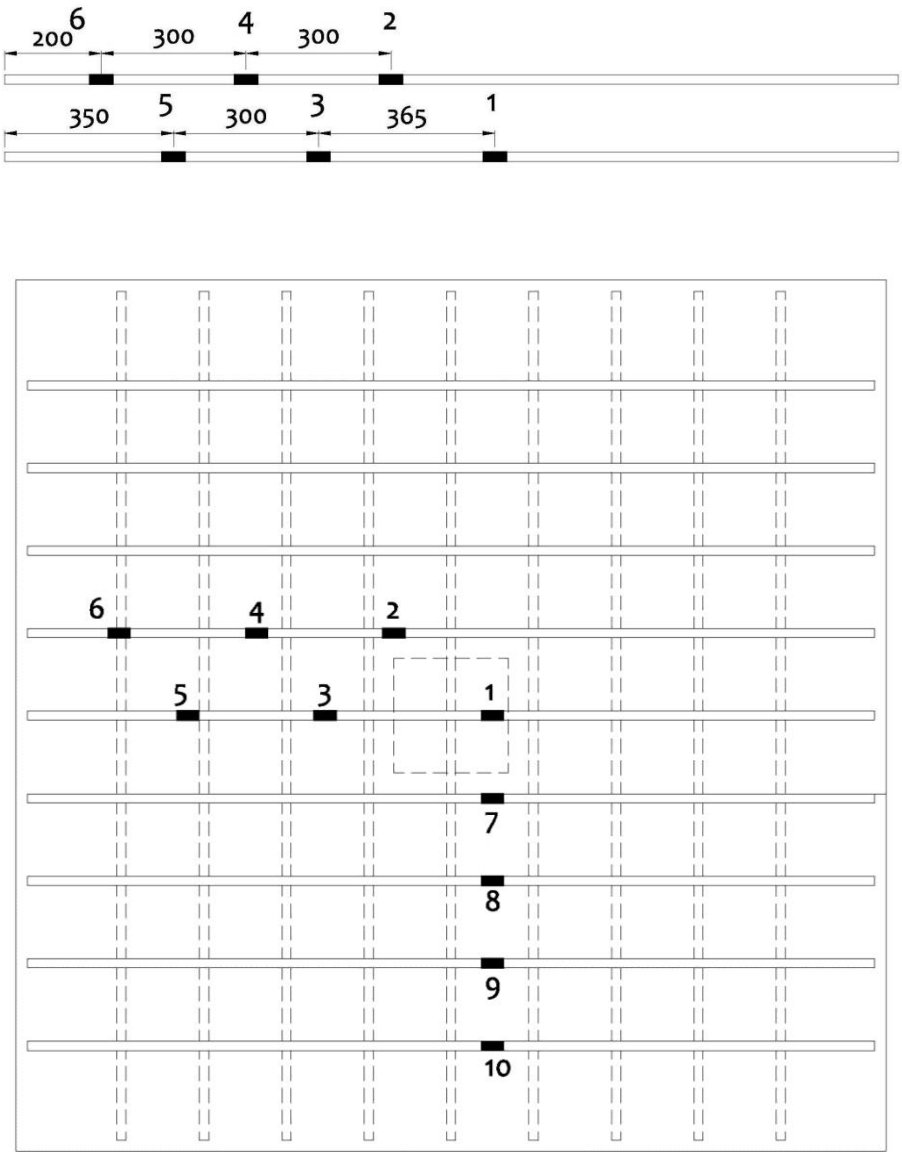

Figure 0.17: Typical Steel Strain Gauges Arrangements for Test Slabs

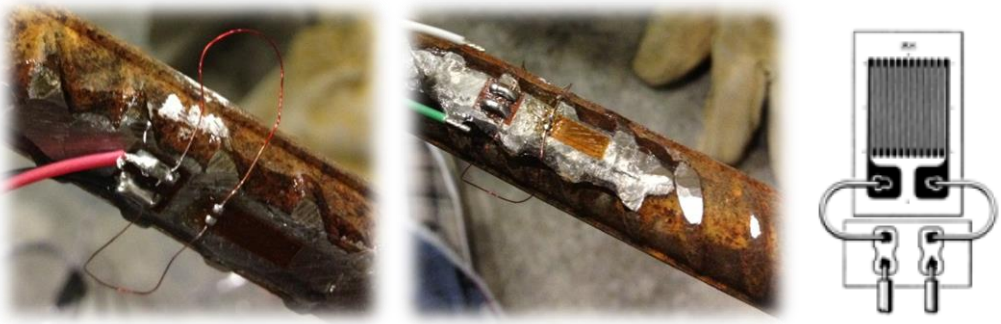

Figure 0.18: Strain Gauge Installation on the Steel Bars

3.8.4 Concrete Strains

Strain gauges were used to measure the concrete strains on the compression side at five different locations. The strain gauges were glued and arranged over the concrete surface as shown in Figure 3.19. The surface of the concrete at the specified locations was grinded and coated with a thin film of epoxy resin. Each strain gauge was wired and connected to the data acquisition system.

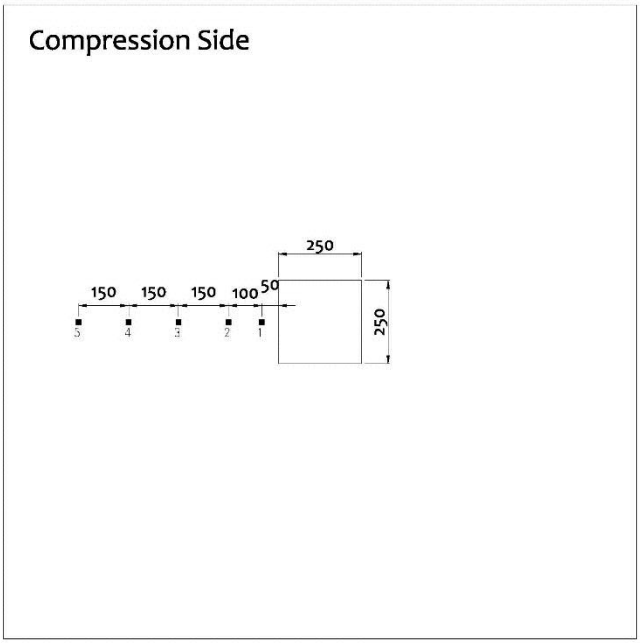

Figure 0.19: Typical Concrete Strain Gauges Arrangements for Tested Slabs

3.8.5 Crack Detection

Crack formation and propagation was carefully inspected for each slab. Formation of early first cracks was detected using naked eye and their widths were measured using a microscope. After detecting these cracks, three Crack Displacement Transducers (CDT) were mounted over the detected cracks to measure the crack opening during the test as shown in Figure 3.20. The (CDT) used are waterproof instruments and are able to measure the crack widths with capacity of ± 2.0 mm.

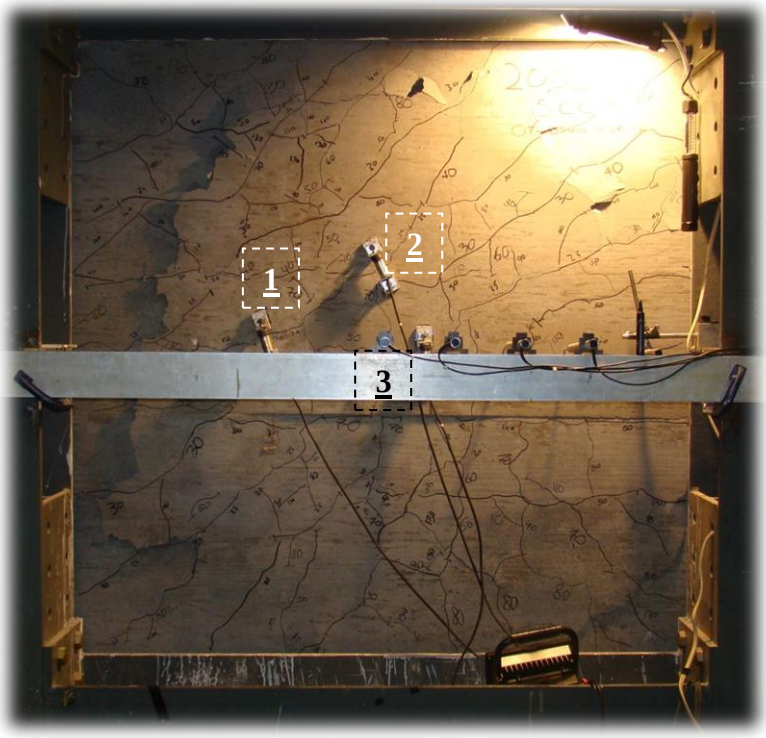

Figure 0.20: Crack Displacement Transducer (CDT) on the Concrete Surface

3.8.6 Data Acquisition System

The measurements from the pressure gauges, strain gauges, LVDTs and CDTs were logged to a high speed data acquisition system. All the data collected using LAB-View software. The data acquisition system was set to note of 3 seconds for data scanning and saving.

3.9 Test Procedure

The slabs were placed in a vertical position. Their position was adjusted to ensure that the column stub center is achieved with the loading actuator axis. They were also carefully inspected to ensure that the slab's four sides are supported on the steel rods attached to the testing frame. At the beginning of the test, an initial load was applied to the slab through the column stub to ensure that all the four sides are rested on the rods and the initial settlements is reduced. The load was applied at a load increment of 8.8 kN (2.0 kips) until the first crack was detected. Then, the test was stopped to

install the crack gauges on the tension surface of the slab using fast setting epoxy glue and left for three hours. The test was then resumed using load increments of 22.5 kN (5 kips). At each load step the test was stopped and the crack propagation was marked as shown in Figure 3.21.

Figure 0.21: A Photograph during Testing and Crack Marking Process

Chapter 4

Results & Discussion

4.1 Introduction

This chapter presents the results from testing the twelve SCC slabs. As mentioned earlier, the main parameters were the aggregate size (10 mm and 20 mm), C/F aggregate ratio (0.7 and 1.2), and slab thickness. The slabs were divided into four groups. Within each group, three slab thicknesses were tested: 150 mm, 200 mm and 250 mm. Group A had an aggregate size of 10 mm, and a C/F aggregate ratio of 0.7, Group B had an aggregate size of 10 mm, and a C/F aggregate ratio of 1.2, Group C had an aggregate size of 20 mm, and a C/F aggregate ratio of 0.7, and Group D had an aggregate size of 20 mm, and a C/F aggregate ratio of 1.2.

The recorded data and the observations during the testing were processed, and are presented in this chapter. This data includes the load-deflection behaviour of the slabs, the gradual development of the concrete and reinforcement strains at each loading step, the crack propagation and the slabs' modes of failure and capacities. Finally, the observed capacities were compared with those calculated using different design codes (CSA A23.3-04, ACI 318-11, BS8110, and EC2 (2010)) as well as the predictions of the Critical Shear Crack Theory (CSCT) that was introduced by Muttoni (2008) and subsequently formed the basis of the Model Code (2010).

4.2 Load – Deflection Characteristics

The deflections of each slab were measured at different locations using four LVDTs arranged as detailed in Section 3.8.2. The deflections were measured on the tension side of the test slabs. Figures 4.1 to 4.4 show the applied load versus the central deflection of all test slabs. The first yielding of the flexural reinforcement is indicated by a circle on the load deflection plots. Some of the strain gauges were damaged during the casting process and, as a result, the steel strains were not measured for some locations in the slabs. The small initial settlement in the load-deflection graphs was corrected. Table 4.1 shows the load and the corresponding deflection values at first cracking, first yield of the flexure reinforcement, and at the ultimate load. The compressive strength and the reinforcement ratio are also listed in this table.

Table 0.1: Deflection Characteristics of Tested Slabs

Slab No.	Comp. Strength f_c'	Rein. Ratio ρ	First Crack load	First Crack Def.	Yield Load P_y	Yield Load Def. Δ_y	Ult. Load P_u	Ult. Load Def. Δ_u
	(MPa)	(%)	(kN)	(mm)	(kN)	(mm)	(kN)	(mm)
SCA150	24.5	1.01	36	1.40	227	9.90	351	17.20
SCA200	26.0	1.08	73	1.30	-	-	533	10.00
SCA250	27.0	0.91	124	1.20	672	6.70	772	8.10
SCB150	29.0	1.01	55	2.70	234	10.90	343	19.30
SCB200	30.0	1.08	62	1.40	457	9.30	598	13.20
SCB250	32.0	0.91	-	-	-	-	764	8.35
SCC150	25.5	1.01	54	2.40	-	-	408	18.10
SCC200	26.0	1.08	57	1.00	-	-	588	11.10
SCC250	27.0	0.91	78	0.70	679	6.40	870	8.90
SCD150	24.0	1.01	45	2.30	221	10.0	342	17.40
SCD200	24.5	1.08	-	-	473	8.80	576	11.40
SCD250	25.0	0.91	100	0.90	751	6.90	836	8.40

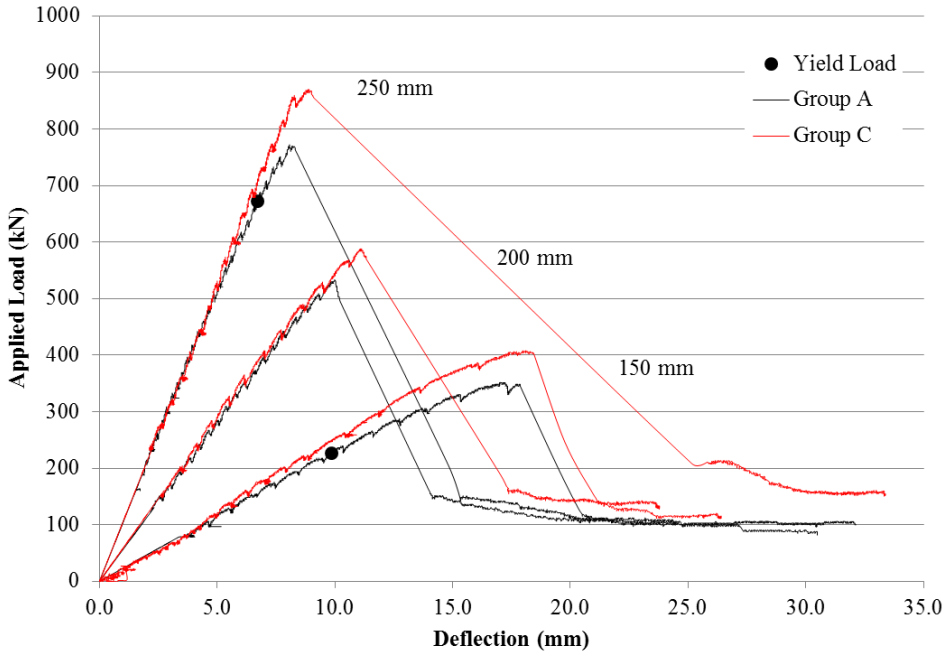

Figure 0.1: Load vs. Central Deflection for Slabs in Groups A and C (C/F Ratio of 0.70 and Coarse Aggregate Size of 10 mm and 20 mm, respectively)

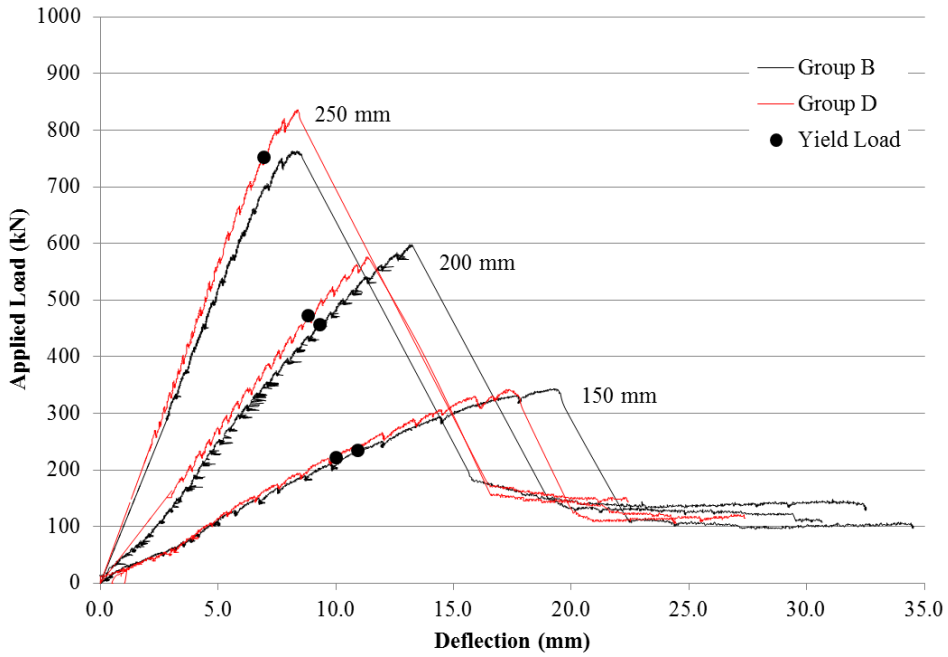

Figure 0.2: Load vs. Central Deflection for Slabs in Groups B and D (C/F Ratio of 1.20 and Coarse Aggregate Size of 10 mm and 20 mm, respectively)

The first crack was observed by the naked eye. The load that corresponds to the first yielding of the flexure reinforcement was determined from the strain gauges' readings. The strain gauges were mounted on the reinforcement as shown in Figures 3.17 and 3.18. The first yielding occurred around the column stub. The yield strains were determined from the actual tests on the reinforcement bars.

In order to examine the effect of changing the maximum aggregate size from 10 mm to 20 mm, the loads versus the central deflection are plotted in Figures 4.1 and 4.2 for the slabs with C/F ratios of 0.7 (Groups A and C) and 1.20 (Groups B and D), respectively. The slabs had similar reinforcement ratios and slight variations in the compressive strength. The figures show that, at the same load values, there is no significant change in the load-deflection curves due to the change in the coarse aggregate size.

Figures 4.3 and 4.4 are plotted to illustrate the influence of changing the C/F ratio from 0.70 to 1.20 for the slabs with the same maximum coarse aggregate; where Figure 0.3 shows Groups A and B with 10 mm coarse aggregate size, and Figure 0.4 shows Groups C and D with 20 mm coarse aggregate size. The figures show that, at the same load values, there is no significant change in the load-deflection curves due to the change in the C/F aggregate ratio. Nonetheless, a minor influence was found on the deflection values when the C/F ratio was increased from 0.70 to 1.20.

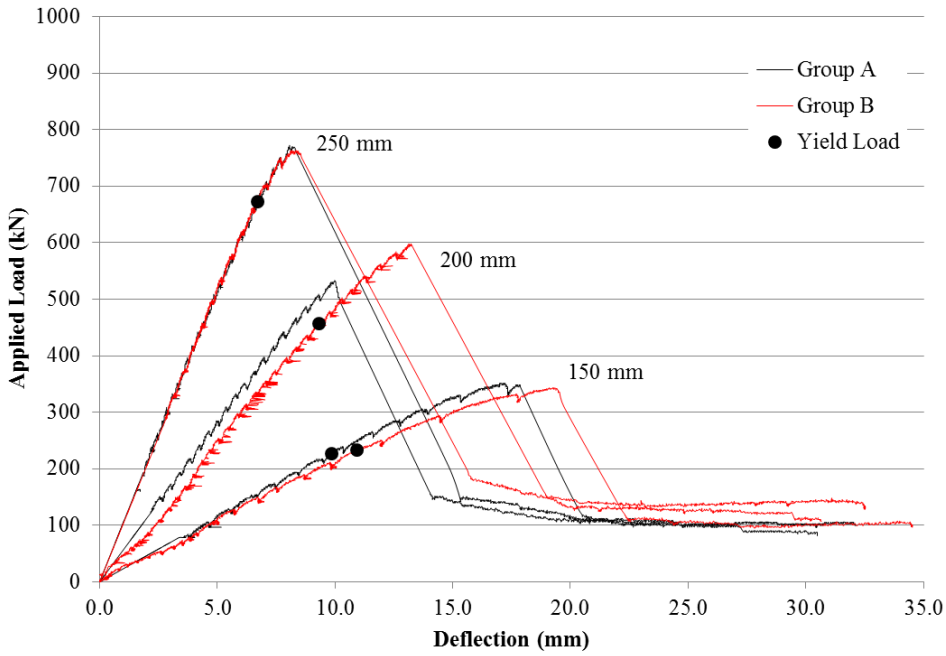

Figure 0.3: Load vs. Central Deflection for Slabs in Groups A and B (Coarse Aggregate Size of 10 mm and C/F Ratio of 0.70 and 1.20, respectively)

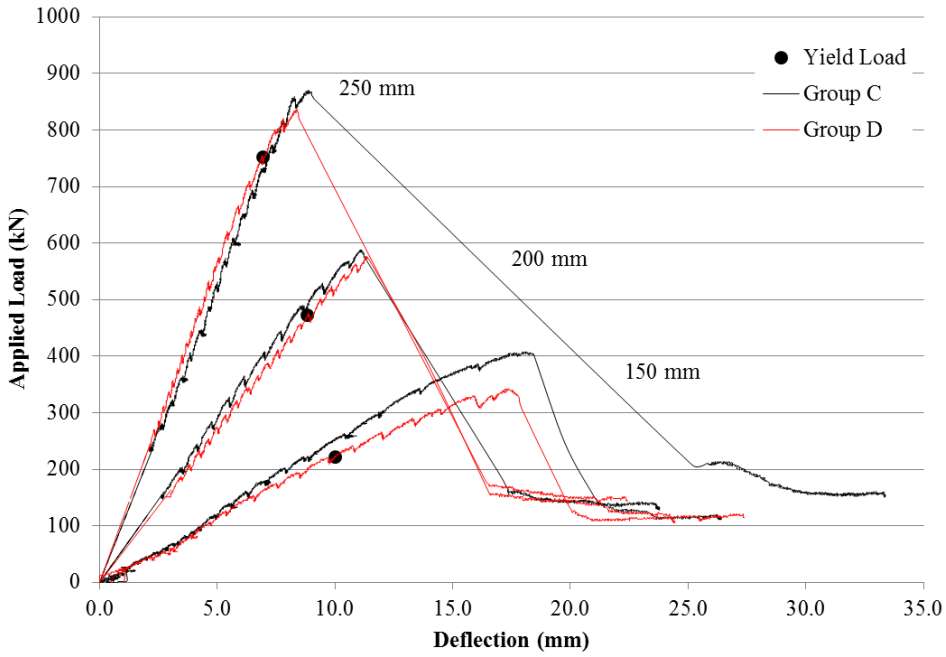

Figure 0.4: Load vs. Central Deflection for Slabs in Groups C and D (Coarse Aggregate Size of 20 mm and C/F Ratio of 0.70 and 1.20, respectively)

The deflection values listed in Table 0.1 illustrate the significant effect of the slab thickness. The deflection at failure for the 250 mm thick slabs was 50% of that of the 150 mm thick slabs. This can be attributed to the increase in stiffness as a result of increasing the slab thickness. The thin slabs showed more ductile failure behaviour as they exhibited higher deflection values. The stiffness and ductility of the slabs are discussed in Sections 4.2 and 4.3. The load deflection curves can be also be used to identify the type of failure (Hussein 1990). Two-way slabs have three possible modes of failure: pure flexure failure, ductile punching failure, and pure punching shear failure. In general, punching shear failure occurs with a sudden drop in the load after the slab reaches the maximum load capacity. The 150 mm thick slabs failed in ductile punching shear. However, thicker slabs (200 mm and 250 mm) failed due to pure punching shear.

The deflection profiles for all slabs are shown in Figures 4.5 to 4.8. The profiles are plotted at different load increments using the deflection measurements from the four LVDTs located at the front side of the slabs as detailed in Section 3.8.2. The same load increments are used for each slab with the same thickness. In addition, the deflection profiles at the ultimate load are also plotted in the deflection profiles. A discontinuity in the deflection profiles was observed inside the shear cracking zone; this discontinuity was more pronounced in the thicker slabs than the thinner ones that exhibited more uniform curvatures. This discontinuity was located approximately at a distance equal to the effective slab depth from the slab center. It was observed that the portion of slab in the outer zone of slabs bounded by the critical shear crack deformed as a rigid body. This behaviour is similar to that of NC two-way slabs. It was first observed by Kinnunen and Nylander (1960) and it subsequently formed the basis of

their mechanical model. Hussein (1990) also made the same observations for normal and high strength concrete slabs. The Critical Shear Crack Theory (CSCT) by Muttoni (2008) uses the same assumptions to determine the load-rotation relationship as discussed in Section 2.3.2.

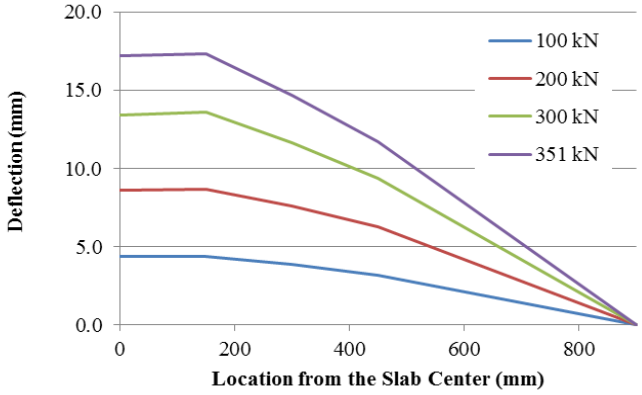

a) 150 mm Thick Slab

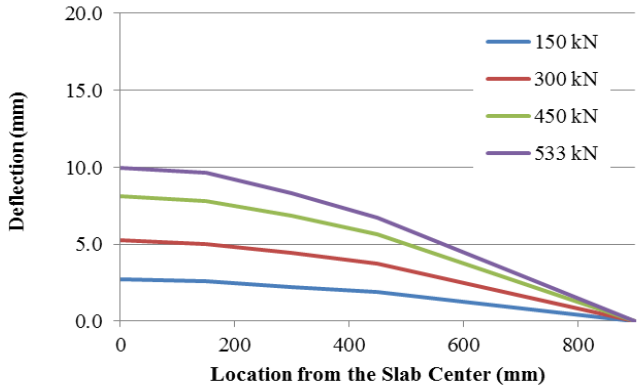

b) 200 mm Thick Slab

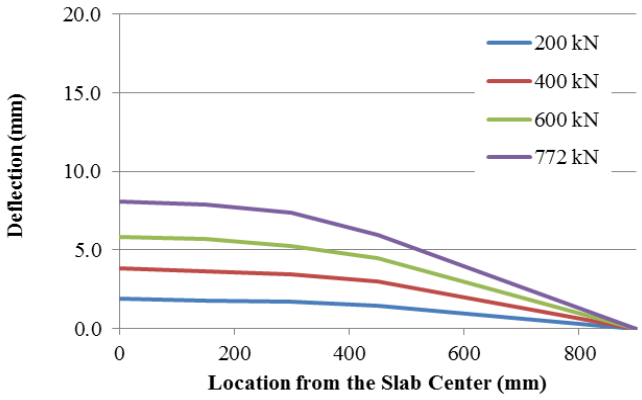

c) 250 mm Thick Slab

Figure 0.5: Deflection Profiles of Group A Slabs

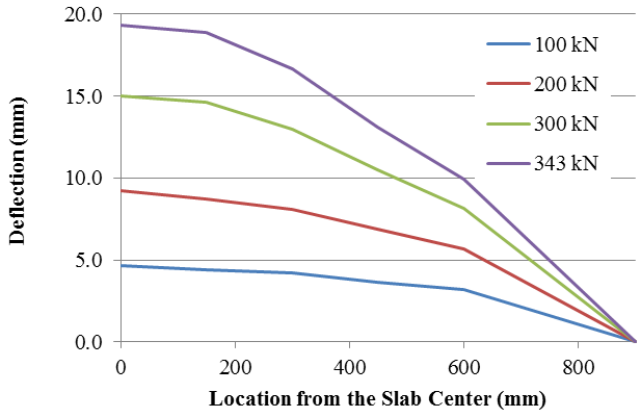

a) 150 mm Thick Slab

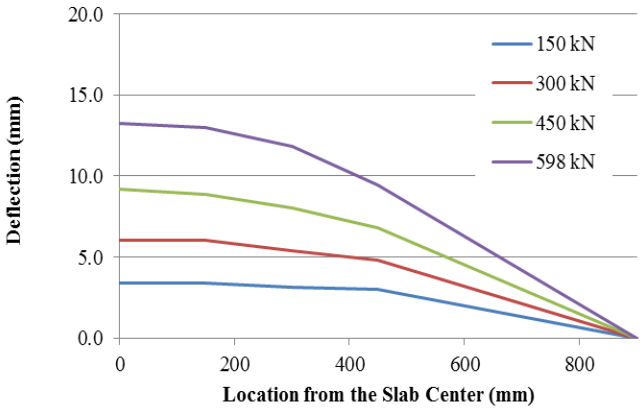

b) 200 mm Thick Slab

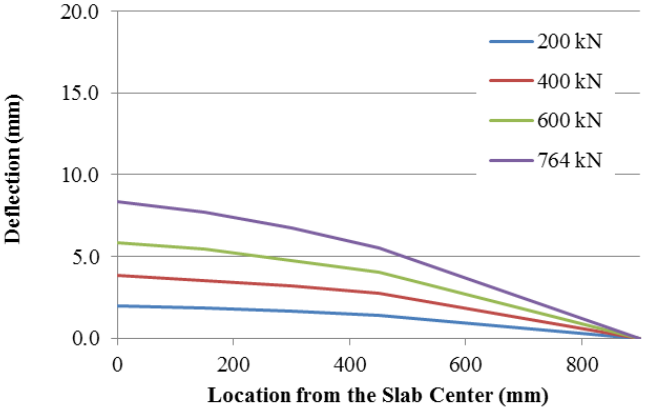

c) 250 mm Thick Slab

Figure 0.6: Deflection Profiles of Group B Slabs

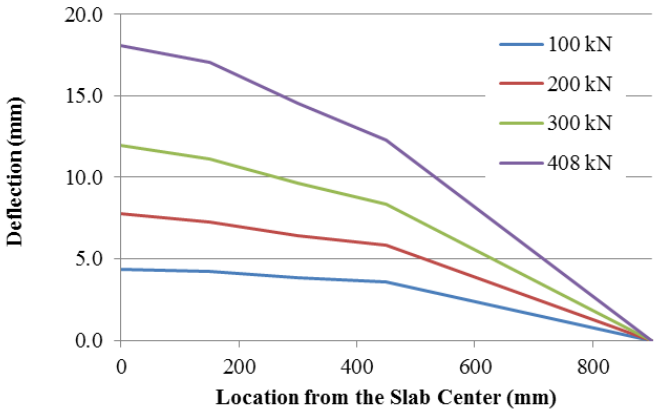

a) 150 mm Thick Slab

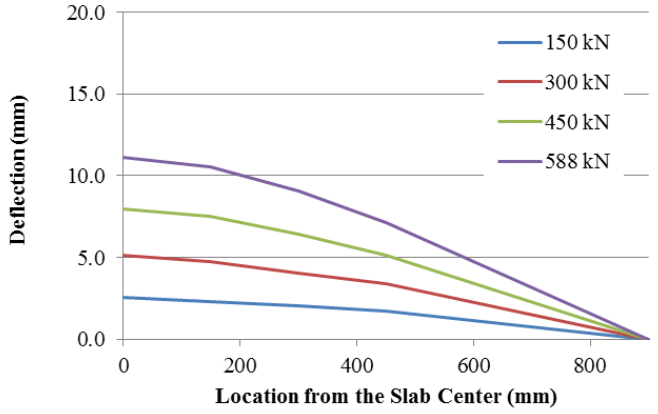

b) 200 mm Thick Slab

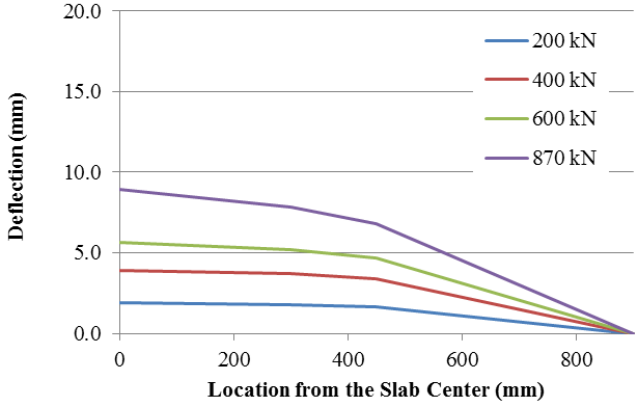

c) 250 mm Thick Slab

Figure 0.7: Deflection Profiles of Group C Slabs

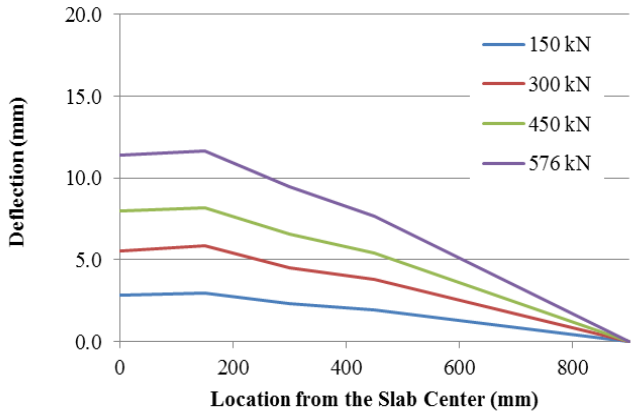

a) 200 mm Thick Slab

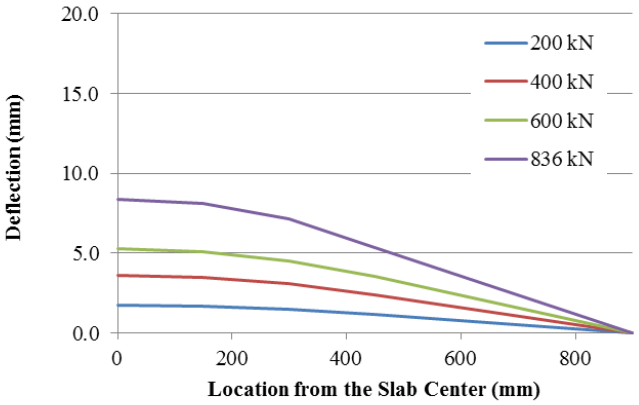

b) 250 mm Thick Slab

Figure 0.8: Deflection Profiles of Group D Slabs

4.3 Stiffness

The stiffness is defined as the slope of the load-deflection curve. In general, for a slab failing in punching shear, a typical load-deflection curve can be represented by three straight lines with different slopes. The first line represents the uncracked slope of the slab. The second line with a lower slope value represents the cracked slab elastic stiffness and ends at the yielding of the reinforcement. The third line represents the slab stiffness after yielding of the flexure reinforcement up to the failure of the slab under punching shear stresses. The smooth transition in slope before and after the formation of the first crack shows that the slabs exhibited a gradual loss in stiffness after the formation of the first crack. A gradual decrease was also observed in the slab stiffness after the yielding of the flexure reinforcement.

The uncracked stiffness, cracked stiffness, first crack deflection and ultimate deflection are listed in Table 4.2. From the experimental results, it is apparent that the slab thickness has the greatest influence on the slab stiffness within each group of slab. The decrease in slab stiffness after cracking was higher in thicker slabs as shown in Table 4.2, except for slabs SCA150 and SCB150 where a higher loss in stiffness was observed. Both slabs were cast using a C/F ratio of 0.70. In general, the loss in slab stiffness correlated with an increase in slab thickness.

There is no significant change in either the uncracked or the cracked stiffness for the slabs due to changing the maximum coarse aggregate size or the C/F ratio used for the four groups of slabs

Table 0.2: Uncracked Stiffness, Cracked Stiffness and Deflections

Slab No.	Comp. Strength f_c'	Uncracked stiffness	Cracked stiffness	Loss in stiffness	First Crack Deflection	Ultimate Deflection
	(MPa)	(kN/mm)	(mm)	%	(mm)	(mm)
SCA150	24.5	25.70	17.0	66.0	1.40	17.20
SCA200	26.0	56.10	49.0	87.0	1.30	10.00
SCA250	27.0	103.30	71.4	69.0	1.20	8.10
SCB150	29.0	20.40	13.0	64.0	2.70	19.30
SCB200	30.0	44.30	36.2	82.0	1.40	13.20
SCB250	32.0	--	75.8	--	--	8.80
SCC150	25.5	22.50	17.4	77.0	2.40	18.10
SCC200	26.0	57.00	40.0	70.0	1.00	11.10
SCC250	27.0	111.43	77.3	69.0	0.70	8.90
SCD150	24.0	19.57	16.4	84.0	2.30	17.40
SCD200	24.5	--	39.6	--	--	12.30
SCD250	25.0	111.11	56.7	51.0	0.90	8.40

Table 0.3: Ductility and Energy Absorption

Slab No.	Comp. Strength f_c'	Slab Thickness	Slab Depth	Rein. Ratio ρ	Ductility $\frac{\Delta_u}{\Delta_y}$	Energy Absorption Capacity
	(MPa)	(mm)	(mm)	%		kN.mm*10^3
SCA150	24.5	150	110	1.01	1.74	3.30
SCA200	26.0	200	155	1.08	--	2.80
SCA250	27.0	250	205	0.91	1.21	3.30
SCB150	29.0	150	110	1.01	1.77	3.80
SCB200	30.0	200	155	1.08	1.42	4.20
SCB250	32.0	250	205	0.91	--	3.50
SCC150	25.5	150	110	1.01	--	4.00
SCC200	26.0	200	155	1.08	--	3.50
SCC250	27.0	250	205	0.91	1.39	4.10
SCD150	24.0	150	110	1.01	1.74	3.30
SCD200	24.5	200	155	1.08	1.30	3.40
SCD250	25.0	250	205	0.91	1.22	3.90

4.4 Ductility and Energy Absorption

Ductility is defined as the ratio between the deflection at the ultimate load, Δ_u, and the deflection at the first yielding of the flexure reinforcement, Δ_y. Hussein (1990) and Zhang (2006) used the same definition for ductility. The slab ductility represents the deformation capacity of the slab prior to failure. The ductility of all test slabs are listed in Table 0.3. From the experimental values, it is apparent that the slab thickness has the most significant influence on the ductility index of the slabs. Group D clearly shows decrease in the slab ductility by approximately 30%. This decrease was a result of increasing the slab thickness from 150 to 250 mm.

The energy absorption capacities for all slabs are listed in Table 0.3. The energy absorption was calculated as the area under the entire load-deflection curve recorded at the center of each slab. The energy absorption values for slabs SCD150, SCD200, and SCD250 are 3.30 kN.mm, 3.40 kN.mm, and 3.90×10^3 kN.mm, respectively. Despite the change in the slab thickness, the energy absorption values remain close. Increasing the slab thickness was not followed by a consequent increase in the energy absorption. This can be explained by the higher load capacity and the lower deflection at ultimate load for thick slabs.

The energy absorption values do not show any significant influence in changing the coarse aggregate size or the C/F ratio on both ductility and energy absorption capacities for the tested slabs. However, the slab thickness is found to have the most significant influence.

4.5 Steel Reinforcement Strain

This section presents the strain development of the flexure reinforcement in the test slabs. The strains were measured using ten strain gauges mounted on the reinforcement at different locations as detailed in Section 3.8.3. These locations were selected to measure the radial and tangential strain development. As mentioned earlier, some strain gauges were damaged during the casting process, and hence, some strain data is missing. The maximum strain was always recorded at the center of the slab and the values are listed in Table 0.4. The maximum recorded strain was higher in the thin slabs and decreased when the slab thickness was increased. Table 0.4 shows that the yielding of the reinforcement in the thin slabs occurred at approximately 65% of the failure load.

Table 0.4: Strain in Concrete and Flexure Reinforcement

Slab No.	Comp. Strength f_c' (MPa)	Yield Load P_y (kN)	Ult. Load P_u (kN)	Yield /Ultimate %	Ultimate Radial Strain ε	Radius of yield (mm)	Ultimate Concrete Strain ε	Ult. Slab Rotation rad.
SCA150	24.5	227	351	65.0	0.0033	341	0.0027	0.0220
SCA200	26.0	--	533	--	0.0026	225	0.0015	0.0128
SCA250	27.0	672	772	87.0	0.0022	62	0.0011	0.0119
SCB150	29.0	234	343	68.0	0.0030	425	0.0016	0.0256
SCB200	30.0	457	598	76.0	--	--	0.0007	0.0162
SCB250	32.0	--	764	--	0.0026	206	0.0005	0.0100
SCC150	25.5	--	408	--	--	--	0.0012	0.0213
SCC200	26.0	--	588	--	--	--	0.0011	0.0139
SCC250	27.0	679	870	78.0	0.0028	212	0.0006	0.0121
SCD150	24.0	221	342	65.0	0.0031	446	0.0025	0.0223
SCD200	24.5	473	576	82.0	0.0025	325	0.0007	0.0115
SCD250	25.0	751	836	90.0	0.0023	334	0.0005	0.0110

Figures 4.9 to 4.12 show the load versus the strain in the flexure reinforcement at the center of each slab. The figures show that the slope of the load-strain curve changes at a load value corresponding to the formation of the first cracking. After the occurrence of the first crack in concrete near the loaded area (column face), the cracks started to propagate on the concrete surface and the stresses were transferred to the flexure reinforcement.

The slab thickness was found to have the most significant influence on the flexure reinforcement strain. The maximum values of the flexure reinforcement strains are listed in Table 4.4. The strains decreased as the slab thickness was increased. For example, the maximum values of strain in Group D for slabs of thickness 150 mm, 200 mm, and 250 mm were 3100, 2500, and 2300 με, respectively. From Figures 4.9 to 4.12, it can be concluded that the C/F aggregate ratio and the coarse aggregate size do not have any significant influence in the development of the steel strains in the slabs.

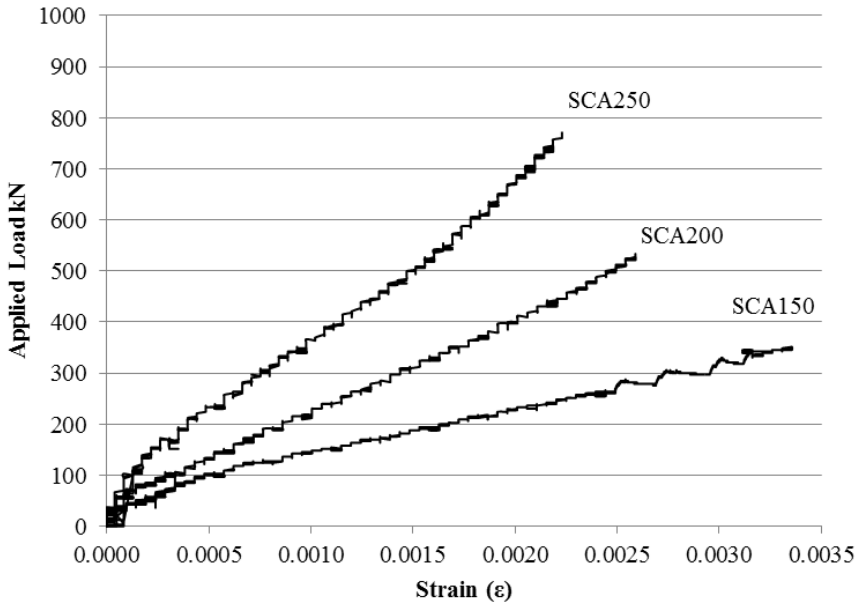

Figure 0.9: Load vs. Reinforcement Strain at Center of Slab for Group A

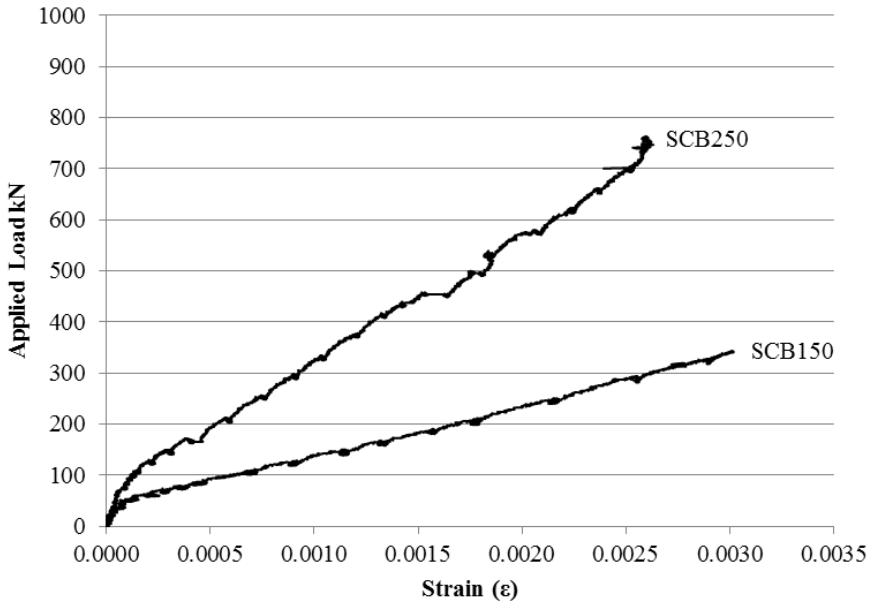

Figure 0.10: Load vs. Strain at Center of Slab for Group B

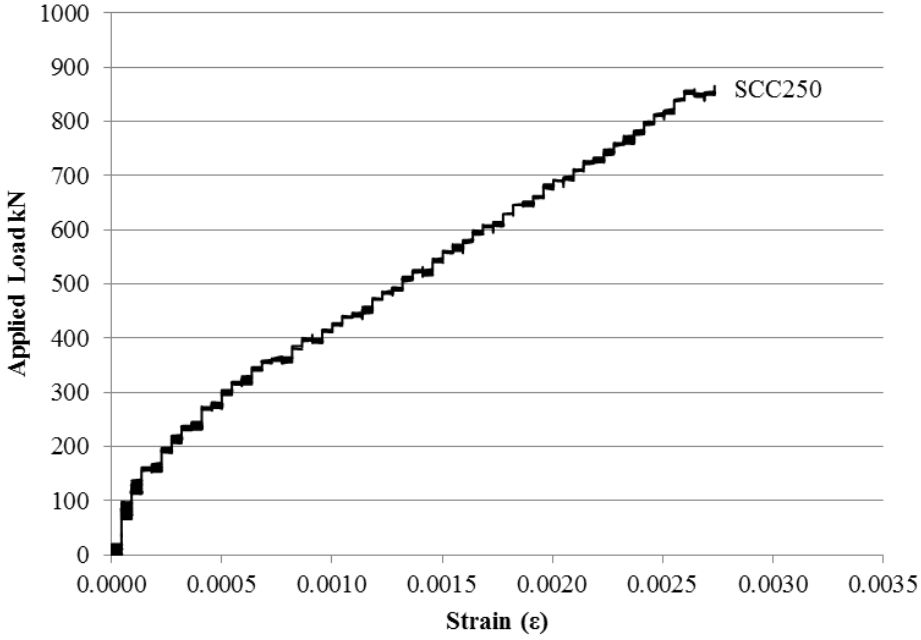

Figure 0.11: Load vs. Strain at Center of Slab for Group C

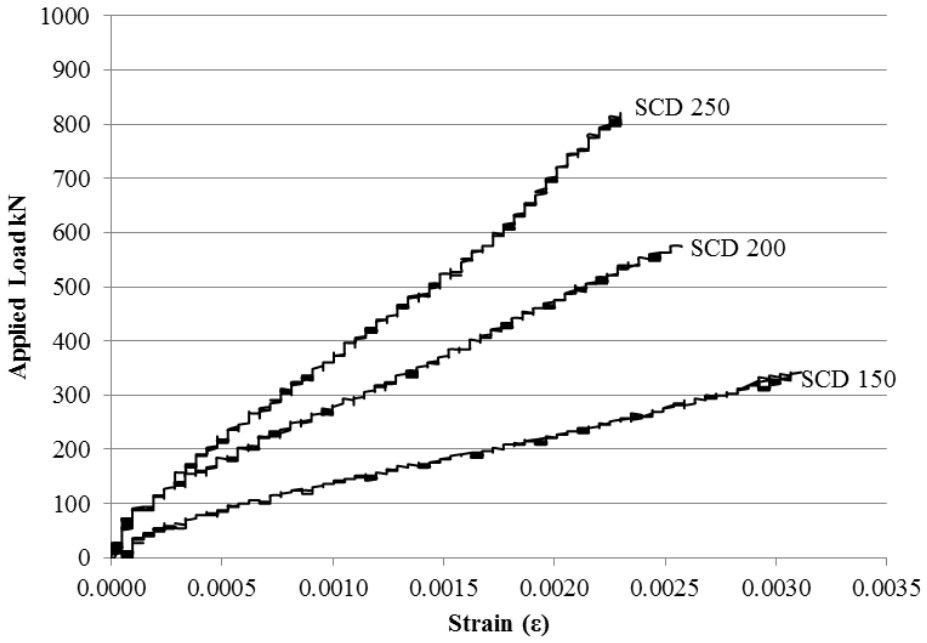

Figure 0.12: Load vs. Strain at Center of Slab for Group D

Figures 4.13 to 4.16 show the flexure reinforcement strain profiles in the radial direction. The profiles are plotted at different load increments using the steel strain gauge measurements. The same load increments were used for each slab with equal thickness. Also, the profiles at ultimate load are plotted in the strain profiles. The tension tests of the reinforcing bars used in the current experimental program showed that yield strain of the bars was approximately equal to 2200 με (Section 3.3). Based on this value and the plotted strain profiles, it can be seen that partial yielding occurred and extended in all slabs before failing under punching shear. Yielding of the reinforcement was spread in the 150 mm thick slabs while a localized yielding, around the column stub, was found in the 200 mm and 250 mm thick slabs.

The general trends of the strain profiles reveal that the strain is inversely proportional to the distance from the slab center. This behaviour is similar to the observation made by Kinnunen and Nylander (1960) for slabs with normal concrete. The strain was

higher around the column up to a certain distance, and then it dropped significantly. Thus, the observations support the inverse relationship of radial strain and distance from the slab center.

Similar to the load deflection profiles stated in Section 4.2, a discontinuity in the load strain profiles was observed at a distance approximately equal to the slab depth from the column face where the critical shear crack was formed for some of the labs. This discontinuity was more pronounced in thicker slabs than thinner ones which exhibited more uniform deformations. This observation was also reported in research conducted by Zhang (2006) on two-way slabs reinforced with CFRP bars. In general, the strain profiles were not conclusive in establishing the effect of C/F aggregate ratio or the aggregate size on such profiles.

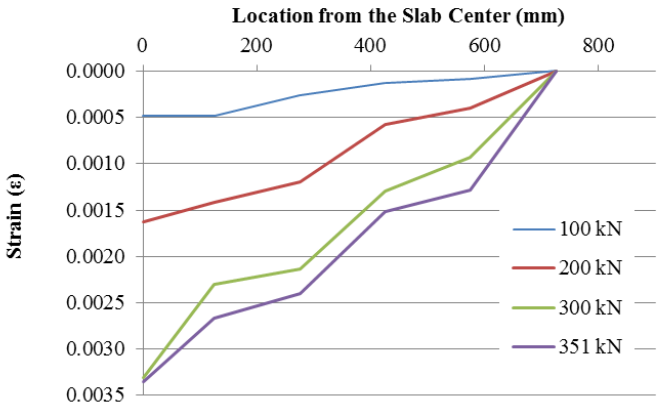

a) 150 mm Thick Slab

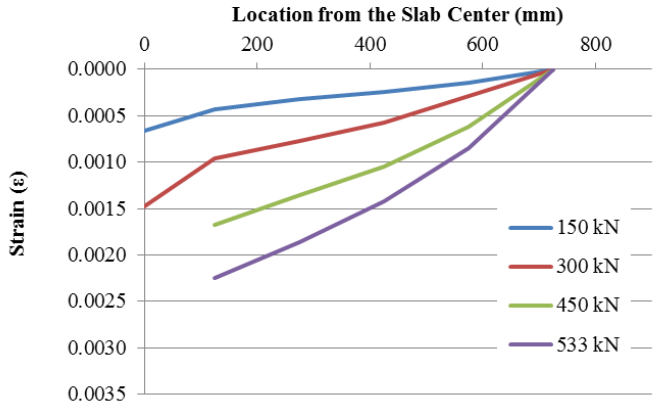

b) 200 mm Thick Slab

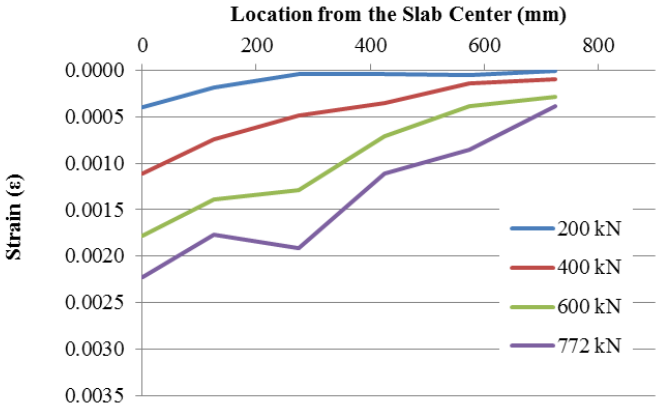

c) 250 mm Thick Slab

Figure 0.13: Reinforcement Strain Profile in the Radial Direction (Group A Slabs)

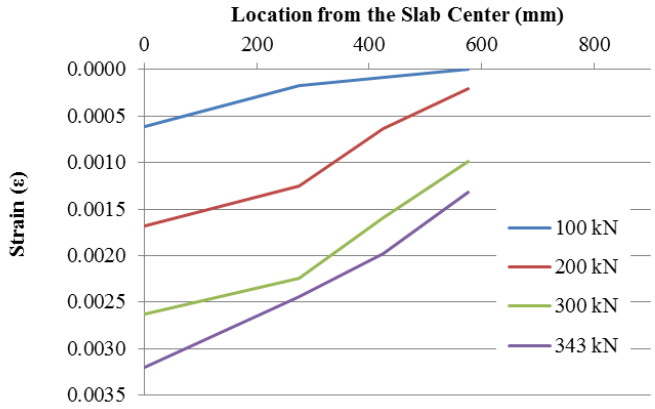

a) 150 mm Thick Slab

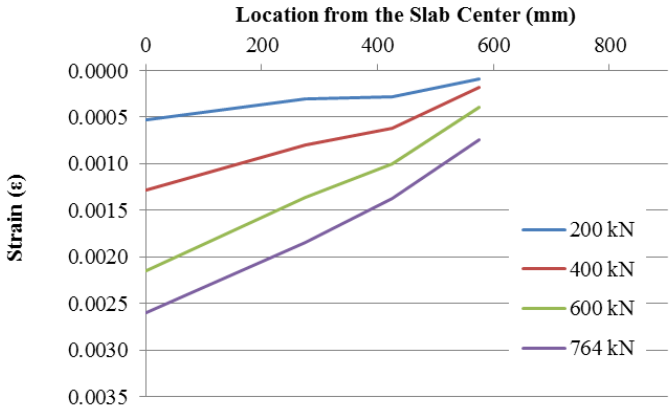

b) 250 mm Thick Slab

Figure 0.14: Reinforcement Strain Profile in the Radial Direction (Group B Slabs)

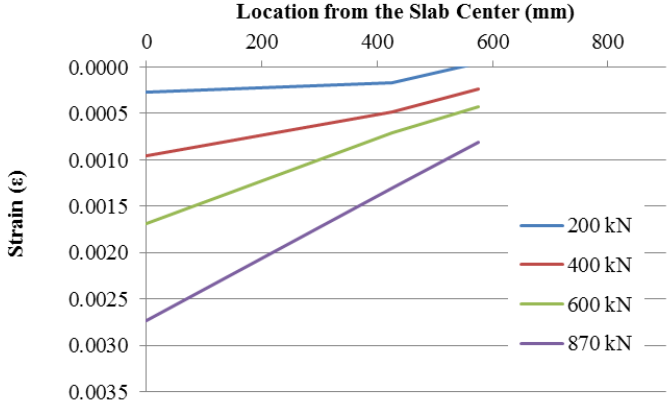

Figure 0.15: Reinforcement Strain Profile in the Radial Direction (Group C Slabs)

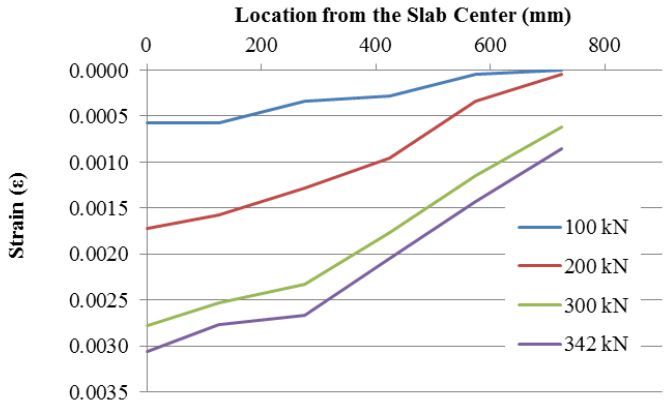

a) 150 mm Thick Slab

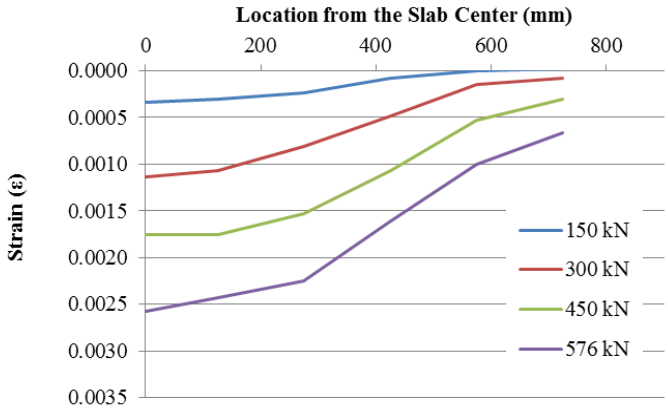

b) 200 mm Thick Slab

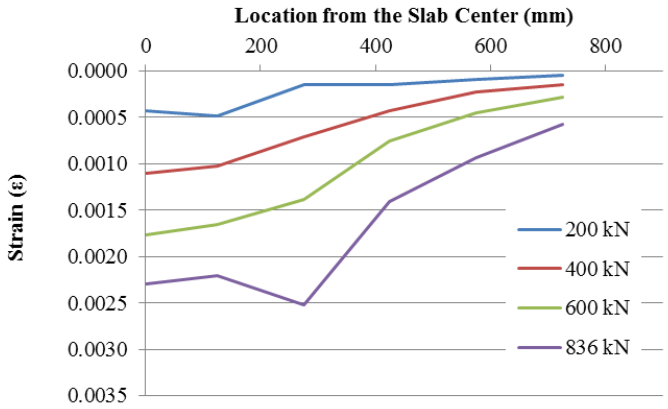

c) 250 mm Thick Slab

Figure 0.16: Reinforcement Strain Profile in the Radial Direction (Group D Slabs)

4.6 Concrete Strains

The concrete strains were measured at different locations on the compression side of the slabs as mentioned and detailed in Section 3.8.4. The concrete strains were only measured in the radial direction which is defined as the perpendicular direction to the column face. The purpose of using strain gauges at different locations is to monitor the distribution of the strain along the slab radius. The maximum concrete strain value for each slab occurred at the column face. These values are listed in Table 0.4. The results show that the maximum concrete strain for all slabs did not reach the limiting value of 0.0035 which is specified by the Canadian Code (CSA-A23.3-04) as the theoretical crushing value of concrete in compression. The radial strain at failure load ranged between 0.0004 and 0.0027; these values were recorded in slabs SCC250 and SCA150, respectively. It can be observed from the listed values that increasing the slab thickness has a significant influence on decreasing the maximum strain in the concrete. For instance, the concrete strain values in slabs of thickness 150, 200, and 250 in Group A were 0.0027, 0.0015, and 0.0011 respectively.

The applied loads versus the concrete strains at the column face are plotted in Figures 4.17 and 4.18. The figures show higher concrete strain values for thin slabs; these values decreased as the slab thickness was increased. The figures could hardly be used to confirm the effect of changing the maximum coarse aggregate size. The concrete strains listed in Table 0.4 as well as the concrete strain profiles did not show any significance for changing the C/F ratio on the developed strains for the test slabs.

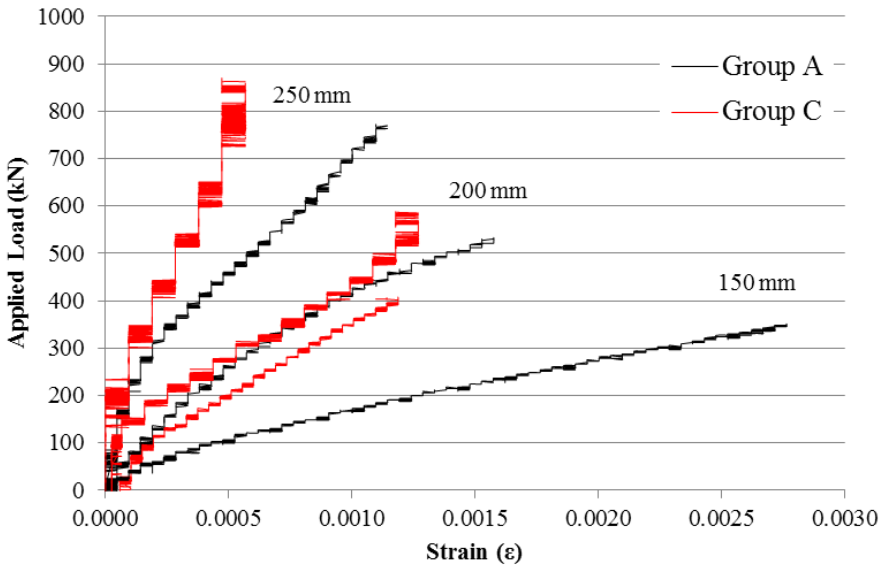

Figure 0.17: Load vs. Concrete Strain for Slabs in Groups A and C (C/F Ratio of 0.70 and Coarse Aggregate Size of 10 mm and 20 mm, respectively)

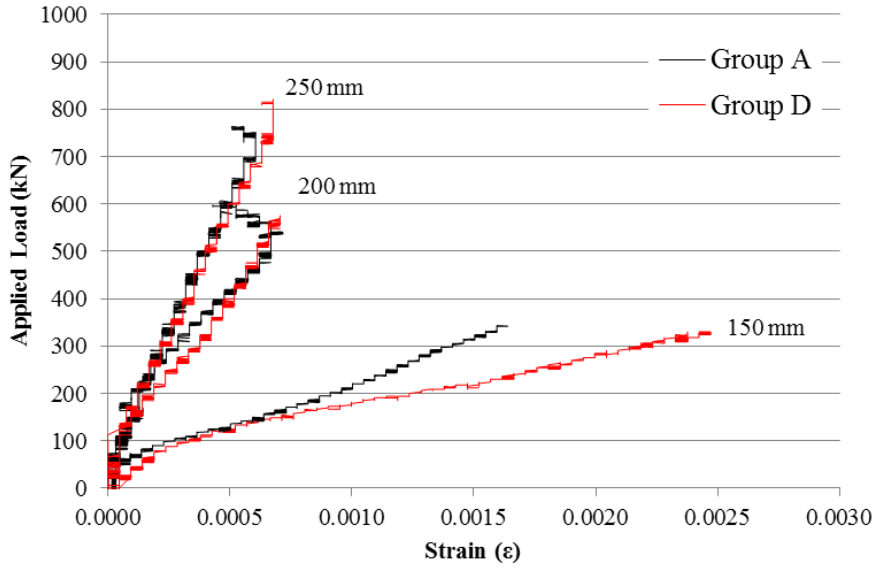

Figure 0.18: Load vs. Concrete Strain for Slabs in Groups B and D (C/F Ratio of 1.20 and Coarse Aggregate Size of 10 mm and 20 mm, respectively)

There is an increasing trend in the concrete strains with increasing the load as shown in Figures 4.17 and 4.18. However, slabs SCB 200, SCB250, SCC200, SCC250, SCD200, and SCD250 showed a decrease in the concrete strain after reaching a certain value before failure. The same observation is found in previous research

conducted by Muttoni (1991), and Imtiaz (2004). Imtiaz (2004) attributed this phenomenon to the strain redistribution in the concrete after the formation of cracks on the tension surface.

Figures 4.19 to 4.22 show the concrete strain profiles in the radial direction for each slab at certain load increments as listed on each figure. The highest strain values were recorded at the column face. A drop in the concrete strain was observed at certain radius of the tested slab. This drop was located approximately at d/2 from the column face. This observation was also reported in research conducted by Zhang (2006) on two-way slabs reinforced with CFRP bars.

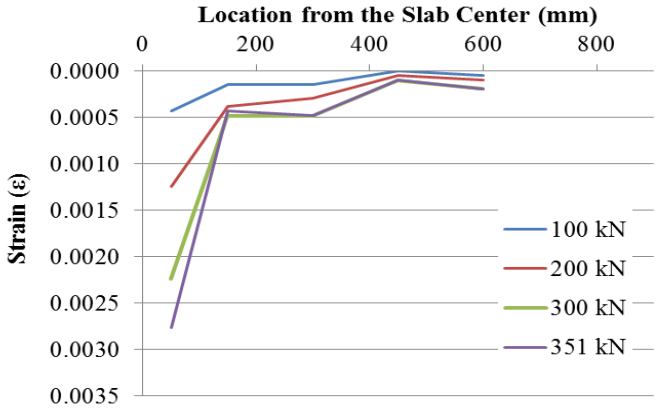

a) 150 mm Thick Slab

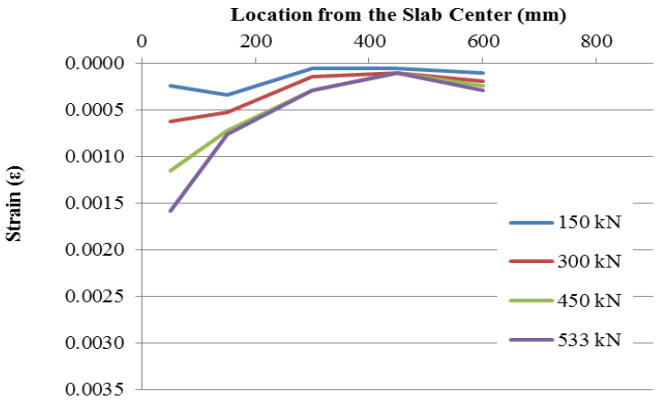

b) 200 mm Thick Slab

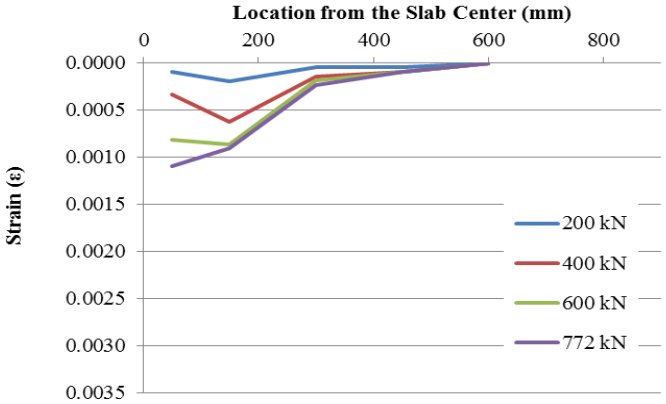

c) 250 mm Thick Slab

Figure 0.19: Concrete Strain Profile for Group A Slabs

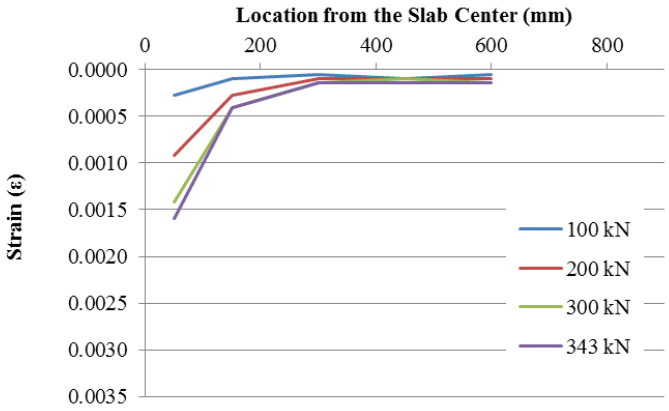

a) 150 mm Thick Slab

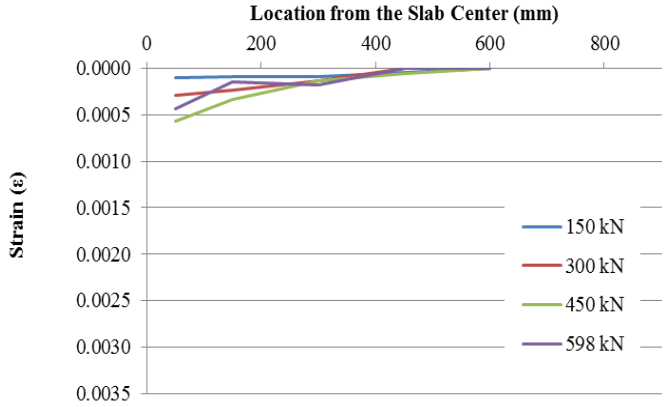

b) 200 mm Thick Slab

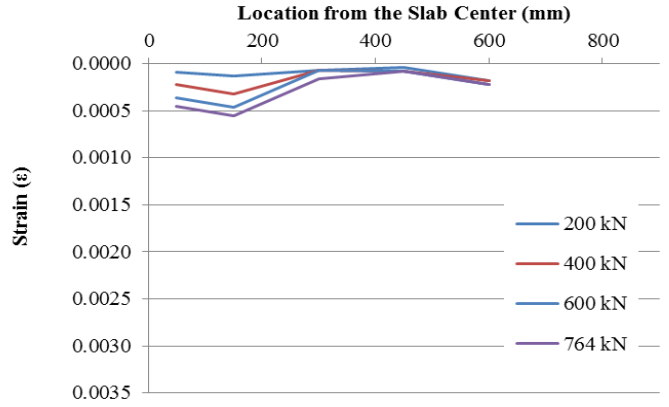

c) 250 mm Thick Slab

Figure 0.20: Concrete Strain Profile for Group B Slabs

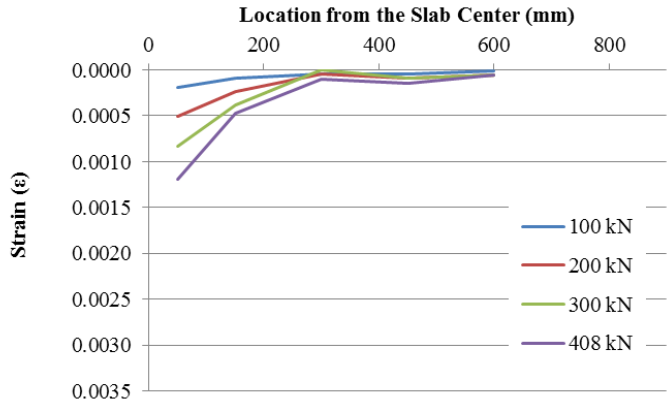

a) 150 mm Thick Slab

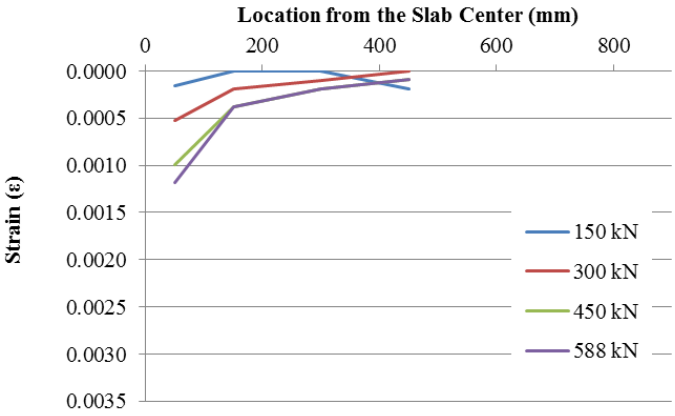

b) 200 mm Thick Slab

Figure 0.21: Concrete Strain Profile for Group C Slabs

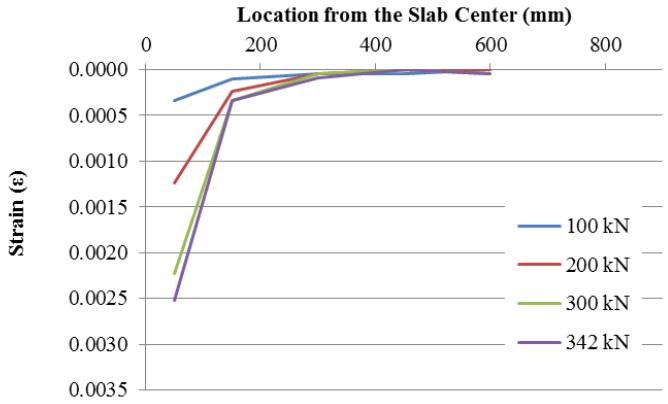

a) 150 mm Thick Slab

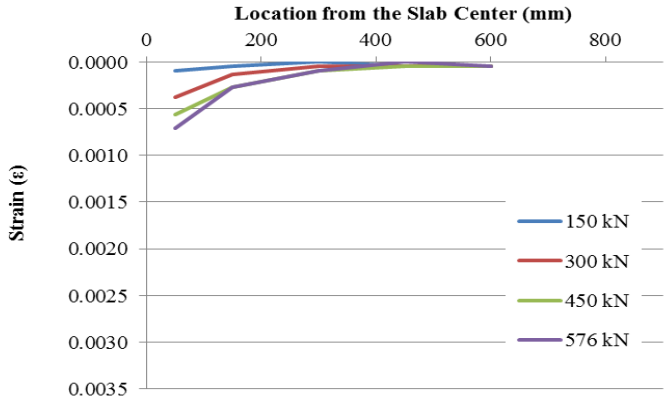

b) 200 mm Thick Slab

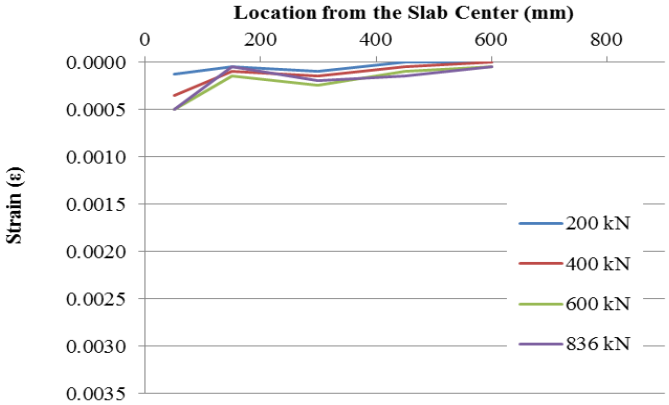

c) 250 mm Thick Slab

Figure 0.22: Concrete Strain Profile for Group D Slabs

4.7 Cracking Characteristics

The testing procedure is mentioned in details in Section 3.9. The crack pattern formation and propagation was carefully observed during testing. The first crack was visually detected by the naked eye and marked on the slab surface. The load value corresponding to the first crack formation was recorded and marked. The test was then stopped to attach the Crack Displacement Transducers (CDT) at the critical crack locations to monitor the crack width development. During the second stage of loading, the propagation of cracks as well as the load values were marked on the slab surface at each load increment of 22 kN (5.0 kips) until the slab failed. In general, the first crack was formed tangentially and passed around the column stub. This was followed by propagation of the radial cracks from the column stub edges to the four corners of the slab. As the applied load was increased, all radial cracks were connected by cracks in the tangential direction. It was observed that no new cracks were formed at approximately 80% of the failure load. Figures 4.23 to 4.34 show photographs of the crack patterns for each slab after failure occurred.

The first crack load values, the corresponding deflection, and the maximum crack widths are listed in The C/F aggregate ratio and the coarse aggregate size did not show any influence of the cracking characteristics of the slab as listed in Table 4.5.

In general, the first crack load for all slabs occurred in a range of 6% to 16% of the failure load. The lowest value of the loads that caused first crack was recorded for slab SCD200 and the highest value was recorded for slab SCA250 and SCB150. Nonetheless, the first crack is observed by the naked eye and hence, there could be some variability in the observed loads.

Figure 0.23: Crack Pattern for SCA150

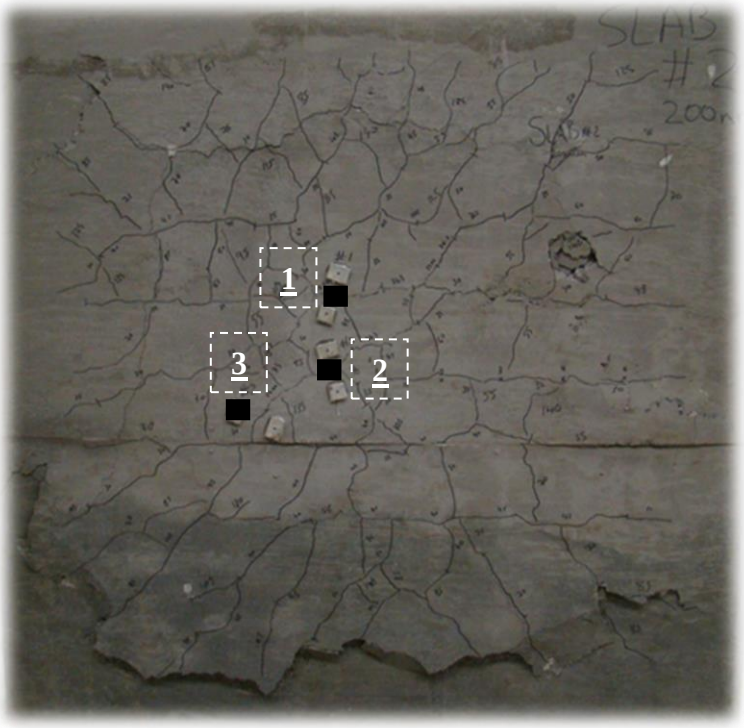

Figure 0.24: Crack Pattern for SCA200

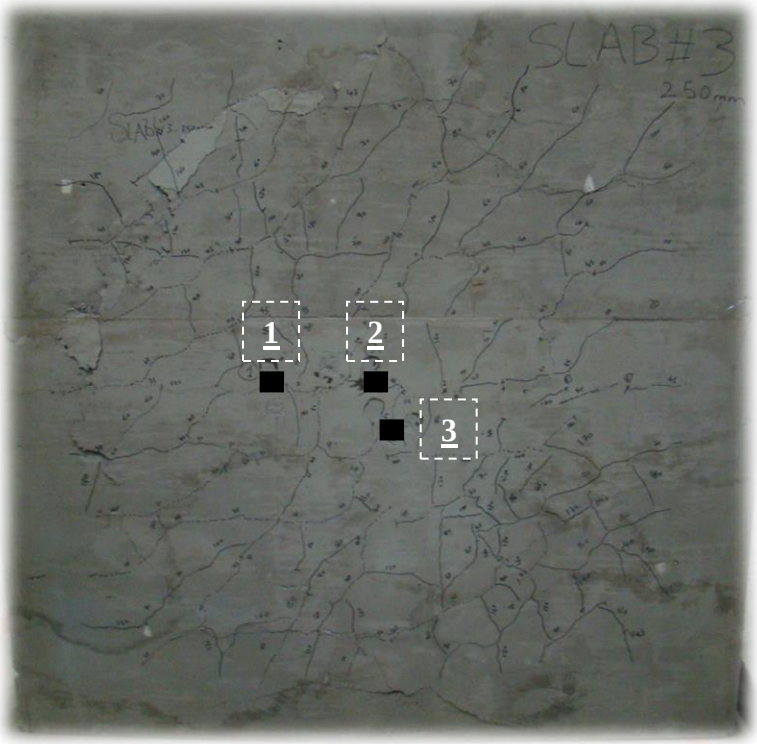

Figure 0.25: Crack Pattern for SCA250

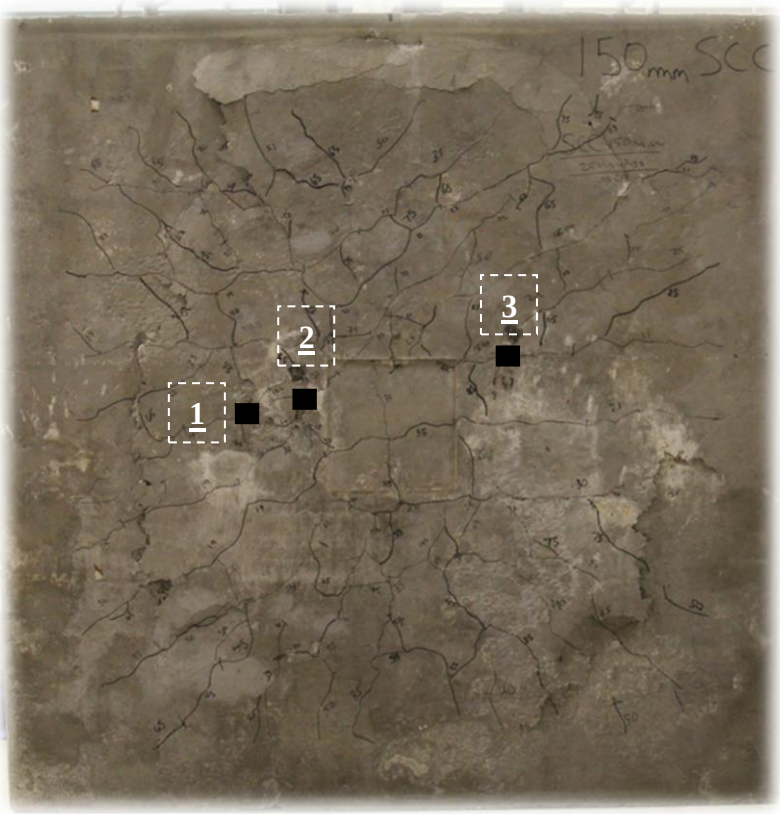

Figure 0.26: Crack Pattern for SCB150

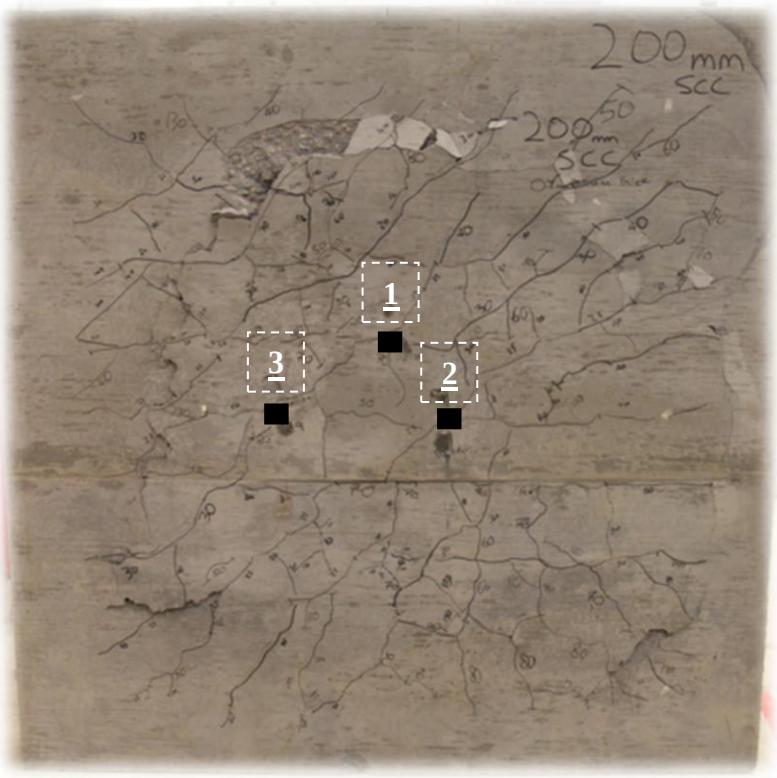

Figure 0.27: Crack Pattern for SCB200

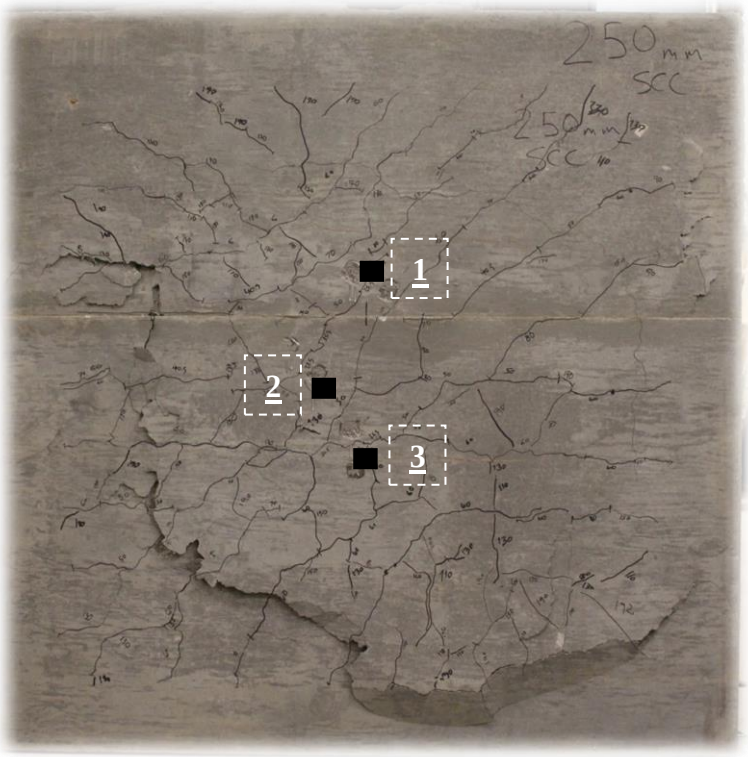

Figure 0.28: Crack Pattern for SCB250

Figure 0.29: Crack Pattern for SCC150

Figure 0.30: Crack Pattern for SCC200

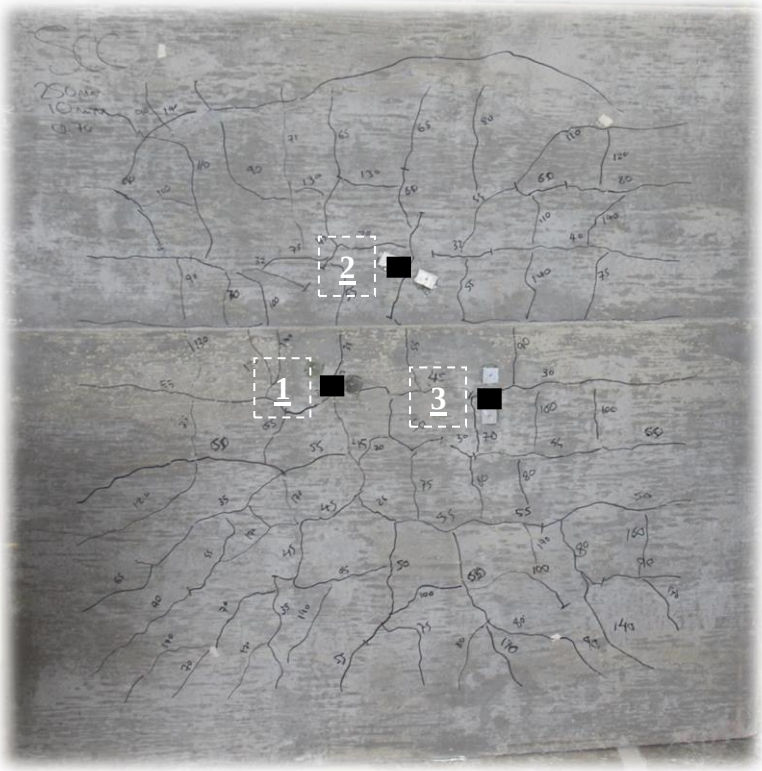

Figure 0.31: Crack Pattern for SCC250

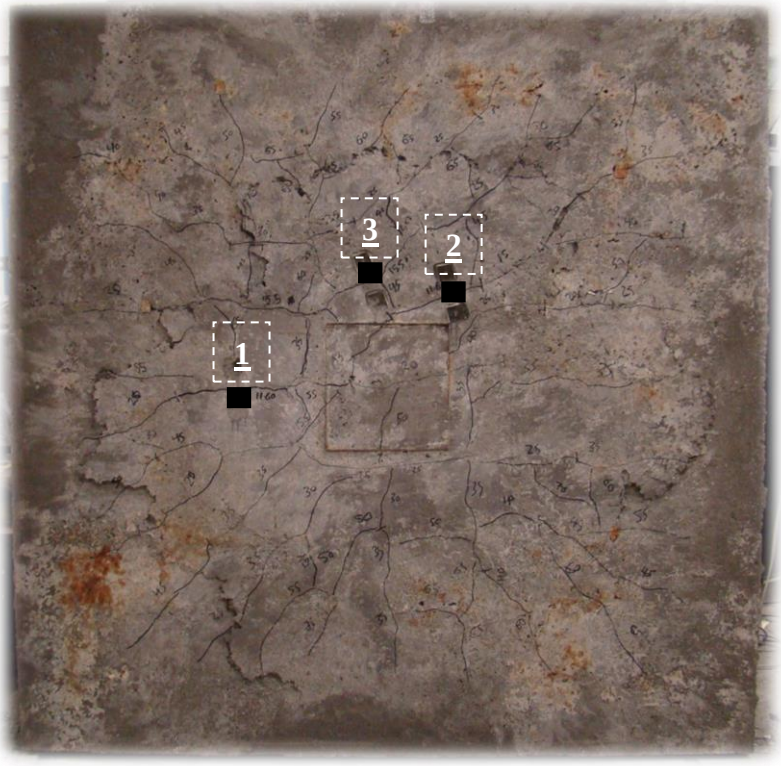

Figure 0.32: Crack Pattern for SCD150

Figure 0.33: Crack Pattern for SCD200

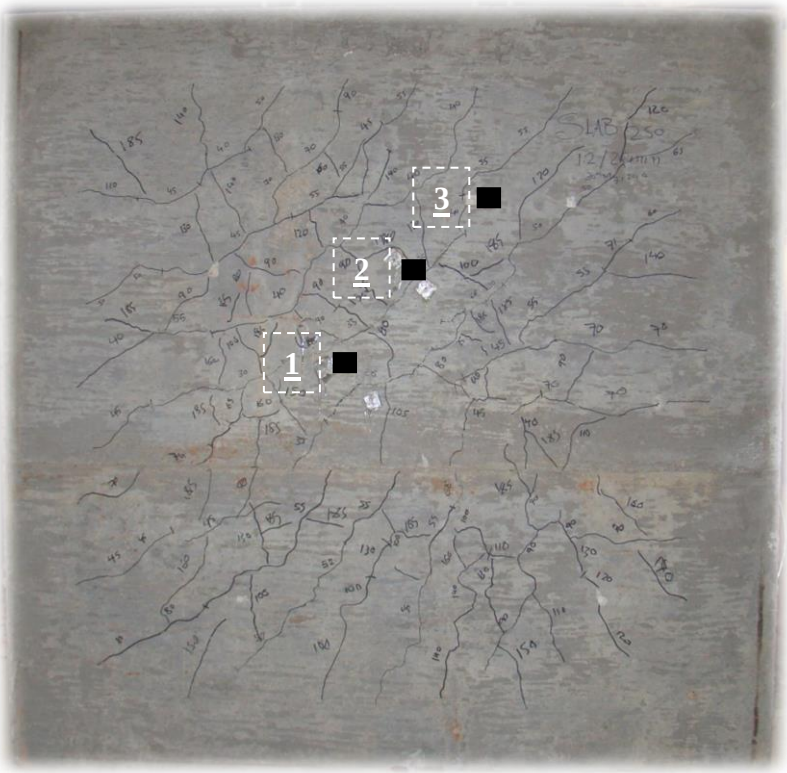

Figure 0.34: Crack Pattern for SCD250

The increased first cracking load, within each group of slabs, shows the significance of increasing the slab thickness. This increase in the load value can be attributed to the increased stiffness as explained in Section 4.3. The effect of the increased stiffness is also confirmed by the recorded crack width. The crack widths values show a decreasing trend with increasing the slab thickness. The largest crack width usually occurred around the column stub. The highest recorded value of the crack width was 1.90 mm in slab SCA150, and the smallest value was 0.31 mm in slab SCC250. The crack widths versus the applied loads are plotted in Figures 4.35 to 4.39. The crack widths in the plots were measured using the data recorded by the CDT mounted on the slab surface. Due to the redistribution of cracking and loads, nonlinear trends can be observed in the plotted figures. The C/F aggregate ratio and the coarse aggregate size did not show any influence of the cracking characteristics of the slab.

Table 0.5: Crack Measurements

Slab No.	Comp. Strength f_c' (MPa)	Rein. Ratio ρ %	First Cracking		Crack / Ultimate %	Max Crack Width mm		
			Load (kN)	Def. (mm)		(1)	(2)	(3)
SCA150	24.5	1.01	36	1.40	10%	1.90	1.30	--
SCA200	26.0	1.08	73	1.30	14%	0.75	0.50	0.75
SCA250	27.0	0.91	124	1.20	16%	--	--	--
SCB150	29.0	1.01	55	2.70	16%	--	--	--
SCB200	30.0	1.08	62	1.40	10%	1.30	0.80	0.60
SCB250	32.0	0.91	--	--	--	0.75	1.00	0.50
SCC150	25.5	1.01	54	2.40	13%	--	--	--
SCC200	26.0	1.08	57	1.00	10%	1.10	0.90	0.50
SCC250	27.0	0.91	78	0.70	9%	0.75	0.70	0.31
SCD150	24.0	1.01	45	2.30	13%	1.00	0.45	0.35
SCD200	24.5	1.08	--	--	--	0.75	0.85	0.40
SCD250	25.0	0.91	100	0.90	12%	0.65	0.50	0.35

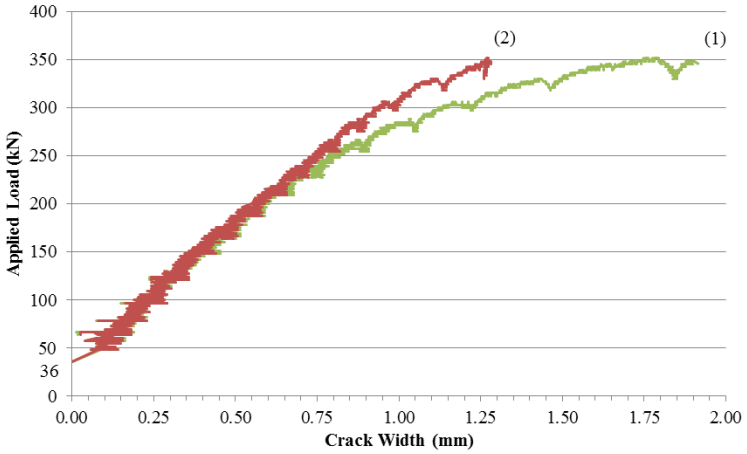

Figure 0.35: Crack Width vs. Applied Load for SCA150

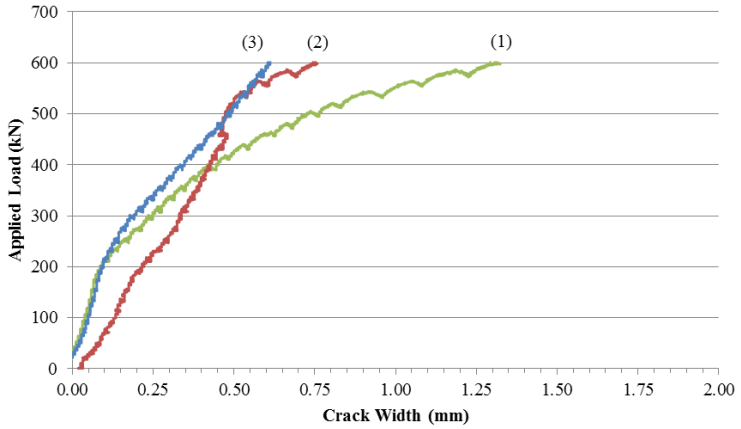

Figure 0.36: Crack Width vs. Applied Load for SCB200

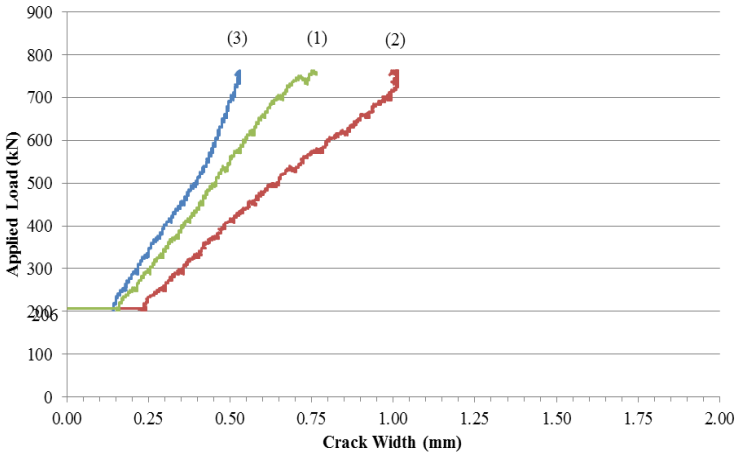

Figure 0.37: Crack Width vs. Applied Load for SCB250

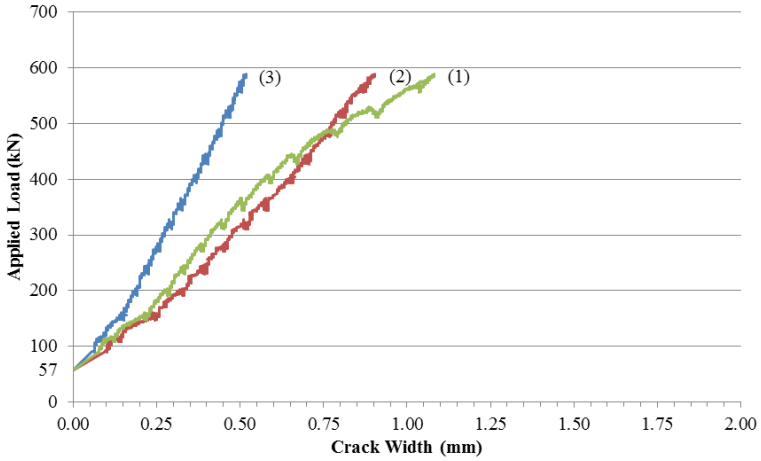

Figure 0.38: Crack Width vs. Applied Load for SCC200

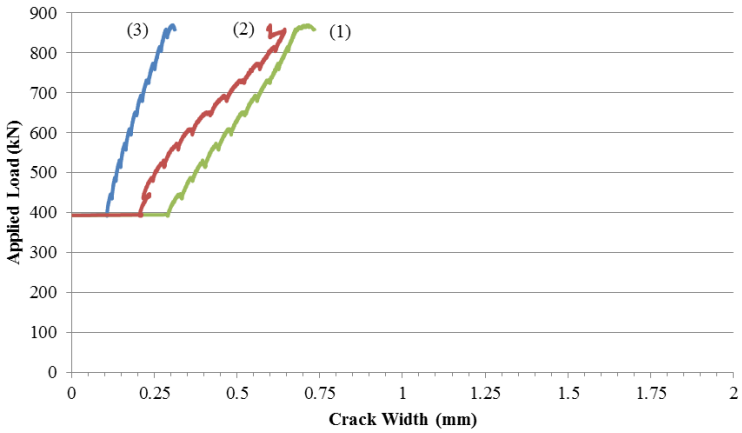

Figure 0.39: Crack Width vs. Applied Load for SCC250

Figures 4.40 to 4.42 show typical plots of the crack widths versus the reinforcement strains recorded closest to the occurrence of the crack. In general, it was observed that the strain versus crack width can be approximated as a straight line for the 200 mm and 250 mm slabs. On the other hand, the 150 mm slabs showed a nonlinear trend for the plotted curve after the strain had reached the yielding value of 2200 με as mentioned.

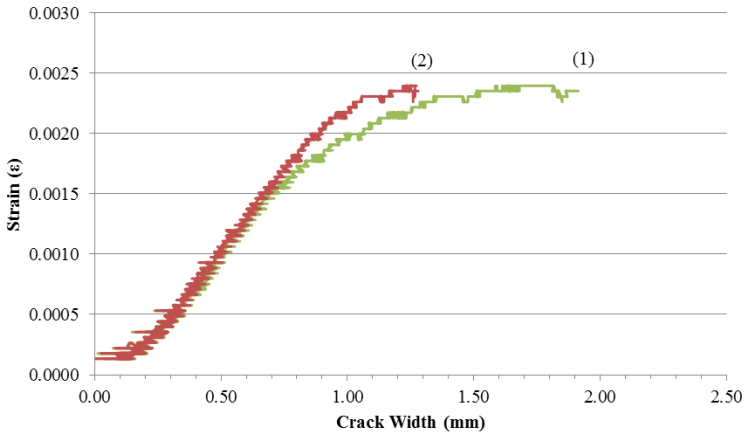

Figure 0.40: Crack Width vs. Reinforcement Strain for SCA150

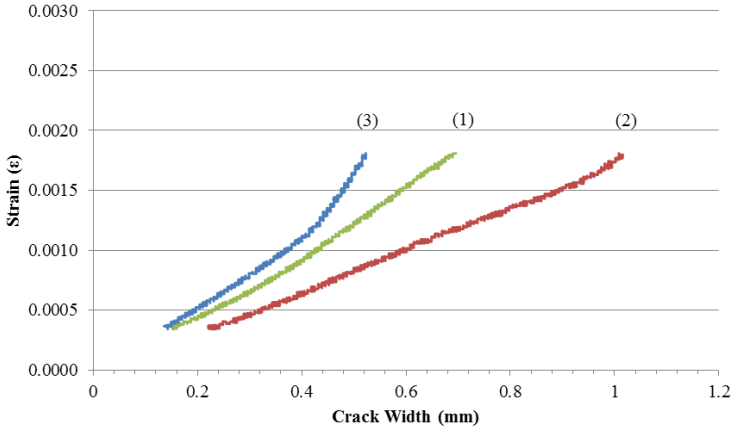

Figure 0.41: Crack Width vs. Reinforcement Strain for SCB250

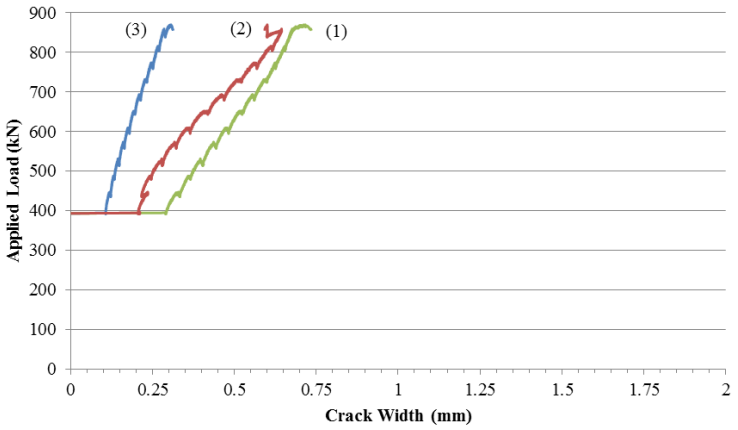

Figure 0.42: Crack Width vs. Reinforcement Strain for SCC200

4.8 Slab Rotation and Ultimate Capacity

The rotation capacity of the slab is defined as the slab rotation at ultimate load. The values of slab rotations are listed in Table 4.6 for all test slabs. These rotations were measured for the slab portion outside the shear crack which rotates as a rigid body as mentioned in Section 4.2. The experimental results show that the slab thickness has the major influence on the slab rotation. Thick slabs were found to have lower rotation capacity compared to thin slabs. There is no significant change in the slab rotation due to changing the coarse aggregate size or the C/F ratio used for the four groups of slabs. The rotation capacities ranged between 0.0256 and 0.0096 rad. The highest value was recorded in slab SCB150, and the lowest value was recorded in slab SCB250. Both slabs were cast using a coarse aggregate size of 10 mm and C/F ratio of 1.20. It should be noted that Group B slabs showed the highest rotation capacity among all slabs as listed in Table 4.6 and shown Figure 0.43 to Figure 0.46.

As mentioned in Section 2.3.2, a rational mechanical model was proposed by Muttoni (2008) and subsequently formed the basis for punching shear provisions in the latest edition of the Model Code (2010). The model is based on the critical shear crack theory (CSCT) which assumes that the shear strength is governed by the width and the roughness of the shear crack developed through an inclined compression strut that carries the shear force as shown in Figure 2.2; assuming that the crack width w is proportional to the slab rotation ψ. The shear strength is calculated from a set of assumed kinematics characterized by the rotation of the slab and integrating the contribution of the concrete tensile stresses, and the aggregate interlock along the failure surface. Most of the shear stress is transferred at the bottom end of the crack where the crack width is small, while any contribution from dowel action of the

reinforcement is ignored due to the expected spalling of the concrete cover. It was shown that the punching shear capacity decreases with increasing rotation since this implies wider cracks; thus reducing both tensile and aggregate contributions.

The details of the CSCT model are mentioned in Section 2.3.2. In Figures 4.43 to 4.46, the dashed lines represent the failure criterion of the CSCT calculated using Eq. 2.6, and the solid lines represent the slab-rotation predicted using Eq. 2.7 and. It should be noted that the CSCT failure criterion takes into account both the slab rotation and the maximum coarse aggregate size. The dotted curve in those figures shows the applied load versus rotation obtained from the experimental measurements. The predicted capacity and corresponding maximum rotation, for each slab, are defined by the intersection of the slab-rotation curve (solid line) with the failure criterion (dashed line).

The measured ultimate loads and rotation capacities, as well as those predicted using CSCT, are listed in Table 4.6. In general, the CSCT seems to reasonably predict the load-rotation behaviour of all test slabs. The load-rotation curves also represent the slab stiffness. The CSCT underestimates the initial stiffness at the first two load stages defined in Section 4.3. This underestimation is more pronounced for the thicker slabs with 200 mm and 250 mm thickness. The underestimation of the stiffness leads to an underestimation of the punching shear strength. This was observed for all slabs except SCB250. The prediction of the capacity of the test slabs using the CSCT is discussed in Section 4.8.

Table 0.6: Test Results vs. CSCT Predictions

Slab No.	f_c' (MPa)	P_{test} (kN)	P_{CSCT} (kN)	Experimental Rotation (rad.)	Rotation CSCT (rad.)	P_{CSCT}/P_{test}	$v_u / \sqrt{f_c'}$
SCA150	24.5	351	263	0.0220	0.0143	0.75	0.448
SCA200	26.0	533	465	0.0128	0.0083	0.87	0.416
SCA250	27.0	772	722	0.0119	0.0058	0.94	0.398
SCB150	29.0	343	276	0.0256	0.0153	0.80	0.402
SCB200	30.0	598	490	0.0162	0.0087	0.82	0.435
SCB250	32.0	764	770	0.0096	0.0061	1.01	0.362
SCC150	25.5	408	287	0.0213	0.0170	0.70	0.510
SCC200	26.0	589	503	0.0139	0.0095	0.85	0.460
SCC250	27.0	870	787	0.0121	0.0064	0.90	0.449
SCD150	24.0	342	282	0.0223	0.0166	0.82	0.441
SCD200	24.5	576	493	0.0115	0.0092	0.86	0.463
SCD250	25.0	836	763	0.0110	0.0063	0.91	0.448

The predicted rotation values show an increasing trend when a larger coarse aggregate size is used. However, the measured slab-rotation for the test slabs showed inconsistency with the predicted values. In general, the experimental results on the SCC slabs did not show any definitive trends for the effect of coarse aggregate size on the slab rotation.

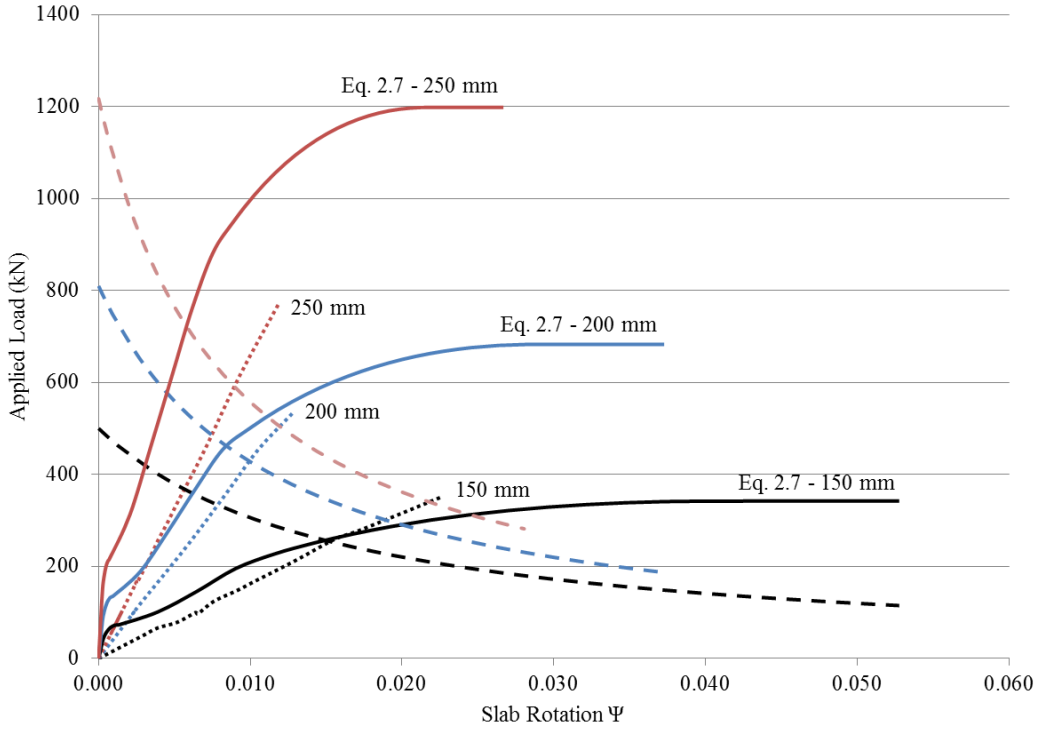

Figure 0.43: Load vs. Rotation (Group A Slabs: C/F 0.70 & Agg. Size 10 mm)

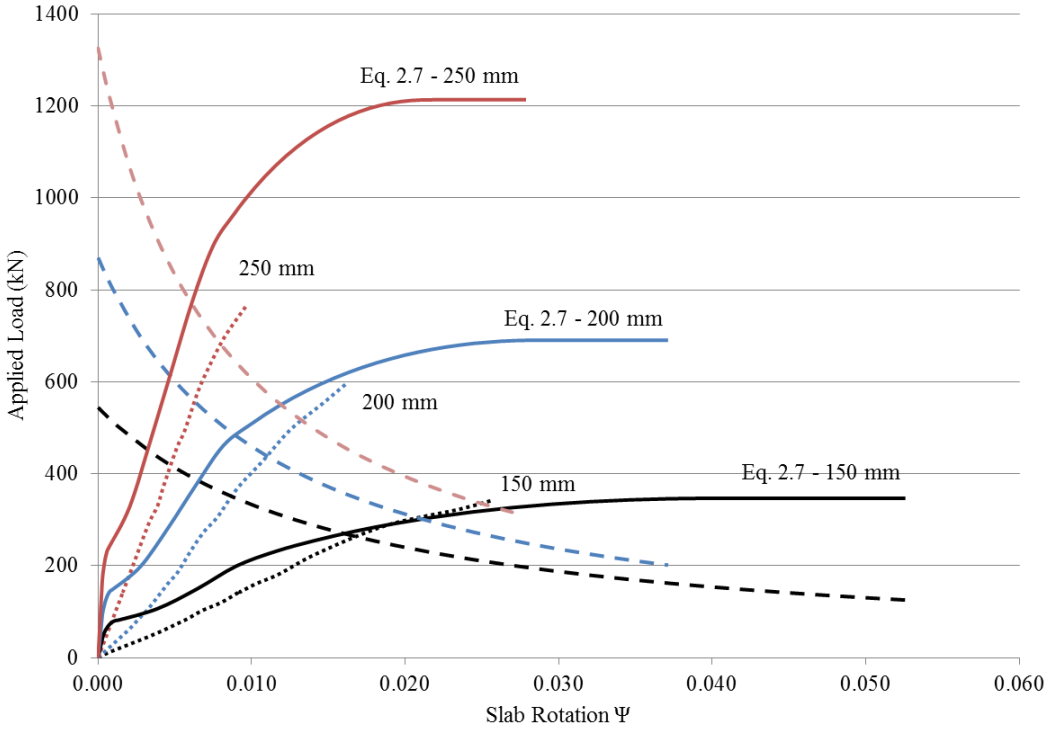

Figure 0.44: Load vs. Rotation (Group B Slabs: C/F 1.20 & Agg. Size 10 mm)

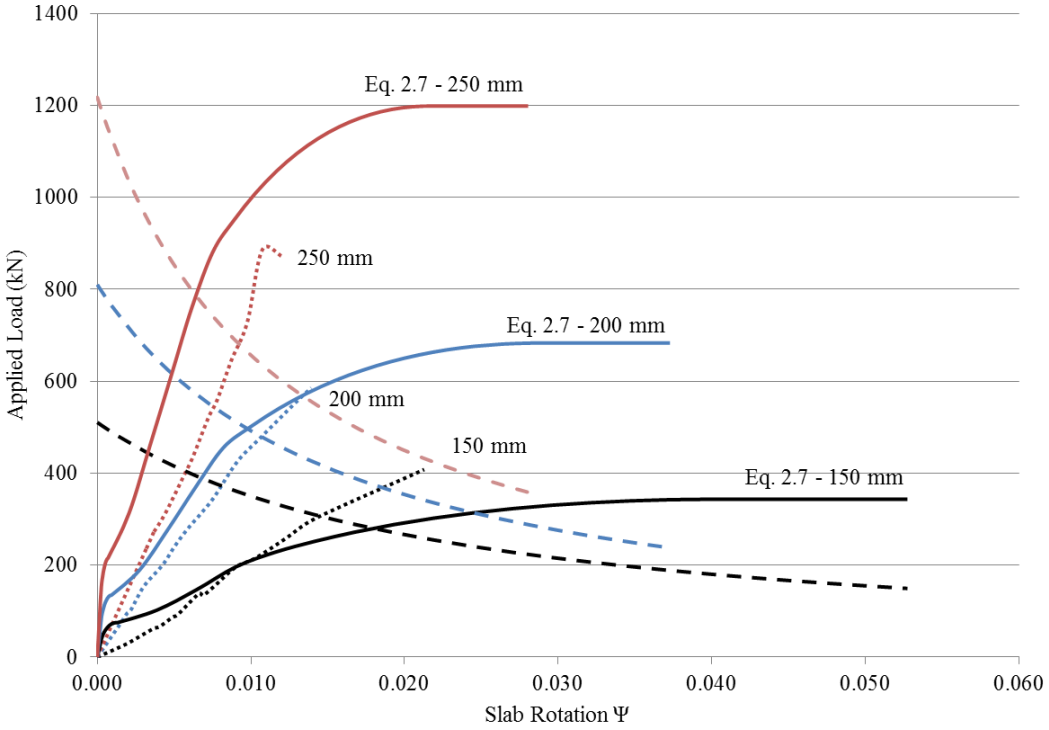

Figure 0.45: Load vs. Rotation (Group C Slabs: C/F 0.70 & Agg. Size 20 mm)

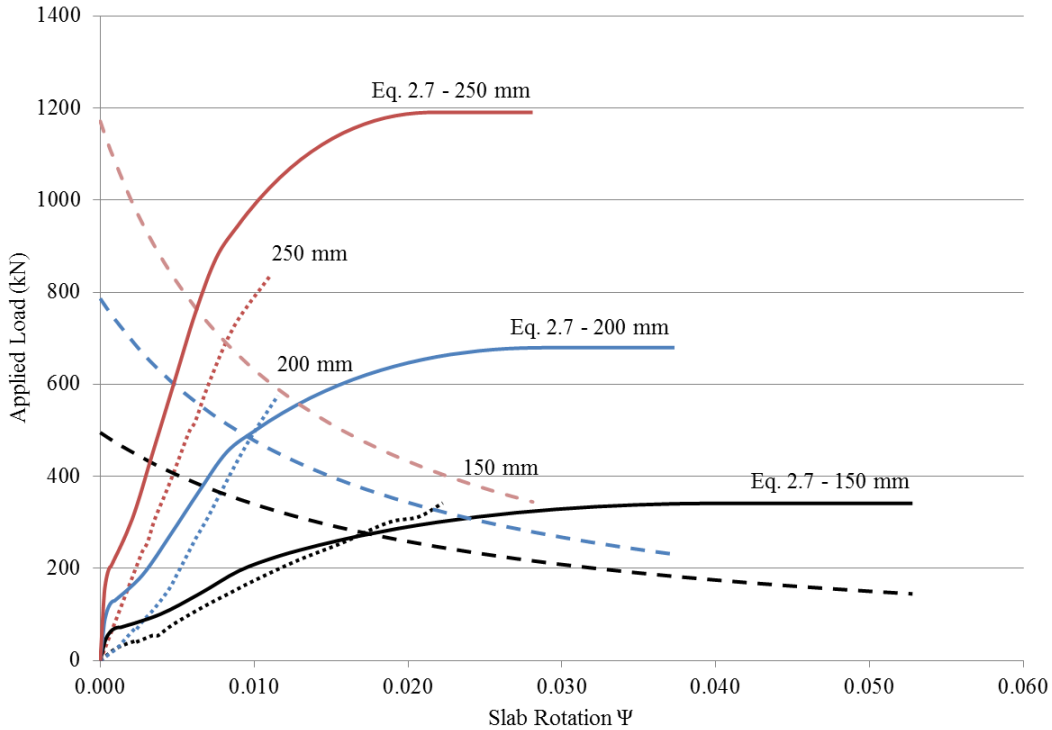

Figure 0.46: Load vs. Rotation (Group D Slabs: C/F 1.20 & Agg. Size 20 mm)

4.9 Shear Strength

The shear strengths for all slabs are presented in this section. The recorded ultimate loads, P_{test}, are listed in Table 0.7. The shear strength, v_u, is determined by dividing the ultimate load by $b_o d$, where b_o is the critical punching perimeter at $d/2$ from the column face, and d is the average slab depth for punching shear stresses calculations. In order to eliminate the small variability in the compressive strength of the different slabs, the shear strength was normalized w.r.t. $\sqrt{f_c'}$.

The relationship between the normalized shear strength and the slab depth is shown in Figure 0.47 for all test slabs. The results of Group A and C slabs indicated a decreasing trend in the normalized shear strength with increasing slab depth. The 200 mm and 250 mm thick slabs in Group B and D also indicated the same trend. However, the 150 mm thick specimens with C/F ratio of 1.2, SCB150 and SCD150, did not show the same trend of decreased normalized shear strength when the slab depth is increased. Hence, these somewhat inconsistent results do not necessarily allow definitive conclusions regarding the size effect for the slabs with C/F ratio of 1.2.

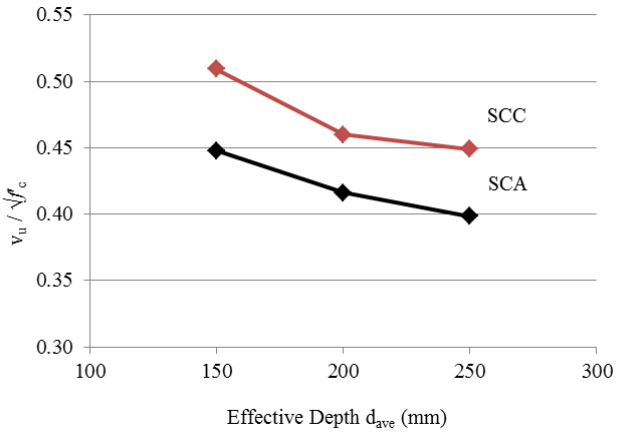

a) Group A and C Slabs (C/F Ratio of 0.70 and Maximum Aggregate Size of 10 mm and 20 mm, respectively)

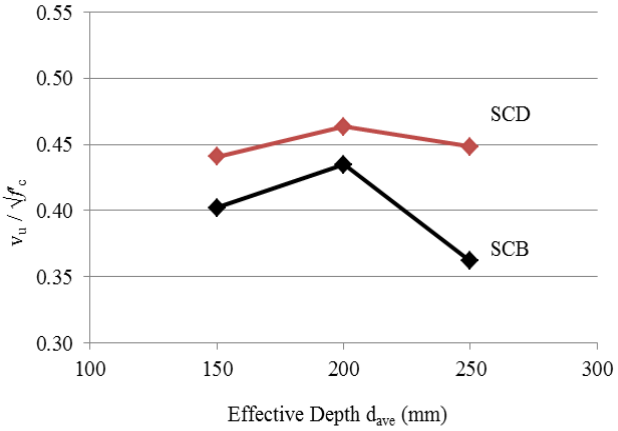

b) Group B and D Slabs (C/F Ratio of 1.20 and Maximum Aggregate Size of 10 mm and 20 mm, respectively)

Figure 0.47: Influence of Slab Thickness on Shear Stress Resistance

Figure 4.48 show the normalized shear strength versus the aggregate size for all test slabs. The figures clearly demonstrate that the coarse aggregate size have a significant influence on the shear strength of the test slabs. The shear strength consistently increased with increasing the maximum coarse aggregate size as shown in Table 4.7. An increase of approximately 12% is found for increasing the maximum coarse aggregate size form 10 mm in Group A to 20 mm in Group C. On the other hand, when the shear strength for Group D slabs were compared with those of Group B, a higher deviation in the increased stresses was found, as for slabs of thickness 200 mm, and 250 mm the strength increased by 6.5%, and 23%, respectively, with increasing the maximum coarse aggregate size from 10 mm to 20 mm.

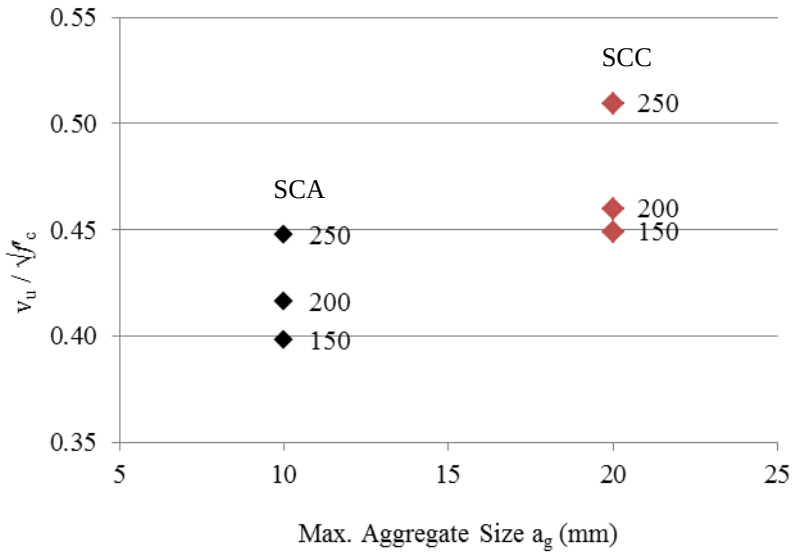

a) Group A and Group C – C/F 0.70

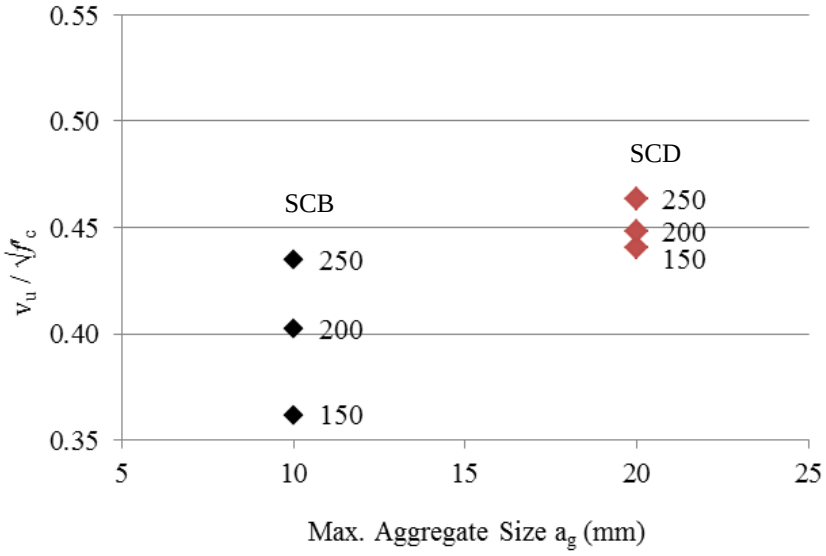

b) Group B and Group D – C/F 1.20

Figure 0.48: Influence of the Coarse Aggregate Size on Shear Strength

Table 0.7: Normalized Shear Strength of Test Slabs

Slab No.	h	d_{ave}	b_o	ρ	$f_c'^{*}$	P_{test}	$v_u^{\dagger}$	$v_u / \sqrt{f_c'}$
	(mm)	(mm)	(mm)	%	(MPa)	(kN)	(MPa)	
SCA150	150	110	1440	1.01	24.5	351	2.22	0.448
SCA200	200	155	1620	1.08	26.0	533	2.12	0.416
SCA250	250	205	1820	0.91	27.0	772	2.07	0.398
SCB150	150	110	1440	1.01	29.0	343	2.17	0.402
SCB200	200	155	1620	1.08	30.0	598	2.38	0.435
SCB250	250	205	1820	0.91	32.0	764	2.05	0.362
SCC150	150	110	1440	1.01	25.5	408	2.57	0.510
SCC200	200	155	1620	1.08	26.0	589	2.34	0.460
SCC250	250	205	1820	0.91	27.0	870	2.33	0.449
SCD150	150	110	1440	1.01	24.0	342	2.16	0.441
SCD200	200	155	1620	1.08	24.5	576	2.29	0.463
SCD250	250	205	1820	0.91	25.0	836	2.24	0.448

* Compressive strength on the testing day, measured using (100 × 200 mm) cylinders

† v_u is the shear strength (ultimate shear strength) = $P_{test} / b_o.d$

4.10 Test Results versus Code Predictions

The flexure reinforcement has an influence on the punching shear capacity of two-way slabs. The reinforcement reduces the crack width through the bond between the concrete and the deformed bars, and results in more uniform distribution of the cracks. Using the yield line theory, the flexural capacity of a slab is calculated as follows:

$$P_{felx} = 8\,(\,s/(a-c) - 1.172\,)\,M_n \qquad (0.1)$$

Where *s*, *a*, and *c* are dimensions shown in Figure 0.49. M_n is the nominal flexure strength for a one meter strip of the slab and is calculated as:

$$M_n = \rho . f_y . d^2 \left[1 - 0.59 \left(\rho . f_y / f_c'\right)\right] \quad (0.2)$$

Where ρ is the tensile flexural reinforcement ratio, and f_y is the specified yield strength for the reinforcement used.

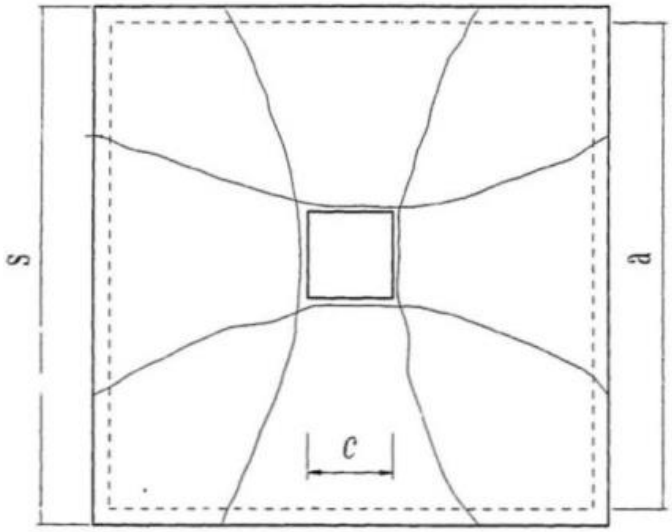

Figure 0.49: Yield Line Patter, Hussien (1991)

Hognestad (1953) introduced the ϕ_o factor which is defined as the ratio between the ultimate capacity P_u and the flexure resistance P_{flex}, calculated by the yield line theory, of a slab. A slab is considered to fail in punching shear when $\phi_o \leq 1$. If $\phi_o > 1$, the slab is considered to fail in flexure. The listed values for ϕ_o in Table 4.8 show that all test slabs failed due to shear. The thin slabs of thickness 150 mm have a higher ϕ_o values. This indicates that those slabs have more ductile behaviour compared to thicker slabs. These findings in addition to the spread of yield in the test slabs support the discussion of the slabs' ductility and stiffness mentioned in Section 4.3.

The punching shear equations of the different design codes are presented in Section 2.4. The resistance factors in these equations are taken as unity when comparing the predication of the code equations to the test results. In the current study, four codes

are presented (the Canadian Code (CSA A23.3-04), the American Code (ACI 318-11), the British Code (BS8110-97), and the European Code (EC2, 2010)).

The influence of the flexure reinforcement is not accounted for in the current North American Codes, CSA A23.3-04 or the ACI 318-11. On the other hand, the British standard and the European code EC2; both include the flexure reinforcement ratio influence on the punching capacity. CSA A23.3-04 does not account for the slab depth if it is less than 300 mm. Both the British Code (BS8110-97), and the European Code (EC2, 2010) contains terms that account for the slab depth as mentioned in Section 2.4.

The comparison between the test results and the code predications are presented in Tables 4.8 and 4.9 for the test slabs with 10 mm and 20 mm coarse aggregate size, respectively. The mean ratio, standard deviation and coefficient of variation of the predicted to the measured capacities for the slabs are also listed in these tables.

The Canadian code CSA A23.3-04 gives safe predictions of the capacity of the SCC test slabs with 10 mm and 20 mm coarse aggregate size. The only unsafe prediction is that for slab SCB250. The ratio of the predicted to the measured capacity is 1.05 for this slab which is unsafe prediction. The mean ratio, standard deviation (S.D) and coefficient of variation (COV) of the predicted to the measured capacities for the slabs of Groups A and B, with 10 mm coarse aggregate size, are 0.93, 0.07 and 7.7%, respectively. For Groups C and D, with 20 mm coarse aggregate size, these values are 0.83, 0.04 and 4.9%, respectively. Hence, the CSA code is more conservative and has less scatter for SCC slabs with 20 mm coarse aggregate size compared to those with

10 mm coarse aggregate size. In general, the Canadian Code can be safely used to check the punching shear capacity of SCC slabs without the need to modify the code equation. The ACI 318-11 code predictions are the most conservative among the four codes and they follow the same trend as the CSA code.

The BS8110-97 code gave the least scatter in the P_{code}/P_{test} ratios among all codes for the slabs with 10 mm coarse aggregate size. The predictions of the BS8110-97 code were very similar to those of CSA A23.3 for the slabs with 20 mm coarse aggregate size. The BS8110-97 gives safe predictions of the capacity of all SCC test slabs.

The predictions of the Eurocode (EC2) are unsafe for all SCC slabs with 10 mm coarse aggregate size and thicknesses of 200 mm and 250 mm. The ratios of P_{code}/P_{test} are higher than unity for those slabs. For slabs with 20 mm coarse aggregate size, the predictions of the Eurocode (EC2) are unsafe for the 250 mm slabs. The EC2 has the highest COV among all codes for the SCC slabs with 10 mm and 20 mm coarse aggregate size. It should be mentioned that the BS 8110 code was superseded by Eurocode (EC2) in 2010.

In conclusion, and with the exception of EC2, the capacity of SCC slabs with different thicknesses and coarse aggregate size can safely and adequately be predicted using the listed codes (CSA23.3-04, ACI318-11 and BS8110). In general, the predictions of all four codes are more conservative and have less scatter when applied to SCC slabs with 20 mm coarse aggregate size compared to those with 10 mm coarse aggregate size.

The CSCT proposed by Muttoni (2008) gives safe predictions of the capacity all test slabs with 10 mm and 20 mm coarse aggregate size. The mean ratio, standard deviation and coefficient of variation of the predicted to the measured capacities for the slabs of Groups A and B, with 10 mm coarse aggregate size, are 0.86, 0.10 and 12.0%, respectively. For Groups C and D, with 20 mm coarse aggregate size, these values are 0.83, 0.08 and 9.7%, respectively. Moreover, the COV of the CSCT predictions are higher than those of CSA23.3-04, ACI318-11 and BS8110. The COV of the CSCT predictions were very close to those of EC2. It should be mentioned that the CSCT considers the coarse aggregate size used when determining the capacity of the slabs. However, all codes do not consider this factor in their design equations. In addition, unlike code equations, the CSCT can reasonably predict the structural behaviour of the test slabs as mentioned in Section 4.7.

Table 0.8: Test Results vs. Code Predictions (Slabs with 10 mm Agg. Size)

Slab No.	v_u	$v_u / \sqrt{f_c'}$	P_{code} / P_{test}				P_{CSCT} / P_{test}	P_{test} / P_{flex}
	MPa	Nominal	CSA23.3	ACI318	BS8110	EC2		ϕ_o
SCA150	2.22	0.448	0.85	0.74	0.86	0.91	0.73	0.78
SCA200	2.12	0.416	0.91	0.79	0.94	1.11	0.87	0.58
SCA250	2.07	0.398	0.95	0.83	0.93	1.18	0.94	0.58
SCB150	2.17	0.402	0.94	0.82	0.94	0.98	0.79	0.75
SCB200	2.38	0.435	0.87	0.76	0.88	1.04	0.81	0.64
SCB250	2.05	0.362	1.05	0.91	0.99	1.26	1.01	0.56
		Mean	0.93	0.82	0.92	1.08	0.86	
		S.D	0.07	0.06	0.05	0.13	0.10	
		COV	7.7%	7.7%	5.2%	12.0%	12.0%	

Table 0.9: Test Results vs. Code Predictions (Slabs with 20 mm Agg. Size)

Slab No.	v_u	$v_u / \sqrt{f_c'}$	P_{code} / P_{test}				P_{CSCT} / P_{test}	P_{test} / P_{flex}
	MPa	Nominal	CSA23.3	ACI318	BS8110	EC2		ϕ_o
SCC150	2.57	0.510	0.75	0.65	0.75	0.79	0.69	0.91
SCC200	2.34	0.460	0.83	0.72	0.85	1.00	0.84	0.64
SCC250	2.33	0.449	0.85	0.74	0.82	1.05	0.90	0.65
SCD150	2.16	0.441	0.86	0.75	0.88	0.92	0.80	0.77
SCD200	2.29	0.463	0.82	0.71	0.85	1.00	0.85	0.63
SCD250	2.24	0.448	0.85	0.74	0.83	1.06	0.91	0.63
		Mean	0.82	0.72	0.83	0.97	0.83	
		S.D	0.04	0.04	0.04	0.10	0.08	
		COV	5.0%	5.0%	5.3%	10.4%	9.7%	

Chapter 5

Conclusions & Recommendations

Four SCC mixtures were developed and used to cast the SCC slabs in the current study. Twelve reinforced concrete slabs were prepared using the four SCC mixtures. The main parameters of the test were the C/F ratio, aggregate size and slab depth. The structural behaviour and characteristics of SCC slabs were examined: load-deflection, steel and concrete strains, capacity, crack propagation and crack profile at failure. The following conclusions can be drawn from the present research:

- The C/F ratio and aggregate size did not show any significant influence on the slab behaviour such as deflection, stiffness, ductility and energy absorption, steel and concrete strains and cracking characteristics.

- A discontinuity in the deflection profiles was observed inside the shear cracking zone. This discontinuity is more pronounced in thicker slabs than in thin slabs which exhibited more uniform deformations. This discontinuity is located approximately at a distance equal to the effective slab depth from the slab center. The portion of slab in outer zone of slabs, bounded by the critical shear crack seemed to deform as a rigid body. This behaviour is very similar to that of NSC slabs.

- The slab thickness has the most significant effect among the test parameters on the behaviour of the test slabs.

- The test result proved that there is no significant difference in term of structural behaviour when using different coarse aggregate size or content. Therefore, the structural behavior of SCC should be similar to that of NC."

- The depth and aggregate size are the most influential parameters on the shear capacity of the slab; increasing the slab thickness lead to a decrease in the normalized shear strength of the slab while increasing the aggregate size lead to an increase in the normalized shear strength of the slab.

- The punching shear provisions in the Model Code (2010) are based on the CSCT proposed by Muttoni (2008). The CSCT is able to reasonably predict the structural behaviour of the test slabs. Nonetheless, the test results did not show any clear trend in the relationship between the aggregate size and the slab rotation.

- The Canadian Code CSA (A23.3-04), the American Code (ACI 318-11) and the British Code (BS8110-97) give safe predictions of the capacity of the SCC test slabs. The only unsafe prediction by CSA A23.3-04 is that for slab SCB250. Therefore, these codes can be safely used to check the punching shear capacity of SCC slabs without the need of any modification to the equations used for such shear check.

- The predictions of the Canadian Code CSA (A23.3-04), the American Code (ACI 318-11) and the British Code (BS8110-97) are more conservative and have less scatter when applied to SCC slabs with 20 mm coarse aggregate size compared to those with 10 mm coarse aggregate size.

- The British Code (BS8110-97) was superseded by Eurocode (EC2) in 2010. The predictions of the Eurocode (EC2) are unsafe for most of the slabs with thicknesses of 200 mm and 250 mm.

- The EC2 has the highest COV among all codes for the SCC slabs with 10 mm and 20 mm coarse aggregate size. The predictions of the Eurocode (EC2) are unsafe for most of the slabs with thicknesses of 200 mm and 250 mm. Hence, further research is needed to examine the use of EC2 in the design of SCC slabs for punching shear.

- The CSCT gives safe predictions of the capacity all test slabs. The COV of the CSCT predictions are higher than those of CSA23.3-04, ACI318-11 and BS8110. The COV of the CSCT predictions were very close to those of EC2.

Reference

ACI Committee 318, “Building Code Requirements for Structural Concrete (ACI 318-11) and Commentary,” American Concrete Institute, Farmington Hills, MI, 2008, 473 pp.

ASTM C39/C39M-04a (2004) “Standard Test Method for Compressive Strength of Cylindrical Concrete Specimens,” ASTM International, West Conshohocken, Pa.

ASTM C78-02 (2002). “Standard Test Method for Flexural Strength of Concrete (Using Simple Beam with Third-Point Loading),” ASTM International, West Conshohocken, Pa.

Birkle, G., and Dilger, W., “Influence of Slab Thickness on Punching Shear Strength,” ACI Structural Journal, V. 105, No. 2, Mar.-Apr. 2008, pp. 180-188.

BS 8110, “Structural Use of Concrete, Part 1: Code of Practice for Design and Construction,” British Standards Institution, London, UK, 1997, 117 pp.

BS EN 1992-1-2, “Eurocode 2: Design of Concrete Structures—Part 1-1: General Rules and Rules for Buildings,” Brussels, Belgium, 2004, 230 pp.

Comité Euro-International du Béton-Fédération de la Précontrainte (CEB-FIP), “Punching of Structural Concrete Slabs,” Bulletin No. 12, Lausanne, Switzerland, 2001, 307 pp

CSA A23.3-04, “Design of Concrete Structures for Buildings,” Canadian Standards Association, Rexdale, ON, Canada, 2004, 258 pp.

EFNARC 2005, "Specification and Guidelines for Self-Compacting Concrete", pp.32, www.efnarce.org.

Fib technical report buletin 57, “Shear and punching shear in rc and frc elements,” tech. rep., The International Federation for Structural Concrete, Salò, Italy, Workshop 15-16 October 2010.

Goodier, C.I., “Development of self-compacting concrete.” Structures & Buildings 156, November 2003 Issue SB4, Pages 405-414

Guandalini, S., Burdet, O. L., and Muttoni, A., “Punching Tests of Slabs with Low Reinforcement Ratios,” ACI Structural Journal, V. 106, No. 1, Jan.-Feb. 2009, pp. 87-85.

Hassan, A. A. A., Hossain, K. M. A., and Lachemi, M., “Behaviour of full-scale Self-consolidating concrete beams in shear.” Cement & Concrete Composites, 30 (2008): 588-596

Hassan, A. A. A., Hossain, K. M. A., and Lachemi, M., "Strength, cracking and deflection performance of large-scale self-consolidating concrete beams subjected to shear failure." Engineering Structures, 32 (2010): 1262-1271

Hussein, A. (1990). "Behaviour of Reinforced Concrete Slabs Made with High-Strength Concrete," Master Thesis, Faculty of Engineering, Memorial University of Newfoundland, St. John's, Canada.

Khaleel, O. R., Al-Mishhadani, S. A., and Abdul Razak, H., "The Effect of Coarse Aggregate on Fresh and Hardened Properties of Self-Compacting Concrete (SCC)," The Twelfth East Asia-Pacific Conference on Structural Engineering and Construction. Procedia Engineering 14 (2011) 805-813

Kinnunen, S. (1963). "Punching of Concrete Slabs with Two-Way Reinforcement with Special Reference to Dowel Effect and Deviation of Reinforcement From Polar Symmetry," Transactions. No. 198, Royal Institute of Technology, Stockholm, Sweden.

Kinnunen, S., and Nylander, H. (1960). "Punching of Concrete Slabs without Shear Reinforcement," Trans., Royal Inst. Of Technol., Stockholm, No. 158, 112p.

Krishna Rao, B., Krishna, A. V., and Rajagopal, A., "Effect of different sizes of coarse aggregate on the properties of NCC and SCC" International Journal of Engineering Science and Technology. Vol. 2(10), 2010, 5959-5965

Lin, C. H., and Chen, J. H., "Shear Behaviour of Self-consolidating concrete Beams," ACI Structural Journal, V. 109, No. 3, May-June 2012, pp. 307-316.

Muttoni, A., "Shear and Punching Strength of Slabs without Shear Reinforcement," Beton-und Stahlbetonbau, V. 98, No. 2, Berlin, Germany, 2003, pp. 74-84.

Muttoni, A., "Punching shear strength of reinforced concrete slabs without transverse reinforcement," ACI Structural Journal, vol. 105, pp. 440–450, July-August 2008.

Muttoni, A., and Ruiz, M. F.,"Applications of critical shear crack theory to punching of reinforced concrete slabs with transverse reinforcement," ACI Structural Journal, vol. 106, pp. 485–494, July-August 2009.

Muttoni, A., and Schwartz, J., "Behaviour of Beams and Punching in Slabs without Shear Reinforcement," IABSE Colloquium, V. 62, Zurich, Switzerland, 1991, pp. 703-708.

Rizk, E., Marzouk, H., and Hussein, A., "Punching Shear of Thick Plates with and without Shear Reinforcement," ACI Structural Journal, V. 108, No. 5, Sept.-Oct. 2011, pp. 581-591.

Sherwood, E. G., Bentz, E. C., and Collins, M. P., "Effect of Aggregate Size on Beam-Shear Strength of Thick Slabs," ACI Structural Journal, V. 104, No. 2, March-April 2007, pp. 180-190.

Standard Norge, Eurocode 2 (EC2): Design of concrete structures - Part 1-1: General rulesand rules for buildings, 2004+NA: 2008.

Vecchio, F. J., and Collins, M. P., "The Modified Compression-Field Theory for Reinforced Concrete Elements Subjected to Shear," ACI JOURNAL, Proceedings V. 83, No. 2, Mar.-Apr. 1986, pp. 219-231.

Walraven, J. C., "Fundamental Analysis of Aggregate Interlock," Journal of Structural Engineering, ASCE, V. 107, No. 11, 1981, pp. 2245-2270.

Zdenek, P., and Kim, J. K., "Size Effect in Shear Failure of Longitudinally Reinforced Beams," ACI Structural Journal, V. 81, No. 4, July-Aug. 1984, pp. 456-468.